



**POLITECNICO**  
MILANO 1863

Dipartimento di Chimica, Materiali e Ingegneria Chimica “G. Natta”

Doctoral Program in Material Engineering

# **Electrospinning of biopolymers for regenerative medicine**

Advisor: Dr. Lorenza Draghi

Candidate: Chiara Marcolin

Tutor: Prof. Luigi De Nardo

Coordinator: Prof. Chiara Castiglioni

XXIX PhD Cycle



## Abstract

Extra-cellular matrix (ECM) is a three-dimensional structure constituted by interconnected nanofibers, which serves as scaffold for cell proliferation and plays also an important role in tissue function. ECM is composed of several types of proteins, polysaccharides and glycoproteins.

In tissue engineering field, a scaffold with adequate composition and properties is fundamental to favor physiological healing process and successful outcome. In this regard, electrospinning (ES) represents a valuable fabrication technique, as it allows the production of nanofibers in a simple and convenient way; moreover, natural polymers, and in particular ECM biopolymers, can be processed by ES, thus allowing the fabrication of membranes whose chemical composition and morphology closely resemble those of physiological ECM. Several studies in literature have focused their attention on ES of biopolymers; however, some limitations remain, as solvents commonly used for ES are not necessary good solvent for natural polymers and they can be toxic or cause extensive molecule denaturation, biopolymer solutions usually lack viscoelastic properties essential for a stable ES, and finally, a crosslinking post-treatment, which is necessary to improve matrix stability, may introduce cytotoxic residues. Therefore, more detailed comprehension and study on biopolymer ES are necessary in order to elucidate possible solutions, thus leading to production of membranes with a tremendous potential as scaffold for tissue engineering.

In Chapter 1, ECM composition and function were reviewed, and the most studied strategies for ECM mimicry were presented. Then, ES process was described, and the influence of several parameters on the process outcome was discussed. Particular attention was dedicated to ES of natural polymers and the relative characterization techniques commonly used in literature.

In the second Chapter, the most abundant ECM macromolecules (i.e. collagen/gelatin, elastin and hyaluronic acid) were used to obtain different composition blends, and their ES process was optimized in order to produce electrospun matrices with tunable composition

that closely mimics ECM of different tissues. The use of a non-fluorinated solvent, namely formic acid, for solution preparation was advantageous in reducing both toxicity and cost of the process with respect to the solvents commonly used in literature for biopolymer ES (i.e. hexafluoroisopropanol, HFIP, and trifluoroethanol, TFE). Influence of collagen batch variability on ES process was also evaluated. Finally, the efficacy of the most common crosslinking methods for natural polymers was compared by evaluating matrix morphology and stability.

The third Chapter is dedicated to the ES of fibrinogen, which has a major role in clot formation and physiological tissue repair, and of fibrinogen/gelatin blend. For the first time fibrinogen was successfully electrospun by means of an acidic solvent system composed of formic and acetic acids, instead of the commonly used HFIP. However, fibrinogen solution gelification at the tip of the spinneret occurred, thus hindering process continuity. As it was not possible to solve this problem, an alternative solution consisted in electrospinning a blend of fibrinogen/gelatin (1/1). Moreover, solution gelification phenomenon was investigated in details, and in particular the effect of acidic pH on fibrinogen molecular structure was examined by means of experimental and computational studies, which elucidated the denaturing effects of the solvent used for ES on the biomolecule.

In Chapter 4 a variation of traditional ES technique, namely co-axial ES, was used to obtain core-shell fibers with application in wound healing. In particular, gelatin and hyaluronic acid were used as core and shell materials, respectively; moreover, CCG-203971 drug to prevent myofibroblast differentiation, which is responsible for excessive scar formation during wound healing, was loaded within the fiber core. The membranes were crosslinked by glutaraldehyde vapor, and influence of different process durations on electrospun matrix chemical structure were investigated. Finally, *in vitro* drug release and cell tests were carried out in order to evaluate the feasibility of drug-loaded bicomponent fibrous membrane for the application intended.

# Index

<b>Chapter 1: Introduction</b> .....	<b>8</b>
1. The extracellular matrix.....	9
1.1 Materials to mimic the extracellular matrix.....	11
1.2 Strategies to mimic the extracellular matrix .....	12
2. Electrospinning .....	13
2.1 Electrospinning apparatus.....	14
2.2 The History of Electrospinning .....	14
2.3 Electrospinning process.....	16
2.4 Effect of ES parameters .....	17
2.5 Non-conventional electrospinning techniques .....	20
3. Electrospinning of natural polymers .....	23
4. Characterization techniques of electrospun membranes .....	31
References.....	36
<b>Aim of the thesis</b> .....	<b>43</b>
<b>Chapter 2 – Electrospinning of gelatin-based blends</b> .....	<b>45</b>
1. Introduction.....	46
2. Materials and methods .....	47
2.1 Solubility tests.....	49
2.2 Electrospinning apparatus.....	49
2.3 Evaluation of process stability .....	50
2.4 Morphological analysis .....	50
2.5 SDS-PAGE analysis .....	52
2.6 Crosslinking methods .....	53
3. Results and discussion .....	56
3.1 Electrospinning of collagen .....	56
3.2 Electrospinning of gelatin .....	62
3.3 Electrospinning of elastin .....	65
3.4 Electrospinning of gelatin/elastin blends.....	67

3.5 Electrospinning of gelatin/elastin/hyaluronic acid blends .....	72
3.6 Crosslinking strategies .....	76
4. Conclusions.....	81
References.....	83
<b>Chapter 3 – Study on fibrinogen stability at acidic pH and electrospinning of fibrinogen/gelatin blend .....</b>	<b>87</b>
1. Introduction.....	88
2. Materials and methods .....	90
2.1 Electrospinning of fibrinogen and fibrinogen/gelatin blends .....	90
2.2 Study of fibrinogen molecular structure and investigation on gelification process .....	93
3. Results and discussion .....	103
3.1 Electrospinning of fibrinogen: effect of solution and process parameters on morphology and gelification kinetics .....	103
3.2 Study of fibrinogen molecular structure and investigation on gelification process .....	107
3.3 Electrospinning of fibrinogen/gelatin blend: solution and parameters optimization .....	116
4. Conclusions.....	119
References.....	120
<b>Chapter 4 – Core-shell electrospinning of natural polymers for wound healing applications .....</b>	<b>123</b>
1. Introduction.....	124
2. Materials and methods .....	130
2.1 Core-shell electrospinning optimization .....	130
2.2 Glutaraldehyde crosslinking process .....	136
2.3 In vitro tests.....	137
3. Results and discussion .....	140
3.1 Core-shell electrospinning optimization .....	140
3.2 Characterization of the crosslinking process.....	160
3.3 Evaluation of CCG-203971 cytotoxicity and efficacy .....	165

3.4 Core-shell electrospinning of drug loaded fibers: release kinetics and cell tests	169
4. Conclusions.....	174
References.....	177
<b>Chapter 5 - Final remarks.....</b>	<b>180</b>

# Chapter 1: Introduction

---



# 1. The extracellular matrix

The extracellular matrix (ECM) is the natural scaffold where cells adhere, proliferate, and migrate. ECM is a complex three-dimensional nanofibrous network, composed of proteins, polysaccharides, and glycoproteins, which serve as substrate to which cells attach via cell-matrix adhesion (Fig. 1.1). The interaction between cells and ECM is reciprocal and dynamic: cells synthesize and manipulate ECM, which in turn influences cell behavior, by both chemical (growth factors, cytokines) and physical (density, stiffness, orientation) signals necessary to cell proliferation, migration and differentiation<sup>1</sup>. In particular, growth factors and signalling molecules can be stored within the ECM, which protects them from premature degradation, and conveniently releases them to function as soluble ligands, or they can attach to the surface of the ECM to present themselves more efficiently to cell receptors and eventually lead cell migration in a concentration-dependent manner (haptotaxis)<sup>2</sup>.

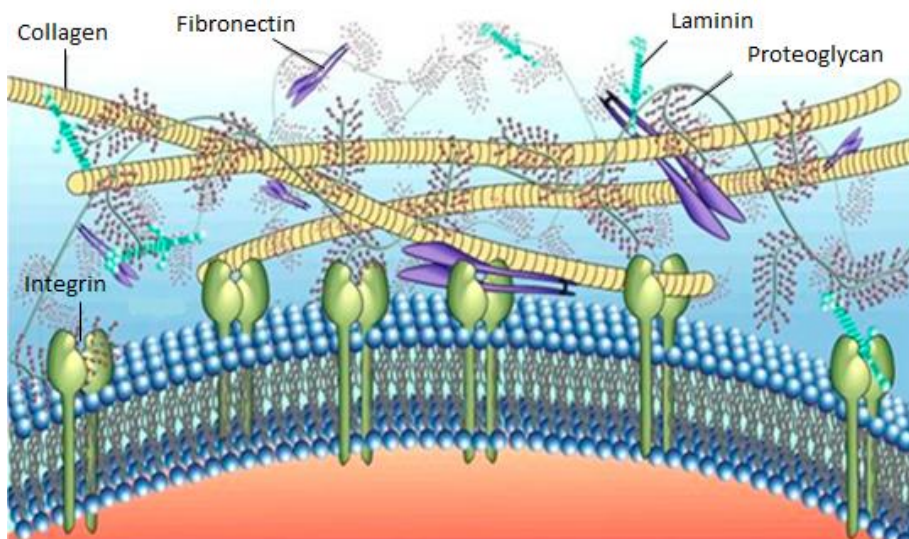


Fig. 1.1: Cellular microenvironment showing the main components of ECM<sup>3</sup>.

Furthermore, cell-environment interactions are specific for each tissue and organ, thus leading to their unique composition and morphology, with respect to the function. Nevertheless, it is possible to identify some main ECM components present in human

tissues, such as collagen, proteoglycans and hyaluronic acid, while other components depend on the specific tissue (fibrin, fibronectin, elastin, laminin, hydroxyapatite – See Table 1.1).

Table 1.1: Major component of native ECM, their locations, and functions in the body<sup>4</sup>.

<b>Component</b>	<b>Location</b>	<b>Function</b>
Collagen	Widely distributed	Key component of tissue architecture, provide tensile strength, cell-matrix interaction, matrix-matrix interaction
Elastin	Highly elastic tissues (lung, blood vessel, skin)	Key component of tissue architecture, provide elasticity
Proteoglycans	Widely distributed	Cell-matrix interaction, matrix-matrix interaction, cell proliferation, cell migration
Hyaluronic acid	Widely distributed	Cell-matrix interaction, matrix-matrix interaction, cell proliferation, cell migration
Laminin	Basement membranes	Basement membrane component, cell migration
Fibronectin	Widely distributed	Component of tissue architecture, cell-matrix interaction, matrix-matrix interaction, cell proliferation, cell migration
Fibrinogen	Blood, sites of wound healing	Cell proliferation, cell migration, hemostasis
Various Adhesion Molecules	Widely distributed	Mediate cell adhesion to matrix, mediate transmembrane signals

Thanks to macromolecule flexibility, fiber dimensions range from tens to hundreds of nanometers, allowing unique control of hierarchical organization<sup>2</sup>. Not only the composition, but also ECM architecture plays an important role in regulating cell behavior, and fiber organization depends on tissue function. For example, collagen fibers in ligaments and tendons are aligned along the load-bearing axis of the tissue, in order to provide the greatest resistance to strain.

The importance of ECM lies in many fundamental physiological processes: in fact, the matrix separates tissues and organs, and is responsible for their mechanical properties; it maintains tissue homeostasis thanks to its buffering action and water retention ability.

Furthermore, it provides substrate for cell anchorage and motility, and it works as a reservoir of biochemical factors important for cellular functions. Finally, ECM regulates cell communications and can influence cell behavior in several ways, both during tissue morphogenesis, homeostasis and wound healing<sup>1</sup>. ECM functions are usually mediated by cell-ECM adhesions: special receptors present on the cell surface recognize and interact with particular ECM chemical sequences. For example, a family of transmembrane cell receptors named integrins can recognize motifs such as RGD (Arg-Gly-Asp) present in several ECM proteins (i.e. collagen, fibrinogen, fibronectin)<sup>5</sup>.

### 1.1 Materials to mimic the extracellular matrix

Considering the fundamental role of ECM in so many cell and tissue processes, several attempts to reproduce cell environment in order to investigate cell-ECM interactions and to fabricate adequate scaffolds for tissue engineering have been made.

With respect to the material used for scaffold production, three main classes can be identified: synthetic polymers, natural polymers, and decellularized tissues.

**Synthetic polymers** are advantageous because they are usually easy to synthesized and process, thus allowing good reproducibility and tunable composition<sup>6</sup>. They can present excellent mechanical properties and can be biodegradable, with tunable degradation kinetics. However, degradation occurs in medium-long term (weeks-months) and byproducts formed can elicit inflammatory response<sup>7</sup>. Furthermore, synthetic biomaterials lack functional sites for cells, as they are not able to provide biochemical similarities with ECM, thus leading to possible foreign body and encapsulation responses post-implantation<sup>7</sup>. To decrease adverse physiological/organism reactions and improve cell interaction, new strategies have been developed, as for example the conjugation of synthetic materials with various ECM peptides, and the coating with natural gels (e.g. collagen and chitosan)<sup>6</sup>.

Because of their similarity with the physiological ECM, **natural polymers** are attractive materials for biomedical applications, as they have the possibility to direct cell migration and proliferation<sup>6,8</sup>. In fact, they are intrinsically biocompatible and biodegradable, and

degradation products are well tolerated and metabolized by human body. One major limit of natural polymers is the possible batch-to-batch variation; however, an innovative strategy to overcome this problem is represented by the recombinant protein technology, where precisely defined natural polymers can be produced, thus making them very attractive for biomedical applications<sup>8</sup>.

To accurately mimic ECM composition and architecture, tissue engineers have obtained scaffolds from **decellularized tissues**, both allogeneic or xenogeneic. Even if similarity in microstructure and biochemical properties to the native tissues can favor the regeneration process, their use is limited because of the possible presence of animal residues and contaminants. Furthermore, decellularized membranes are not chemically and physically controlled, thus presenting scarce reproducibility<sup>1</sup>.

## **1.2 Strategies to mimic the extracellular matrix**

Due to the extreme complexity of ECM, it is almost impossible to totally replicate its precise structure; for this reason, strategies of ECM biomimicry in literature focuses on the reproduction of only some properties considered the most important for the application envisioned<sup>9</sup>. Initially, scaffolds have been designed to match the properties of the tissue to be replaced on a macroscopic level, without considering the complexity and nanoscale details of the matrix<sup>2</sup>. More recent researches in tissue engineering field try to combine micro and nanostructured scaffolds with naturally derived biopolymers in order to provide biochemical signals important for cell adhesion, proliferation and migration<sup>10-11</sup>. For example, **3D printing** technique allows the control of scaffold three-dimensional architecture and pore size. As the process can be performed at ambient temperature, it is compatible with natural polymers and proteins (i.e. gelatin, collagen, chitosan, alginate hydrogels)<sup>12-14</sup>. The main limitation of the technique relies in the feature dimensions that can be obtained, which range from micron to millimeter, thus being much bigger than ECM dimensions.

Another widely studied technique for the production of scaffolds from natural biomaterials is **freeze-drying**, or lyophilization. This method allows the fabrication of porous matrices

with high surface area and specific three-dimensional shape for the desired application; however, these traditional scaffolds have a microporous structure with a bigger magnitude than nano-scale fibrillar network of native ECM<sup>15-17</sup>.

In order to better reproduce ECM structure and dimensions, there has been a great interest in developing techniques which allow the fabrication of matrices with nanometric features. In this regard, one possible strategy is to use the ability of molecules of autonomously organizing into patterns (**self-assembly**). For example, collagen molecules and synthetic collagen-based peptides have been used to obtain very thin fibrils, with diameter typically less than 10 nm<sup>2</sup>. Nevertheless, self-assembled nano-fibers systems are limited to hydrogel format; collagen gels, in particular, are quite heterogeneous and have poor physical strength, which limits their application<sup>1,18</sup>.

Among the wide variety of technological processes that allow the fabrication of nano-structured scaffolds, **electrospinning** is of particular interest because it can generate 3D structure with micro to nano-scale features, and it offers great flexibility in terms of choice of material, scaffold geometry, and fiber orientation<sup>11</sup>. In fact, nanometer fibers in the same range of ECM dimensions (50-500 nm) can be obtained utilizing natural polymers, thus mimicking both the structure and the chemical composition of the physiological matrix. Furthermore, electrospinning apparatus is simple, convenient and has low operating cost; the process can promisingly be scalable to industrial dimensions and is relatively reproducible.

## 2. Electrospinning

The term “electrospinning” derives from “electrostatic spinning”, and even if it is an old technique the process has gained much attention in the last twenty years, due to its versatility and ability to consistently produce micro- and nano-fibers with high surface-to-volume ratio. Because of these advantages, electrospun membranes have been studied in the past several years for different applications, such as filtration, optical sensors, and biological scaffolds<sup>6, 19-20</sup>. Nevertheless, there are still some challenges to be solved, such

as the difficulty to produce consistent amount of nanofibers with traditional single-needle setup. Furthermore, a major challenge for tissue engineering applications is the lack of cellular migration in the electrospun scaffold because of its high fiber density and low porosity<sup>6</sup>.

## **2.1 Electrospinning apparatus**

In the traditional ES system, a polymeric solution is loaded into a plastic syringe connected to a metal needle (spinneret). A high voltage (10-30 kV) is then applied to the solution, and a grounded or oppositely charged target (collector) is placed some distance from the polymer solution in order to collect the produced fibers (Fig. 1.2). In particular, the polymer solution is held by its surface tension at the tip of the spinneret; when the electric field is applied, charges are induced and accumulated on solution surface, where mutual charge repulsion causes a force opposite to the surface tension. As the electric force increases, the surface of the solution drop elongates to form a conical shape (Taylor cone). When the electric field reaches a critical value, electrostatic force overcomes viscoelastic force and drop surface tension: a charged jet of the solution is then formed. This jet, starting from Taylor cone, travels through the instability region, where bending and whipping movements, together with solvent evaporation, cause jet thinning. Bending movement becomes more and more rapid as the jet travels, thus making it appears as spraying droplets or separated fibers to human eyes, even if only one single fiber is ejected. Finally, continuous fibers are deposited on the collector, thus forming a non-woven and interconnected fabric. The process is conducted at room temperature with atmosphere conditions<sup>21</sup>.

## **2.2 The History of Electrospinning**

Electrospinning technique is based on observations of physical phenomena occurred very long time ago. In fact, in XVI century Sir William Gilbert described for the first time the behavior of a liquid exposed to electrostatic forces: he observed that when a suitably electrically charged piece of amber was brought near a droplet of water it would form a

cone shape and small droplets would be ejected from the tip of the cone. This was the first recorded observation of what will be later called “electrospraying”.

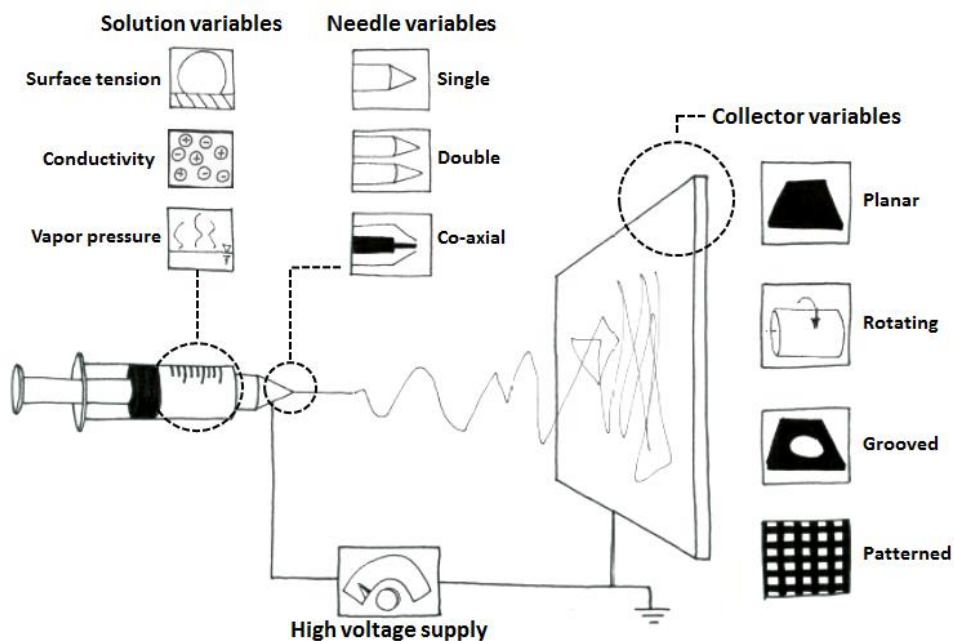


Fig. 1.2: Electrospinning setup scheme with indication of possible variables as example.

In 1745, Bose created an aerosol spray through the application of a high potential to a liquid at the end of a glass capillary tube. In 1882, Lord Rayleigh calculated the maximum amount of charge a drop can hold before electrical forces overcome its surface tension<sup>22</sup>.

The first patents about electrospinning date back to 1902 by J.F. Cooley and W.J. Morton<sup>20</sup>, and over one hundred years more than 200 polymers have been electrospun. In 1917 John Zeleny described and photographed electrospaying phenomena, and was the first to attempt to mathematically model the behavior of fluids under electrostatic forces<sup>6</sup>.

Developments toward commercialization were made by Anton Formhals in 1934-44, and described in a sequence of patents for the fabrication of textile yarns<sup>20</sup>. In 1938 N.D Rozenblum and I.V Petryanov-Sokolov generated electrospun fibers as smoke filter materials for gas masks, which led to the establishment of a factory<sup>6</sup>. Between 1964 and 1969 Sir Geoffrey Ingram Taylor produced the theoretical background of electrospinning: he analyzed and mathematically modelled the shape of a droplet that is deformed by an

electric field<sup>22</sup>; this characteristic droplet shape is now known as the Taylor cone. Since 1980s electrospinning process has gained new attention because of the strong interest in nanotechnology field.

In the early 1990s several research groups (notably that of Reneker who popularized the name electrospinning for the process<sup>21-22</sup>) demonstrated that many organic polymers could be electrospun into nanofibers. More recently, efforts have focused also on the comprehension and the modeling of electrostatic and fluidodynamic forces involved in the process<sup>23-25</sup>.

### **2.3 Electrospinning process**

A stable electrospinning process can be divided into four distinct regimes or zones<sup>22</sup> (Fig. 1.3).

Region I – Taylor cone: in the first region, the jet emerges from the solution droplet. The geometry of the jet near the base is a tapered cone, which results from a combination of charge repulsion and surface tension. When a strong enough electric field is applied at the liquid surface, it produces a force that allows a jet of liquid ejection from the surface. Electrical conductivity of polymer solutions, in particular, is high enough to supply the small currents that are required for the electrospinning. In electrospinning, initiation and maintenance of a stable jet are essential steps which have to be carefully considered.

Region II – Jet: beyond the base, electrical stress accelerates polymer solution towards the grounded collector. The electrical forces which stretch the fiber are resisted by the elongational viscosity of the jet. The forces accelerating the polymer in the solution are mediated by the transfer through the viscoelastic jet, in which the viscoelastic parameters are changing at the same time, as the solvent is evaporating from the jet and the temperature of the jet changes. The charges in the jet carry the liquid polymer from the reservoir towards the collector, in an attempt to close the circuit.

The speed of the solution jet increases as it travels away from the needle tip and for increasing applied voltage; estimated values using a high-speed camera or a laser doppler velocimetry are about 0.5-5 m/s.



Region III – Whipping jet: the solution jet ejected from the Taylor cone will remain stable for a certain distance, depending on the solution properties and electrical configuration; in this region the jet axis is parallel to the flow direction. As the jet progresses toward the collector, a bending perturbation – due to Coulomb forces – occurs and accelerates rapidly, causing the jet to form an irregular coil with many turns, which expands in diameter as the jet continues to elongate in response to the Coulomb repulsion of the charge. The trajectory of each short segment of the coil is roughly perpendicular to its axis. Moreover, the effect of solvent evaporation has to be considered. Therefore, both the elongation due to the electric field and the evaporation thin the jet.

Region IV - Collection: finally, the fiber remained after solvent evaporation can be collected on a metal screen. For polymers dissolved in non-volatile solvents, an appropriate liquid bath can be used as collector in order to remove the solvent and solidify the fiber.

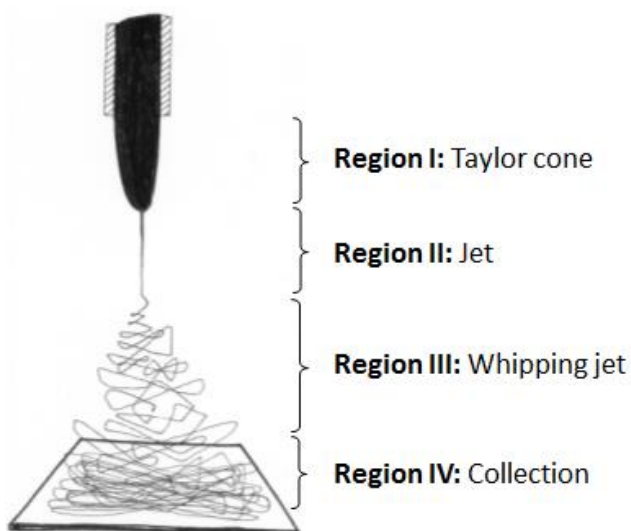


Fig. 1.3: Four regions of ES process: (I) Taylor cone, (II) jet, (III) whipping jet, and (IV) collection of the fibers.

## 2.4 Effect of ES parameters

ES is a simple technique but there are various parameters that significantly affect fiber dimensions, orientation and morphology; by proper tuning of these parameters, is therefore possible to obtain nanofibers with desired morphology and diameter<sup>21</sup>: 1)

solution properties including viscosity, conductivity, surface tension, concentration and molecular weight of the polymer; 2) processing parameters including flow rate, electric field strength, needle-to-collector distance, collector geometry; 3) ambient parameters including temperature, humidity and air flow.

In particular, from the physics under ES process described above, the influence of some variables can be deduced:

1) Solution properties

- a. **Concentration:** solution concentration should be in an optimal range, as for low concentrations beads and not fibers are formed, while at high concentrations the process stability is hindered because of the impossibility to maintain a continuous flow of the solution at the tip of the spinneret<sup>26</sup>. Within the optimal concentration range, researchers found out that a direct correlation between concentration and fiber dimension exists<sup>27</sup>.
- b. **Molecular weight:** molecular weight of the polymer influences rheological and electrical properties of the solution, such as viscosity and conductivity. It has been observed that too low molecular weight solutions cause beads formation, while high molecular weight solutions produce fibers with larger average diameters<sup>28-29</sup>. This derives from the fact that polymer molecular weight greatly affects the number of chain entanglements in a solution, that play an important role in ES process stability.
- c. **Viscosity:** solution viscosity plays an important role in determining fiber size and morphology. In fact, for solutions with low viscosity, surface tension is the dominant force and no continuous fiber formation is possible, thus resulting in bead or beaded-fiber formation. On the contrary, for very high viscosity values it is difficult to have jet ejection from the solution droplet. An optimal viscosity value is therefore necessary; depending on different polymer-solvent combinations, the optimal range can vary between 1 to 215 poise<sup>21, 30-31</sup>. Viscosity, polymer concentration and molecular weight are correlated to each other.

- d. **Surface tension:** surface tension of the solution is related to the solvent composition; when surface tension is too high, jet instability and generation of sprayed droplets occur, thus inhibiting ES process<sup>32-33</sup>. By reducing the surface tension of the solution, fibers without beads can be obtained.
- e. **Conductivity:** solution conductivity is mostly related to the polymer type, the solvent used and the presence of ionisable salts. If solution conductivity is too low, the jet is not sufficiently elongated by electrical force to produce fibers, and beads are usually obtained. Anyway, highly conductive solutions are unstable when a strong electric field is applied, thus forming fibers with broad diameter distribution<sup>34</sup>. Therefore, an optimal conductivity range for fiber formation is necessary; within this range, an increase of solution conductivity determines the decrease in fiber diameter<sup>30</sup>.

## 2) Processing parameters

- a. **Applied voltage:** electric field strength is a fundamental parameter in ES process, as fiber formation occurs only if the voltage applied to the solution is above a threshold value. Within a certain range, an increase of the voltage increases electrostatic repulsive forces, which determines a decreasing of fiber dimensions<sup>35</sup>.
- b. **Flow rate:** the flow rate is also a fundamental parameter as it influences jet velocity and material transfer rate; in particular, higher flow rates usually increase fiber diameter<sup>36</sup>.
- c. **Tip-to-collector distance:** it has been reported that if needle and collector are too close or too far from each other, bead formation occurs<sup>37-38</sup>. Furthermore, it is important that electrospun fibers collected are dry from the solvent used; thus, an adequate distance between the tip and the collector is necessary to obtain complete solvent evaporation.
- d. **Types of collector:** the collector is used as conductive substrate where fibers are deposited. The most popular collector is metal plate, but also other materials can be used, such as conductive paper, wire mesh, pin, parallel bars,

rotating cylinder or wheel, and bath of liquid that is non-solvent for the polymer spun<sup>39-42</sup>. Furthermore, by varying collector geometry it is possible to obtain orientation and patterning of the fibers: for example, rotating mandrel or disc allow the deposition of aligned nanofibers<sup>31, 42</sup>.

### 3) Environmental parameters

- a. **Temperature:** an increase in temperature causes a decrease in solution viscosity, thus usually decreasing fiber diameter<sup>43</sup>. Moreover, the solvent evaporation rate increases with increasing temperature.
- b. **Relative humidity:** the effect of relative humidity on ES process is not simple and easily predictable, and it varies a lot for different polymer solutions. Generally, very low humidity values cause fast evaporation of volatile solvents, thus determining tip clog after few minutes<sup>30</sup>. Another effect related to humidity is the appearance of pores on fiber surface, usually related to increasing humidity values<sup>44</sup>.

## 2.5 Non-conventional electrospinning techniques

As already remarked, versatility of ES process is one of its major advantages and in the past few years this interesting ES ability has allowed the birth of novel branches derived from the nanotechnology. Different structures of nanofibers, such as core-shell, bicomponent, hollow and porous can be obtained by using special spinnerets or by playing with solvent type and ambient conditions<sup>45</sup>.

**Coaxial ES** or **core-shell ES** was developed about ten years ago and it became extensively studied in many different fields such as drug delivery and nanofluidics<sup>46</sup>. In fact, with this technology it is possible to impart specific functional properties onto the surface of the nanofibers (shell solution), while keeping the intrinsic properties of it (core solution). Furthermore, it allows encapsulation in the core or wrapping as a shell of non-spinnable polymers or non-polymeric materials. Core-shell fibers are also attractive in regenerative medicine field, as it is possible to make nanofibers with better cytocompatible properties as cell scaffolds, or to incorporate drug or bioactive agents in the core solution thus

controlling the release rate and protecting them from harsh solvents used for the shell<sup>20</sup>. The process is very similar to traditional ES one: two different liquids are delivered with individual syringe pumps and flow through a specific core-shell needle with two separated and concentrically aligned nozzles; usually the outer liquid is a solution and forms the shell, while either a polymeric solution or a small molecule liquid is filled in the inner capillary (core). The needle is connected to high voltage power supply; when the electric field is strong enough, the composite drop is transformed in a composite Taylor cone and a compound jet is formed, which subsequently undergoes to electrically-driven bending instability characteristic of the ordinary ES process. Thus the core-shell jet solidifies and core-shell fibers are formed on the collector<sup>46</sup>. Anyway, using core-shell needle does not imply formation of core-shell fibers as many intricate physical processes are involved in the process, and there is still no adequate full model of core-shell jet bending driven by electrical force. For example, the flow rate of the two components affects the stability of the jet and influences the shell thickness. Other parameters, such as immiscibility, viscosity and conductivity of the solvents used for core and shell phases also play a crucial role in determining the uniform formation of core-shell fibers. In particular, both miscible and immiscible polymer blends have been successfully electrospun into core-shell nanofibers, but for miscible fluids low interfacial tension between the two liquids is required<sup>47</sup>.

The same ES setup for fabricating core-shell nanofibers can be used to produce **hollow fibers**, if the core material is dissolved with a selective solvent at the end of the process. It has been demonstrated that hollow fibers of composites, ceramic, and polymers can be obtained by electrospinning two immiscible liquids through a coaxial spinneret, choosing the right solvent and controlling the heating rate<sup>20,48</sup>. Furthermore, by modifying the core liquid, it is possible to produce hollow nanofibers filled with different functional components (e.g. fluorescent dye, iron oxide)<sup>49</sup>. Tubular nanostructures can be particularly useful in catalysis, fluidics, purification, separation, gas storage, energy conversion, drug release and environmental protection.

Other efforts have been made to fabricate core-shell nanofibers without the use of a coaxial spinneret; this is possible when an emulsion of two polymer solutions is used as

working liquid (**emulsion ES**). The jet is generated from the emulsion droplet at the tip of an ordinary single-nozzle spinneret, and stretched into fibers. Usually, the dispersed phase in the emulsion moves towards the core of the fiber, and the continuous phase becomes the shell<sup>50</sup>. However, emulsion ES does not always result in core-shell fibers, but also fibers with dispersed phase embedded as separate spots are obtained<sup>46</sup>. Both water-in-oil and oil-in-water emulsions can be spun, according to the specific application<sup>51</sup>. The main application of emulsion ES is in drug delivery field; for example, water-in-oil emulsion ES is used for the encapsulation of hydrophilic drug or bioactive molecules, in order to avoid burst release and preserve molecule activity from harsh organic solvents<sup>52</sup>. In fact, initial release can be reduced by adjusting aqueous to organic phase ratio. Furthermore, this technique is also used to spin insoluble compounds, that can be mixed with solutions of different polymers. Usually, apart from suitable solvents, a surfactant or emulsifying agent is also necessary to lower the surface tension and increase emulsion stability, thus avoiding agglomeration of the drug which can cause its migration on the surface of electrospun fibers, resulting in an unwanted burst release<sup>53</sup>. Emulsion ES is a relatively easy technique, as it needs a simpler set-up than coaxial ES which requires two concentric needles, and provides a good encapsulation of bioactive molecules, favoring their sustained release. The high versatility of ES allows also the production of **porous fibers**, very interesting because of their high surface area for different applications: filtration, fuel cell, catalysis, tissue engineering and drug delivery<sup>20</sup>. Porous nanofibers can be obtained by choosing particular solvents or solvent systems, by controlling humidity conditions, or by using polymer mixtures. For example, one possible method is based on phase separation into polymer-rich and polymer-poor regions; after solvent evaporation, pores can be formed in the polymer-poor regions. Another strategy is to carry out the ES in a very humid environment in order to favor jet cooling and condensation, and precipitation of tiny water droplets onto the jet. These droplets will subsequently form pores on the fiber surface<sup>50</sup>. Finally, another way to obtain porous fibers is by selective dissolution: a mixture of immiscible polymers is electrospun in the same solvent; porous nanofibers are then formed by removing one of the two polymers using a specific solvent<sup>45</sup>.

In the last years, several authors have focused their attention in developing new forms of ES systems where, instead of a single jet formed at the needle tip, multiple jets are contemporary formed. The process is named “**needleless**” ES, and it is potentially more efficient, as it avoids the use of capillaries and needles and their inherently related limits, thus allowing the production of greater amount of fibers<sup>54</sup>. The spinnerets used in this case can be rotating cylinders, balls, and coils, in which the jets are ejected from the spinneret surfaces, or stationary wire spinnerets. For example, the commercial equipment Elmarco Nanospider™ consists of a cylindrical spinneret rotating on the surface of the solution bath to be spun. The multiple jets generated on the spinnerets form fibers that are collected on a moving belt used as collector, which allows rapid coating of big substrates<sup>55</sup>. Needleless ES system has better productivity compared to single needle solution and improved fiber deposition in contrast to multi-needle ES, because of the reduction in mutual fiber repulsion.

### **3. Electrospinning of natural polymers**

ES of natural polymers is extremely advantageous for applications in tissue engineering, wound healing and drug delivery. In fact, natural polymer nanofibers can mimic properties and composition of natural ECM, and biopolymers also have specific binding sequences (e.g. RGD for proteins) that are recognized by the cells.

However, with respect to synthetic polymers, their processability by ES is poor and the procedure appears more challenging and less versatile<sup>9,20</sup>. Indeed, natural polymers usually possess a stable three-dimensional structure, due to intra-molecular weak bonding, and, in some cases, their bioactivity strictly depends on their native structure<sup>9</sup>. Therefore, for ES purposes it is necessary to find an adequate solvent that can solubilize the polymer without compromising its integrity; it is not possible to predict how much the process and the solvent preserve or alter the native structure of biomolecules, so sometimes molecular structure after ES is studied with specific characterization techniques (e.g. vibrational spectroscopy, circular dichroism spectroscopy, thermal analysis<sup>6,8</sup>). However, in latest

years several conflicting results have been reported in literature concerning structural and functional properties of biomolecule electrospun fibers<sup>56-57</sup>.

Furthermore, rigidity of the molecule hinders its unraveling along the ES jet axis, thus resulting in a solution which lacks the viscoelastic properties essential for a stable process<sup>56</sup>. Finally, as the solvents used are usually organic and eventual residues in the membrane are potentially harmful for cell interaction, high volatility properties are desired<sup>8</sup>.

Other strategies to improve natural polymer processability with ES are the introductions of chemical modifications to improve spinnability, solubility/non-solubility, or blending with synthetic polymers (e.g. PEO, PVA, PLA, PCL)<sup>20</sup>.

The most used solvent for biomolecule ES is hexafluoro-isopropanol (HFIP), as it favors natural polymer solubility by virtue of strong hydrogen-bonding properties and ability to break hydrophobic interactions<sup>6,8</sup>; however, HFIP is toxic and has corrosive nature. In addition, it has been demonstrated that HFIP induces protein denaturation, in particular it increases  $\alpha$ -helical percentage<sup>56,58</sup>. For this reason, new solvents for natural polymer ES, less cytotoxic and causing lower molecular denaturation, are constantly investigated.

Natural polymers are extracted from animal or plant sources; therefore, the composition is not always controlled and tends to vary by batch. This drawback could be solved by using biomolecules synthesized by genetically modified bacteria<sup>8</sup>.

Another characteristic of natural polymers is their intrinsic biodegradability: this represents an advantage as eliminates the need for a second surgical operation to remove the biomaterial implanted. However, degradation kinetics is usually too fast and crosslinking reaction is necessary in order to prolong scaffold stability. Different crosslinking agents have been studied in literature (e.g. glutaraldehyde, formaldehyde, genipin, carbodiimides)<sup>59</sup>. These substances are usually cytotoxic in origin, but after crosslinking treatment residual reagent can be neutralized or eliminated; however, it is always necessary to evaluate if the cytocompatibility and bioactivity of the scaffolds are preserved. As one of the major problems of electrospun scaffolds for tissue engineering applications is the small pore dimension<sup>60</sup> which does not allow cell migration through the membrane,



fast degradation of the matrix can anyway represent an advantage, as bigger pores are formed by the degradation, thus favoring cell penetration.

Natural-origin polymers used for ES can be divided into two major categories: proteins and polysaccharides. **Polysaccharides** can have very different origin: for example, alginate, cellulose and starch have algal or plant origin; chitosan and hyaluronic acid have animal origin.

**Alginate** is an anionic polysaccharide derived from brown seaweed; its chemical structure consists of mannuronic acid and guluronic acid. Alginate has been used for different biomedical applications in different forms (e.g. hydrogel, sponge, microfibers), as it possesses biocompatibility and low toxicity properties, non-immunogenicity and relatively low cost. Although alginate can be easily dissolved in water, electrospinning of this biopolymer is still a challenge due to the lack of chain entanglements caused by the rigid and extended chain conformation in aqueous solution<sup>61</sup>. Nie et al.<sup>62</sup> reported that alginate can be successfully electrospun using glycerol as a co-solvent, as glycerol enhances the entanglement of alginate chains by forming new hydrogen bonds. Another strategy to overcome the poor electrospinnability of alginate is to blend it with water-soluble synthetic polymers such as poly(ethylene oxide) (PEO) and poly(vinyl alcohol) (PVA)<sup>63-64</sup>.

**Cellulose** consists of linked  $\beta$ -D-glucose units and has been of particular interest due to its abundance as a renewable resource, biodegradability, and compatibility with biological systems<sup>61</sup>. Cellulose based materials have been extensively used in the pharmaceutical and biomedical fields, including applications as adsorbent beads, filters, artificial tissue/skin, and protective clothing. However, the processability of cellulose is extremely restricted by its limited solubility in common organic solvents due to strong inter and intra-molecular hydrogen bonds<sup>61</sup>. Solvent systems such as N-methyl morpholine N-oxide/water, lithium chloride/dimethyl acetamide, ionic liquids and ethylene diamine/salt have been investigated to produce electrospun cellulose fibers<sup>65-66</sup>. However, some of these solvents have low volatility, so they cannot completely evaporate during the ES process; furthermore, it is difficult to totally remove lithium or chlorine ions after the ES process.

Alternatively, the synthesis of cellulose derivatives with enhanced solubility to facilitate the ES process, and the possibility to convert these derivatives back to cellulose opened new possibilities to create pure cellulose electrospun fibers. Cellulose derivatives used for electrospinning include cellulose acetate, cellulose triacetate, ethyl cellulose and others<sup>61</sup>. Electrospun cellulose-based nanofiber matrices have been used as affinity or barrier membranes, antimicrobial membranes, membranes for tissue engineering and drug delivery, and membranes for enzyme immobilization<sup>67-69</sup>.

**Chitosan**, a polysaccharide derived from the deacetylation of chitin, is composed of glucosamine and N-acetyl glucosamine, and is obtained from shrimp and crab shells. Chitosan has received particular attention in food, cosmetic, biomedical and pharmaceutical applications due to its biological properties, including biocompatibility, biodegradability, similar structure to glycosaminoglycans in the ECM, hemostatic activity, and anti-bacterial and anti-fungal properties<sup>61</sup>. Because of its polycationic character in acidic aqueous solution due to the many amino groups in its backbone, chitosan is difficult to electrospin; in fact, its polycationic nature excessively increases the surface tension of the solution. High electrical force is thus required to produce electrospun chitosan nanofibers, and particles are often formed during the ES process, likely due to the repulsive forces between ionic groups in the chitosan backbone in acidic solution<sup>70</sup>. However, electrospun fibrous structures were successfully formed by chitosan solutions in aqueous acetic acid solution or by using trifluoroacetic acid (TFA)<sup>38,71</sup>. In fact, TFA destroys strong interactions between the chitosan chains, and its high volatility is advantageous for the rapid solidification of the electrified jet. Chitosan nanofibers can also be fabricated using HFIP as solvent<sup>70</sup>. Unluckily, both TFA and HFIP are environmentally harmful and toxic. Moreover, the resultant chitosan fibers need to be cross-linked to maintain their structural integrity, as they can readily dissolve or swell in aqueous solution. Since the ES of chitosan itself proved to be difficult, chitosan was mixed with other synthetic or natural polymers, such as PEO poly(lactic acid) (PLA), silk fibroin, and collagen<sup>72-75</sup>. As an alternative approach to improve the solubility and electrospinnability of chitosan, several chitosan derivatives, (e.g. hexanoyl chitosan), were also synthesized and electrospun<sup>76</sup>.

**Hyaluronic acid** is a linear polysaccharide consisting of alternating disaccharide units of D-glucuronic acid and N-acetyl-D-glucosamine. HA belongs to the family of glycosaminoglycans (GAGs), being structurally the simplest among them, the only one not covalently associated with a core protein, and non-sulfated one. The molar mass of HA can reach millions of Dalton; such high molar mass and its associated unique viscoelastic and rheological properties predispose HA to play important physiological roles<sup>77</sup>. HA is a main component of the ECM of connective tissues and skin; it can also influence cell proliferation, differentiation, and tissue repair. It has various important biological functions, such as molecular filter, load distribution, but it also plays important roles in embryogenesis, signal transduction and cell motility. Because of excellent biocompatibility and biodegradability, HA has been extensively used in many biomedical applications including ophthalmology, dermatology, tissue engineering, wound dressings, and drug delivery<sup>61</sup>.

Similar to alginate, it is very difficult to electrospin an aqueous HA solution because the unusually high viscosity and surface tension hinder the process. In addition, the strong water retention ability of HA leads to the fusion of electrospun nanofibers on the collector due to the insufficient evaporation of the solvents during ES<sup>77</sup>. The fabrication of HA into nanofibrous membranes from aqueous solution was successfully carried out only after the development of blowing-assisted ES (electro-blowing system), and using a dimethylformamide (DMF)/ water mixture, as DMF significantly decreased the surface tension without changing the viscosity of HA solution<sup>78</sup>. Another strategy adopted to favor HA spinnability has been to use a high temperature (60°C) air flow at the spinneret to facilitate fiber formation<sup>78</sup>. More recently, new solvent systems such as NaOH/DMF or water/formic acid/DMF have proven to be beneficial for fiber formation, as they break strong intra-molecular H bonds thus increasing molecule flexibility and chain entanglements<sup>79-80</sup>. After ES, it is generally necessary to crosslink HA membranes, usually with carbodiimides or in aqueous acidic solutions or vapors<sup>81</sup>.

**Protein** fibers can be considered building blocks of organisms, enabling scaffolding, stabilization, protection, elasticity, and motility at length scales ranging from nanometers

to meters. The great majority of protein-oriented ES studies have involved organic solvents: HFIP, tetrahydrofuran, chloroform, ethanol, DMF, trifluoroacetic acid, dichloromethane, formic acid, and hydrochloric acid<sup>8</sup>. These solvents are necessary to solubilize the proteins and make them spinnable. However, a chief concern of protein ES is the partial or complete and irreversible loss of protein functionality after solubilization. In order to reduce protein denaturation required to obtain spinnability, synthetic polymers have often been blended with proteins and milder solvents have been used<sup>8</sup>.

**Collagen** is the most abundant protein in the human body, it has a typical triple helical structure, and its main function is to provide structural support to tissues; therefore, it is considered as “ideal” scaffold material for tissue engineering. Additionally, collagen is resorbable, has high water affinity, low antigenicity, very good cell compatibility and ability to promote tissue regeneration. This protein has cell adhesion ability in the native ECM, enhancing cell attachment and proliferation through specific interactions between domains in collagen molecules and integrin receptors in the cell membrane (i.e. RGD)<sup>82-83</sup>. The identification of a solvent that suitably dissolves collagen at sufficient concentrations to accomplish ES and the volatility of the solvent for rapid drying where the key issues for ES of collagen. Initially, it has been electrospun in fluorinated solvents (e.g. HFIP, TFE); however, lowering of denaturation temperature and loss of triple helical structure after ES process have been reported<sup>84</sup>. More recently, mixture of PBS/ethanol, and aqueous acetic acid solutions have been used to spin collagen: results showed that the protein is well solubilized and spun, and these solvents lead to a lower denaturation of native molecular structure<sup>85</sup>.

As with other collagenous scaffolds, fabricated as gels or sponges, electrospun collagen lacks mechanical and structural stability upon hydration. In order to increase the strength of electrospun collagen, cross-linking with glutaraldehyde vapors, formaldehyde, carbodiimides, genipin, transglutaminase and epoxy compounds has been evaluated<sup>86</sup>. Another strategy to improve mechanical integrity of the membrane and also enhance collagen spinnability is to spin a blend of collagen and synthetic polymers such as PEO, PLA,

and PCL<sup>8</sup>. In fact, the presence of collagen in a synthetic polymer scaffold is intended to impart biocompatibility and bioactivity.

**Gelatin** is a natural polymer derived from collagen by controlled hydrolysis, and is commonly used for pharmaceutical and medical applications because of its biodegradability, biocompatibility, non-immunogenicity and availability. Gelatin contains RGD-like sequences that promotes cell adhesion and migration<sup>4, 87</sup>.

Gelatin is soluble in water at mild temperature (above 37°C), but its ionizable side chains and strong hydrogen bonding promote aggregation, making ES a challenge. Gelatin nanofibers have been electrospun from organic solvents as HFIP and trifluoroethanol (TFE), as well as formic acid, and acetic acid<sup>27, 87-89</sup>. However, it has been demonstrated that acetic acid and formic acid prevent the partial renaturation of gelatin that occurs during gelling from aqueous solution and implies a partial rearrangement of its structure from random coil to triple helix<sup>27</sup>.

As for collagen, electrospun gelatin matrices immediately dissolve in aqueous environment; therefore, electrospun gelatin is often cross-linked or combined with synthetic polymers in order to maintain a fibrous structure. Several studies have demonstrated the successful effect of different cross-linkers, including 1,6-diisocyanatohexane (HMDI), glutaraldehyde, genipin, and carbodiimide<sup>4</sup>.

**Elastin** is a structural component of ECM in many tissues, and it confers elasticity and recoil to skin, blood vessels, ligaments and intestines. It is a chemically inert, highly insoluble polymer composed of covalently cross-linked molecules of its precursor, tropoelastin, a soluble, non-glycosylated and highly hydrophobic protein<sup>8</sup>. Because of elastin insolubility, tropoelastin or synthetic forms of elastin produced in genetically modified organisms are used in ES. In fact, elastin peptides still retain some important functions, as they influence cell signaling, chemotaxis, proliferation, and protease release via the elastin receptor<sup>4</sup>. Alpha-elastin and tropoelastin have been electrospun using HFIP as only solvent; subsequently analysis on tropoelastin secondary structure revealed that the solvent does not affect protein native form<sup>90</sup>.

As for electrospun collagen, one of the limitations of pure electrospun soluble elastin is its inherently poor mechanical properties. It has also been shown that electrospun elastin dissolves in water instantaneously if uncross-linked<sup>90</sup>; therefore, crosslinking agents such as disuccinimidyl suberate (DSS), glutaraldehyde, EDC and HMDI have been used to stabilize electrospun membranes<sup>8</sup>. Another solution to this problem is to blend elastin with synthetic polymers, which not only help to maintain the structural integrity of the scaffold, but also retains the elastin within the scaffold<sup>4</sup>. Collagen and elastin are often electrospun together to produce tissue engineering scaffolds for vascular graft applications, as they are the two main constituents of native blood vessel<sup>91</sup>. Synthetic polymers have also been used in combination with collagen and elastin to create scaffolds with desirable biological and mechanical properties<sup>92</sup>.

**Fibrinogen** is the precursor of fibrin, that constitutes the natural provisional wound healing matrix; for its physiological role, it appears very interesting as material for fabrication of tissue engineering scaffolds and wound dressings. In fact, it induces cellular interaction and promotes cellular migration, it is easily degradable and non-immunogenic. Furthermore, it has the capacity to bind a wide array of molecules that could be beneficial for tissue regeneration (e.g. different growth factors and cytokines), and contains RGD integrin binding sites which commonly bind fibroblasts and endothelial cells<sup>93</sup>. A variety of solvents have been tried for fibrinogen ES; however, the only solvent system that successfully allowed nanofiber formation is constituted by HFIP/MEM (Minimal Essential Medium)<sup>8</sup>. Similar to other natural polymers, electrospun fibrinogen lacks the mechanical integrity to serve as a tissue engineering scaffold on its own for long periods of time. Therefore, cross-linking of fibrinogen scaffolds has been used to increase mechanical strength and slow degradation rate; common crosslinkers used are glutaraldehyde, EDC and genipin<sup>93</sup>. Another solution is to blend fibrinogen with synthetic polymers, e.g. PDO<sup>94</sup>.

**Silk** is a natural fiber obtained from silkworms and spiders. Fibroin is one of the two protein components of silk, and it has been widely investigated for biomedical applications. In fact, fibroin is biocompatible and slowly biodegradable, it causes minimal inflammatory response when implanted *in vivo* and has excellent mechanical properties, such as high

elasticity, strength and toughness, and resistance to failure in compression<sup>8</sup>. Early tentative of silk fibroin (SF) ES encountered difficulties with protein solubilization and conformational change during processing. SF was first electrospun from HFIP<sup>95</sup>. Then, successfully electrospinning of SF/PEO blends from an aqueous solution have been obtained<sup>96</sup>. Further studies, however, suggested that residual PEO in the SF scaffolds inhibited cell attachment and proliferation as well as adversely affected the mechanical properties of the scaffold. Nowadays, SF is electrospun from formic acid or water<sup>26</sup>; the process is stable and continuous and good fiber morphology can be obtained. Post-ES treatment of scaffolds with methanol can significantly decrease the scaffold rate of degradation.

#### **4. Characterization techniques of electrospun membranes**

In order to evaluate the chemical and physical properties of electrospun membranes, different characterization techniques are commonly used in literature. In particular, for natural biopolymer ES, specific characterization to evaluate the effects of solvent and process on the native structure are of great interest and importance.

Electrospun membranes made of natural polymers are usually characterized with regards to their physical, chemical, mechanical and biological properties; the characterization techniques most commonly used are briefly reported hereafter.

Regarding **physical characterization**, structure and morphology of the fibers are of primary importance, as they also determine physical and mechanical properties of the sample<sup>6</sup>. Geometric properties of nanofibers are usually characterized by various microscopic techniques. The most common and fundamental analysis is by scanning electron microscope (SEM): diameter, morphology (e.g. cross-section shape and surface roughness) and orientation of fibers can be determined. SEM is capable of detecting fiber diameters and morphologies, but the resolution is lower at extreme magnifications. For SEM analysis, there is a requirement for the sample to be electrically conductive, therefore a gold or platinum coating must be applied on the electrospun samples produced. SEM remains the fastest method to observe fibers produced and it requires very small sample

size for its operation<sup>6</sup>. Moreover, elaboration of SEM images can be used to determine matrix porosity or to quantify fiber alignment; for example, fast Fourier transformation is used to convert image data from real space to frequency space, and the distribution of greyscale values is assumed to reflect the degree of fiber alignment in the original image<sup>8</sup>. Another technique widely used for morphological analysis is transmission electron microscopy (TEM), that is particularly useful for analyzing extremely small fibers (<200 nm) and co-axial fiber structure. In general, biological specimens are difficult to image in TEM because of their low contrast; strategies used for increasing the contrast include staining by the addition of heavy atoms both in the polymeric solution before ES or as vapor phase in contact with the electrospun sample.

Atomic force microscopy (AFM) is also used to determine fiber diameter in case of single molecular thickness nanofibers (< 10nm), but accurate measurements become more difficult due to tip convolution. However, AFM is the best instrument to study any type of surface morphology and obtain exact descriptions of the fiber surface<sup>6</sup>.

In addition to fiber dimensions and structure, other important features of nanofibrous matrices are porosity, pore dimensions and density, especially for materials with application in filtration, tissue engineering and drug delivery. For the determination of these characteristics, different techniques have been used in literature, including capillary flow porosimetry, mercury porosimetry, liquid displacement, and SEM<sup>8</sup>. The last method is the simplest and most popular: the area encompassed by adjacent fibers in SEM images is quantified, and eventually normalized with respect to an area used as reference<sup>97</sup>.

When biopolymers, and in particular proteins, are used for ES, it is important to investigate if solubilization and ES process have caused protein denaturation, and if the fibers produced are stable or they need a crosslinking process; for these purposes, Differential Scanning Calorimetry (DSC) has been used by some researchers<sup>6</sup>. Stability of the electrospun membranes in aqueous environment can be further assessed by means of water uptake and mass loss analysis<sup>98</sup>. Usually, mass of the specimen before immersion and after blotting are used to calculate the percentage of medium absorbed or the degradation kinetics of the sample as function of the time.



As for **chemical characterization**, polymer structure within the nanofibers, chemical composition, molecular orientation, and internal molecular interactions have been characterized in different ways.

For example, optical polarizing microscopy has been used not only to visualize fiber morphology, but also to detect a preferred orientation of polymer molecules in the fibers<sup>99</sup>. This is the easiest method to obtain information about the crystallinity of the sample; alternative methods, which need a reference of known crystallinity to measure against, include X-ray diffraction, both wide-angle and small-angle (WAXS and SAXS) and differential scanning calorimetry (DSC)<sup>6</sup>. In particular, for biomolecule electrospun fibers, modifications in crystallinity or in crystal structure of the molecule can provide useful information about its denaturation caused by the solvent or the process<sup>100</sup>. These techniques allow also the characterization of super molecular structure, i.e. macromolecule configuration.

Another technique that can be used to study protein denaturation caused by ES process is Circular Dichroism (CD) spectroscopy, which provides information on protein secondary and tertiary structures in solution<sup>8</sup>. In fact, the very high shear forces acting during the ES process can limit biomolecule physiological folding, while inducing conformational changes (strain-induced crystallization). CD spectrum can be analyzed to provide the content of regular secondary structural features such as  $\alpha$ -helices and  $\beta$ -sheets; for example, fluoroalcohols have been reported to induce an increase in  $\alpha$ -helical conformation in collagen and fibrinogen, and induce transformation from  $\alpha$ -helix to random coil in gelatin<sup>27</sup>. In addition, also FTIR and Raman spectroscopy have been used to study molecular structure of a nanofiber, estimate modifications in secondary structure of proteins after the ES process, and evaluate eventual changes at molecular level. In particular, proteins present common bands in vibrational spectroscopies, related to motion of amidic bonds (i.e. amide I, II, III, and A). Frequency shift or change in intensity of the peaks can be related to modification of protein secondary structure, such as unfolding of helical structure in random coils<sup>8</sup>. Furthermore, as natural polymer membranes often need crosslinking

treatment to improve stability and mechanical properties, presence of new bonds after crosslinking can be investigated by FTIR<sup>6</sup>.

Another technique that can be used to characterize polymer structure in fibers is nuclear magnetic resonance (NMR) spectroscopy. For example, for ES of blend of two polymers, not only can the structure of two materials be detected, but the intermolecular interactions (i.e. hydrogen bonds) can be determined by the use of these methods<sup>8</sup>.

In cases where the knowledge of the elemental composition of fiber surface is required, X-ray photoelectron spectroscopy (XPS) can be utilized. In particular, this technique is useful to investigate core-shell fiber structure or to determine the surface density of polymers in an electrospun blend<sup>101</sup>.

Adequate **mechanical properties** are often fundamental for the electrospun membrane application intended, and they are especially important for a biomedical material. For example, scaffold in tissue engineering must be able to withstand the forces exerted by growing and surrounding tissues or during physiological activities and related biomechanics, e.g. pulsed blood flow. In general, electrospun membranes with randomly deposited fibers have isotropic properties, while membranes obtained using a rotating drum as collector have different properties in different directions according to the fiber orientation<sup>6</sup>. Tensile strength and Young's modulus are only two of the many mechanical parameters that can be defined for electrospun membranes; other parameters are measured depending on the specific application (e.g. compliance and burst pressure for vascular tissue engineering)<sup>8</sup>.

Apart from mechanical characterization of the whole electrospun matrix, researchers have put great interest also in single fiber property determination. With this aim, AFM has been used, as it can accurately apply forces on the nanometer length scale in the picoNewton-to-nanoNewton range<sup>8</sup>. Micromechanical bending tests and nanoindentation are now common techniques, used for the analysis of the bending modulus, tensile strength and elastic modulus of individual electrospun fibers. Although this method has been used successfully for mechanical characterization, there are certain limitations too, such as

uncertainties from the nanoindenter tip shape, the effect of fiber surface curvature and roughness, and the adhesion force between the sample and the indenter.

If the electrospun membrane is intended for biomedical applications, cytocompatibility and biofunctionality are important requirements, that are usually investigated by **biological characterization**. In this regard, the review by Braghirolli et al.<sup>102</sup> gives a complete description of the most used *in vitro* tests for electrospun membrane characterization.

## References

1. Frantz, C.; Stewart, K. M.; Weaver, V. M., The extracellular matrix at a glance. *J Cell Sci* **2010**, *123* (24), 4195-4200.
2. Stevens, M. M.; George, J. H., Exploring and engineering the cell surface interface. *Science* **2005**, *310* (5751), 1135-1138.
3. Fechheimer, M.; Karp, G., Cell and Molecular Biology: Concepts and Experiments. JSTOR: 2000.
4. Sell, S. A.; Wolfe, P. S.; Garg, K.; McCool, J. M.; Rodriguez, I. A.; Bowlin, G. L., The use of natural polymers in tissue engineering: a focus on electrospun extracellular matrix analogues. *Polymers* **2010**, *2* (4), 522-553.
5. Hynes, R. O., Integrins: bidirectional, allosteric signaling machines. *Cell* **2002**, *110* (6), 673-687.
6. Bhardwaj, N.; Kundu, S. C., Electrospinning: a fascinating fiber fabrication technique. *Biotechnology advances* **2010**, *28* (3), 325-347.
7. Han, D.; Cheung, K. C., Biodegradable cell-seeded nanofiber scaffolds for neural repair. *Polymers* **2011**, *3* (4), 1684-1733.
8. Khadka, D. B.; Haynie, D. T., Protein-and peptide-based electrospun nanofibers in medical biomaterials. *Nanomedicine: Nanotechnology, Biology and Medicine* **2012**, *8* (8), 1242-1262.
9. Wang, X.; Ding, B.; Li, B., Biomimetic electrospun nanofibrous structures for tissue engineering. *Materials today* **2013**, *16* (6), 229-241.
10. Nie, Z.; Kumacheva, E., Patterning surfaces with functional polymers. *Nature materials* **2008**, *7* (4), 277-290.
11. Rogina, A., Electrospinning process: Versatile preparation method for biodegradable and natural polymers and biocomposite systems applied in tissue engineering and drug delivery. *Appl Surf Sci* **2014**, *296*, 221-230.
12. Billiet, T.; Gevaert, E.; De Schryver, T.; Cornelissen, M.; Dubrue, P., The 3D printing of gelatin methacrylamide cell-laden tissue-engineered constructs with high cell viability. *Biomaterials* **2014**, *35* (1), 49-62.
13. Lam, C. X. F.; Mo, X.; Teoh, S.-H.; Huttmacher, D., Scaffold development using 3D printing with a starch-based polymer. *Materials Science and Engineering: C* **2002**, *20* (1), 49-56.
14. Duan, B.; Hockaday, L. A.; Kang, K. H.; Butcher, J. T., 3D bioprinting of heterogeneous aortic valve conduits with alginate/gelatin hydrogels. *J Biomed Mater Res A* **2013**, *101* (5), 1255-1264.
15. Zhong, S. P.; Teo, W. E.; Zhu, X.; Beuerman, R.; Ramakrishna, S.; Yung, L. Y. L., Development of a novel collagen-GAG nanofibrous scaffold via electrospinning. *Materials Science and Engineering: C* **2007**, *27* (2), 262-266.
16. O'Brien, F. J.; Harley, B. A.; Yannas, I. V.; Gibson, L., Influence of freezing rate on pore structure in freeze-dried collagen-GAG scaffolds. *Biomaterials* **2004**, *25* (6), 1077-1086.

17. Wu, X.; Liu, Y.; Li, X.; Wen, P.; Zhang, Y.; Long, Y.; Wang, X.; Guo, Y.; Xing, F.; Gao, J., Preparation of aligned porous gelatin scaffolds by unidirectional freeze-drying method. *Acta Biomater* **2010**, *6* (3), 1167-1177.
18. Ma, P. X., Scaffolds for tissue fabrication. *Materials today* **2004**, *7* (5), 30-40.
19. Lu, W.; Sun, J.; Jiang, X., Recent advances in electrospinning technology and biomedical applications of electrospun fibers. *Journal of Materials Chemistry B* **2014**, *2* (17), 2369-2380.
20. Greiner, A.; Wendorff, J. H., Electrospinning: a fascinating method for the preparation of ultrathin fibers. *Angewandte Chemie International Edition* **2007**, *46* (30), 5670-5703.
21. Doshi, J.; Reneker, D. H. In *Electrospinning process and applications of electrospun fibers*, Industry Applications Society Annual Meeting, 1993., Conference Record of the 1993 IEEE, IEEE: 1993; pp 1698-1703.
22. Reneker, D. H.; Chun, I., Nanometre diameter fibres of polymer, produced by electrospinning. *Nanotechnology* **1996**, *7* (3), 216.
23. Reneker, D. H.; Yarin, A. L., Electrospinning jets and polymer nanofibers. *Polymer* **2008**, *49* (10), 2387-2425.
24. Spivak, A.; Dzenis, Y.; Reneker, D., A model of steady state jet in the electrospinning process. *Mechanics research communications* **2000**, *27* (1), 37-42.
25. Bellan, L. M.; Craighead, H. G.; Hinestroza, J. P., Direct measurement of fluid velocity in an electrospinning jet using particle image velocimetry. *J Appl Phys* **2007**, *102* (9), 094308.
26. Sukigara, S.; Gandhi, M.; Ayutsede, J.; Micklus, M.; Ko, F., Regeneration of Bombyx mori silk by electrospinning—part 1: processing parameters and geometric properties. *Polymer* **2003**, *44* (19), 5721-5727.
27. Ki, C. S.; Baek, D. H.; Gang, K. D.; Lee, K. H.; Um, I. C.; Park, Y. H., Characterization of gelatin nanofiber prepared from gelatin–formic acid solution. *Polymer* **2005**, *46* (14), 5094-5102.
28. McKee, M. G.; Wilkes, G. L.; Colby, R. H.; Long, T. E., Correlations of solution rheology with electrospun fiber formation of linear and branched polyesters. *Macromolecules* **2004**, *37* (5), 1760-1767.
29. Burger, C.; Hsiao, B. S.; Chu, B., Nanofibrous materials and their applications. *Annu. Rev. Mater. Res.* **2006**, *36*, 333-368.
30. Baumgarten, P. K., Electrostatic spinning of acrylic microfibers. *J Colloid Interf Sci* **1971**, *36* (1), 71-79.
31. Deitzel, J. M.; Kleinmeyer, J.; Harris, D.; Tan, N. B., The effect of processing variables on the morphology of electrospun nanofibers and textiles. *Polymer* **2001**, *42* (1), 261-272.
32. Hohman, M. M.; Shin, M.; Rutledge, G.; Brenner, M. P., Electrospinning and electrically forced jets. I. Stability theory. *Physics of Fluids (1994-present)* **2001**, *13* (8), 2201-2220.
33. Hohman, M. M.; Shin, M.; Rutledge, G.; Brenner, M. P., Electrospinning and electrically forced jets. II. Applications. *Physics of Fluids (1994-present)* **2001**, *13* (8), 2221-2236.

34. Hayati, I.; Bailey, A.; Tadros, T. F., Investigations into the mechanisms of electrohydrodynamic spraying of liquids: I. Effect of electric field and the environment on pendant drops and factors affecting the formation of stable jets and atomization. *J Colloid Interf Sci* **1987**, *117* (1), 205-221.
35. Larrondo, L.; St John Manley, R., Electrostatic fiber spinning from polymer melts. I. Experimental observations on fiber formation and properties. *Journal of Polymer Science: Polymer Physics Edition* **1981**, *19* (6), 909-920.
36. Megelski, S.; Stephens, J. S.; Chase, D. B.; Rabolt, J. F., Micro-and nanostructured surface morphology on electrospun polymer fibers. *Macromolecules* **2002**, *35* (22), 8456-8466.
37. Lee, J. S.; Choi, K. H.; Ghim, H. D.; Kim, S. S.; Chun, D. H.; Kim, H. Y.; Lyoo, W. S., Role of molecular weight of atactic poly (vinyl alcohol)(PVA) in the structure and properties of PVA nanofabric prepared by electrospinning. *J Appl Polym Sci* **2004**, *93* (4), 1638-1646.
38. Geng, X.; Kwon, O.-H.; Jang, J., Electrospinning of chitosan dissolved in concentrated acetic acid solution. *Biomaterials* **2005**, *26* (27), 5427-5432.
39. Wang, X.; Um, I. C.; Fang, D.; Okamoto, A.; Hsiao, B. S.; Chu, B., Formation of water-resistant hyaluronic acid nanofibers by blowing-assisted electro-spinning and non-toxic post treatments. *Polymer* **2005**, *46* (13), 4853-4867.
40. Li, D.; Wang, Y.; Xia, Y., Electrospinning nanofibers as uniaxially aligned arrays and layer-by-layer stacked films. *Adv Mater* **2004**, *16* (4), 361-366.
41. Ki, C. S.; Kim, J. W.; Hyun, J. H.; Lee, K. H.; Hattori, M.; Rah, D. K.; Park, Y. H., Electrospun three-dimensional silk fibroin nanofibrous scaffold. *J Appl Polym Sci* **2007**, *106* (6), 3922-3928.
42. Xu, C.; Inai, R.; Kotaki, M.; Ramakrishna, S., Aligned biodegradable nanofibrous structure: a potential scaffold for blood vessel engineering. *Biomaterials* **2004**, *25* (5), 877-886.
43. Mit-uppatham, C.; Nithitanakul, M.; Supaphol, P., Ultrafine electrospun polyamide-6 fibers: effect of solution conditions on morphology and average fiber diameter. *Macromolecular Chemistry and Physics* **2004**, *205* (17), 2327-2338.
44. Casper, C. L.; Stephens, J. S.; Tassi, N. G.; Chase, D. B.; Rabolt, J. F., Controlling surface morphology of electrospun polystyrene fibers: effect of humidity and molecular weight in the electrospinning process. *Macromolecules* **2004**, *37* (2), 573-578.
45. Khajavi, R.; Abbasipour, M., Electrospinning as a versatile method for fabricating coreshell, hollow and porous nanofibers. *Scientia Iranica* **2012**, *19* (6), 2029-2034.
46. Yarin, A., Coaxial electrospinning and emulsion electrospinning of core-shell fibers. *Polym Advan Technol* **2011**, *22* (3), 310-317.
47. Kurban, Z.; Lovell, A.; Bennington, S. M.; Jenkins, D. W.; Ryan, K. R.; Jones, M. O.; Skipper, N. T.; David, W. I., A solution selection model for coaxial electrospinning and its application to nanostructured hydrogen storage materials. *The Journal of Physical Chemistry C* **2010**, *114* (49), 21201-21213.
48. Li, D.; Xia, Y., Direct fabrication of composite and ceramic hollow nanofibers by electrospinning. *Nano letters* **2004**, *4* (5), 933-938.
49. McCann, J. T.; Li, D.; Xia, Y., Electrospinning of nanofibers with core-sheath, hollow, or porous structures. *J Mater Chem* **2005**, *15* (7), 735-738.

50. Persano, L.; Camposeo, A.; Tekmen, C.; Pisignano, D., Industrial upscaling of electrospinning and applications of polymer nanofibers: a review. *Macromol Mater Eng* **2013**, *298* (5), 504-520.
51. Angeles, M.; Cheng, H. L.; Velankar, S. S., Emulsion electrospinning: composite fibers from drop breakup during electrospinning. *Polym Advan Technol* **2008**, *19* (7), 728-733.
52. Rieger, K. A.; Birch, N. P.; Schiffman, J. D., Designing electrospun nanofiber mats to promote wound healing—a review. *Journal of Materials Chemistry B* **2013**, *1* (36), 4531-4541.
53. Zhang, H.; Zhao, C.; Zhao, Y.; Tang, G.; Yuan, X., Electrospinning of ultrafine core/shell fibers for biomedical applications. *Science China Chemistry* **2010**, *53* (6), 1246-1254.
54. Wang, X.; Niu, H.; Lin, T.; Wang, X., Needleless electrospinning of nanofibers with a conical wire coil. *Polymer Engineering & Science* **2009**, *49* (8), 1582-1586.
55. Holopainen, J.; Penttinen, T.; Santala, E.; Ritala, M., Needleless electrospinning with twisted wire spinneret. *Nanotechnology* **2014**, *26* (2), 025301.
56. Bürck, J.; Heissler, S.; Geckle, U.; Ardakani, M. F.; Schneider, R.; Ulrich, A. S.; Kazanci, M., Resemblance of electrospun collagen nanofibers to their native structure. *Langmuir* **2013**, *29* (5), 1562-1572.
57. Jha, B. S.; Ayres, C. E.; Bowman, J. R.; Telemeco, T. A.; Sell, S. A.; Bowlin, G. L.; Simpson, D. G., Electrospun collagen: a tissue engineering scaffold with unique functional properties in a wide variety of applications. *Journal of Nanomaterials* **2011**, *2011*, 7.
58. Liu, T.; Teng, W. K.; Chan, B. P.; Chew, S. Y., Photochemical crosslinked electrospun collagen nanofibers: synthesis, characterization and neural stem cell interactions. *J Biomed Mater Res A* **2010**, *95* (1), 276-282.
59. Reddy, N.; Reddy, R.; Jiang, Q., Crosslinking biopolymers for biomedical applications. *Trends in biotechnology* **2015**, *33* (6), 362-369.
60. Kim, T. G.; Chung, H. J.; Park, T. G., Macroporous and nanofibrous hyaluronic acid/collagen hybrid scaffold fabricated by concurrent electrospinning and deposition/leaching of salt particles. *Acta Biomater* **2008**, *4* (6), 1611-1619.
61. Lee, K. Y.; Jeong, L.; Kang, Y. O.; Lee, S. J.; Park, W. H., Electrospinning of polysaccharides for regenerative medicine. *Adv Drug Deliver Rev* **2009**, *61* (12), 1020-1032.
62. Nie, H.; He, A.; Zheng, J.; Xu, S.; Li, J.; Han, C. C., Effects of chain conformation and entanglement on the electrospinning of pure alginate. *Biomacromolecules* **2008**, *9* (5), 1362-1365.
63. Lu, J.-W.; Zhu, Y.-L.; Guo, Z.-X.; Hu, P.; Yu, J., Electrospinning of sodium alginate with poly (ethylene oxide). *Polymer* **2006**, *47* (23), 8026-8031.
64. Bhattarai, N.; Li, Z.; Edmondson, D.; Zhang, M., Alginate-based nanofibrous scaffolds: Structural, mechanical, and biological properties. *Adv Mater* **2006**, *18* (11), 1463-1467.
65. Zhang, L.; Menkhaus, T. J.; Fong, H., Fabrication and bioseparation studies of adsorptive membranes/felts made from electrospun cellulose acetate nanofibers. *Journal of Membrane Science* **2008**, *319* (1), 176-184.

66. Kim, C. W.; Frey, M. W.; Marquez, M.; Joo, Y. L., Preparation of submicron-scale, electrospun cellulose fibers via direct dissolution. *Journal of Polymer Science Part B: Polymer Physics* **2005**, *43* (13), 1673-1683.
67. Son, W. K.; Youk, J. H.; Lee, T. S.; Park, W. H., Preparation of antimicrobial ultrafine cellulose acetate fibers with silver nanoparticles. *Macromolecular rapid communications* **2004**, *25* (18), 1632-1637.
68. Son, W. K.; Youk, J. H.; Park, W. H., Preparation of ultrafine oxidized cellulose mats via electrospinning. *Biomacromolecules* **2004**, *5* (1), 197-201.
69. Wang, Y.; Hsieh, Y. L., Enzyme immobilization to ultra-fine cellulose fibers via amphiphilic polyethylene glycol spacers. *Journal of Polymer Science Part A: Polymer Chemistry* **2004**, *42* (17), 4289-4299.
70. Min, B.-M.; Lee, S. W.; Lim, J. N.; You, Y.; Lee, T. S.; Kang, P. H.; Park, W. H., Chitin and chitosan nanofibers: electrospinning of chitin and deacetylation of chitin nanofibers. *Polymer* **2004**, *45* (21), 7137-7142.
71. Ohkawa, K.; Cha, D.; Kim, H.; Nishida, A.; Yamamoto, H., Electrospinning of chitosan. *Macromolecular rapid communications* **2004**, *25* (18), 1600-1605.
72. Duan, B.; Dong, C.; Yuan, X.; Yao, K., Electrospinning of chitosan solutions in acetic acid with poly (ethylene oxide). *Journal of Biomaterials Science, Polymer Edition* **2004**, *15* (6), 797-811.
73. Li, L.; Hsieh, Y.-L., Chitosan bicomponent nanofibers and nanoporous fibers. *Carbohydrate research* **2006**, *341* (3), 374-381.
74. Duan, B.; Yuan, X.; Zhu, Y.; Zhang, Y.; Li, X.; Zhang, Y.; Yao, K., A nanofibrous composite membrane of PLGA–chitosan/PVA prepared by electrospinning. *Eur Polym J* **2006**, *42* (9), 2013-2022.
75. Chen, Z.; Mo, X.; He, C.; Wang, H., Intermolecular interactions in electrospun collagen–chitosan complex nanofibers. *Carbohydrate Polymers* **2008**, *72* (3), 410-418.
76. Neamark, A.; Rujiravanit, R.; Supaphol, P., Electrospinning of hexanoyl chitosan. *Carbohydrate Polymers* **2006**, *66* (3), 298-305.
77. Li, J.; He, A.; Han, C. C.; Fang, D.; Hsiao, B. S.; Chu, B., Electrospinning of hyaluronic acid (HA) and HA/gelatin blends. *Macromolecular rapid communications* **2006**, *27* (2), 114-120.
78. Um, I. C.; Fang, D.; Hsiao, B. S.; Okamoto, A.; Chu, B., Electro-spinning and electro-blowing of hyaluronic acid. *Biomacromolecules* **2004**, *5* (4), 1428-1436.
79. Brenner, E. K.; Schiffman, J. D.; Thompson, E. A.; Toth, L. J.; Schauer, C. L., Electrospinning of hyaluronic acid nanofibers from aqueous ammonium solutions. *Carbohydrate Polymers* **2012**, *87* (1), 926-929.
80. Liu, Y.; Ma, G.; Fang, D.; Xu, J.; Zhang, H.; Nie, J., Effects of solution properties and electric field on the electrospinning of hyaluronic acid. *Carbohydrate Polymers* **2011**, *83* (2), 1011-1015.
81. Xu, S.; Li, J.; He, A.; Liu, W.; Jiang, X.; Zheng, J.; Han, C. C.; Hsiao, B. S.; Chu, B.; Fang, D., Chemical crosslinking and biophysical properties of electrospun hyaluronic acid based ultra-thin fibrous membranes. *Polymer* **2009**, *50* (15), 3762-3769.
82. Shoulders, M. D.; Raines, R. T., Collagen structure and stability. *Annual review of biochemistry* **2009**, *78*, 929.



83. Fratzl, P., *Collagen: structure and mechanics*. Springer Science & Business Media: 2008.
84. Zeugolis, D. I.; Khew, S. T.; Yew, E. S.; Ekaputra, A. K.; Tong, Y. W.; Yung, L.-Y. L.; Hutmacher, D. W.; Sheppard, C.; Raghunath, M., Electro-spinning of pure collagen nano-fibres—just an expensive way to make gelatin? *Biomaterials* **2008**, *29* (15), 2293-2305.
85. Dong, B.; Arnoult, O.; Smith, M. E.; Wnek, G. E., Electrospinning of collagen nanofiber scaffolds from benign solvents. *Macromolecular rapid communications* **2009**, *30* (7), 539-542.
86. Jiang, Q.; Reddy, N.; Zhang, S.; Roscioli, N.; Yang, Y., Water-stable electrospun collagen fibers from a non-toxic solvent and crosslinking system. *J Biomed Mater Res A* **2013**, *101* (5), 1237-1247.
87. Heydarkhan-Hagvall, S.; Schenke-Layland, K.; Dhanasopon, A. P.; Rofail, F.; Smith, H.; Wu, B. M.; Shemin, R.; Beygui, R. E.; MacLellan, W. R., Three-dimensional electrospun ECM-based hybrid scaffolds for cardiovascular tissue engineering. *Biomaterials* **2008**, *29* (19), 2907-2914.
88. Powell, H.; Boyce, S., Fiber density of electrospun gelatin scaffolds regulates morphogenesis of dermal–epidermal skin substitutes. *J Biomed Mater Res A* **2008**, *84* (4), 1078-1086.
89. Okutan, N.; Terzi, P.; Altay, F., Affecting parameters on electrospinning process and characterization of electrospun gelatin nanofibers. *Food Hydrocolloids* **2014**, *39*, 19-26.
90. Nivison-Smith, L.; Rnjak, J.; Weiss, A. S., Synthetic human elastin microfibers: stable cross-linked tropoelastin and cell interactive constructs for tissue engineering applications. *Acta Biomater* **2010**, *6* (2), 354-359.
91. Boland, E. D.; Matthews, J. A.; Pawlowski, K. J.; Simpson, D. G.; Wnek, G. E.; Bowlin, G. L., Electrospinning collagen and elastin: preliminary vascular tissue engineering. *Front Biosci* **2004**, *9* (1422), e32.
92. Buttafoco, L.; Kolkman, N.; Engbers-Buijtenhuijs, P.; Poot, A.; Dijkstra, P.; Vermes, I.; Feijen, J., Electrospinning of collagen and elastin for tissue engineering applications. *Biomaterials* **2006**, *27* (5), 724-734.
93. Sell, S. A.; Francis, M. P.; Garg, K.; McClure, M. J.; Simpson, D. G.; Bowlin, G. L., Cross-linking methods of electrospun fibrinogen scaffolds for tissue engineering applications. *Biomedical Materials* **2008**, *3* (4), 045001.
94. McManus, M. C.; Sell, S. A.; Bowen, W. C.; Koo, H. P.; Simpson, D. G.; Bowlin, G. L., Electrospun fibrinogen-polydioxanone composite matrix: potential for in situ urologic tissue engineering. *J Eng Fiber Fabr* **2008**, *3* (2), 12-21.
95. Cappello, J.; McGrath, K. P., Spinning of protein polymer fibers. *Silk polymers* **1994**, *544*, 311-327.
96. Jin, H.-J.; Fridrikh, S. V.; Rutledge, G. C.; Kaplan, D. L., Electrospinning Bombyx mori silk with poly (ethylene oxide). *Biomacromolecules* **2002**, *3* (6), 1233-1239.
97. Ayres, C.; Bowlin, G. L.; Henderson, S. C.; Taylor, L.; Shultz, J.; Alexander, J.; Telemeco, T. A.; Simpson, D. G., Modulation of anisotropy in electrospun tissue-engineering scaffolds: analysis of fiber alignment by the fast Fourier transform. *Biomaterials* **2006**, *27* (32), 5524-5534.

98. Zhang, X. H.; Baughman, C. B.; Kaplan, D. L., In vitro evaluation of electrospun silk fibroin scaffolds for vascular cell growth. *Biomaterials* **2008**, *29* (14), 2217-2227.
99. Srinivasan, G.; Reneker, D. H., Structure and morphology of small diameter electrospun aramid fibers. *Polym Int* **1995**, *36* (2), 195-201.
100. Kołbuk, D.; Sajkiewicz, P.; Maniura-Weber, K.; Fortunato, G., Structure and morphology of electrospun polycaprolactone/gelatine nanofibres. *Eur Polym J* **2013**, *49* (8), 2052-2061.
101. Zhang, Y.; Huang, Z.-M.; Xu, X.; Lim, C. T.; Ramakrishna, S., Preparation of core-shell structured PCL-r-gelatin bi-component nanofibers by coaxial electrospinning. *Chemistry of Materials* **2004**, *16* (18), 3406-3409.
102. Braghirolli, D. I.; Steffens, D.; Pranke, P., Electrospinning for regenerative medicine: a review of the main topics. *Drug discovery today* **2014**, *19* (6), 743-753.
103. Nuansing, W. Electrospinning of Biomolecules. Universidad del País Vasco, 2014.

# Aim of the thesis

---

The loss of tissue function due to injury, disease or aging is currently an unresolved problem with high impact on quality of life and large social and economic costs<sup>102</sup>. Tissue Engineering (TE) appears as the most promising alternative for restoration of damaged tissues and organs. However, some open problems remain. In particular, regarding the scaffold component, numerous studies aimed to reproduce the architecture of ECM, whose complex nanoscale fiber structure is the natural scaffold where cells adhere, proliferate, and migrate. Moreover, ECM chemical composition is a heterogeneous mixture of proteins, polysaccharides, and glycoproteins. Therefore, mimicry of ECM network and composition is a challenging goal.

In this regard, ES appears as a powerful technique for nanofiber production, as it is simple, allows great flexibility and control over nanofiber outcome, and has low operating cost. Moreover, it seems to be the only technique that has the possibility to scale up the process to an industrial scale<sup>103</sup>. The combination of ES technique with biopolymers, which are the natural component of ECM, has tremendous potential for the fabrication of biocompatible scaffold for TE, and is therefore extensively studied. However, ES of biopolymers appears challenging because of their solubility issues in solvents suitable for the process, possible charged nature, batch-to-batch variation, and lack of viscoelastic properties. The solvent most commonly used for biopolymer ES is HFIP, however it is toxic, corrosive, and extremely expensive (260€ / 100 grams), thus representing a limitation for possible electrospun membrane production on a large scale.

In this scenario, the objectives of this thesis are as follows:

- 1) investigating alternative solvents to HFIP for ES solution, with special attention on toxicity and cost;
- 2) studying the effect of the solvent and the process on biopolymer native structure with detailed analyses from nano to macro scale;
- 3) evaluating ES process stability and defining highly reproducible solution and process parameters;

- 4) identifying suitable biopolymer blends with tunable compositions for specific applications in TE field;
- 5) comparing the most commonly used crosslinking methods for natural polymers (i.e. dehydrothermal treatment, UV radiation, glutaraldehyde, genipin, carbodiimide) in order to evaluate their efficacy in preserving electrospun morphology while providing adequate membrane stability.

In particular, in Chapter 2 the most abundant biopolymers present in ECM, i.e. collagen (or its derivative gelatin), elastin and hyaluronic acid, are employed and mixed together in order to mimic physiological matrix composition; optimal blend composition for ES process, in terms of process reproducibility and adequate fiber morphology, is determined in order to produce scaffolds with promising application in soft tissue engineering.

In Chapter 3 another biopolymer, which has a fundamental role in physiological wound healing process and therefore appears extremely interesting for TE applications, is studied: fibrinogen. The aim of this section consists in finding a strategy to obtain stable fibrinogen ES without employing fluorinated solvents commonly used in literature, in order to obtain cytocompatible electrospun scaffolds.

In the last Chapter, experimental activity focuses on the fabrication of a natural, drug-loaded membrane by means of core-shell ES technique with potential application as wound dressing.

## Chapter 2 – Electrospinning of gelatin-based blends

---

---

*Collagen/gelatin, elastin and hyaluronic acid were blended and electrospun to produce nanostructured membranes able to mimic the ECM structure and composition. In order to avoid instantaneous degradation of the matrices, different crosslinking methods were investigated. In this regard, dehydrothermal treatment and glutaraldehyde vapor proved to be effective in increase matrix stability.*

---

# 1. Introduction

Gelatin is a biopolymer derived from partial hydrolysis of native collagen and due to its biological origin, non-immunogenicity, biodegradability and biocompatibility it has been widely used in the pharmaceutical and medical fields<sup>1-3</sup>. Its commercial availability at relatively low cost paved the way for its application in the biomedical area, such as carrier for drug delivery<sup>4</sup>, sealants for vascular prostheses<sup>5</sup> or dressings for wound healing<sup>6</sup>. Gelatin has good film-forming attitude and accordingly it was firstly used in the form of films<sup>7</sup>. In the biomedical field, gelatin nanofibers can be potentially useful in developing biomimicking artificial extra-cellular matrix (ECM) for engineering tissues, and dressings for wound healing<sup>8</sup>. However, this material is poor in fiber processing and only electrospinning (ES) technology proved to be successful into nanoscale fibers production<sup>9</sup>.

A mandatory requirement in this case is the selection of a proper solvent to precisely tune physical parameters fundamental for the process, in order to produce gelatin fibers with nanoscale features. In this regard solvents such as fluorinated alcohol (e.g. hexafluoroisopropanol, HFIP, and trifluoroethanol, TFE)<sup>6, 8</sup>, acetic acid<sup>10</sup>, and formic acid<sup>3</sup> have been used. Electrospun gelatin membranes with nanofiber structure are very promising in a variety of applications, especially in conditions where surface area is highly required. Nonetheless gelatin electrospun matrices are water soluble and mechanically weak and these drawbacks limit their applications<sup>11-12</sup>. For this reason, the attention moved in defining efficient crosslinking strategies to enhance fiber stability and in particular to the development of crosslinking treatment to improve both *in vivo* stability and thermomechanical performance of the nanofibrous membranes<sup>7</sup>. In the literature, several physical and chemical methods have been reported for crosslinking gelatin. Physical methods include dehydrothermal treatment and UV-irradiation<sup>13</sup> whereas the use of chemicals include formaldehyde, glutaraldehyde<sup>14</sup>, genipin<sup>15</sup> and carbodiimides<sup>16</sup>. Chemical treatments proved to be more efficient in term of mechanical stability, but with potential drawbacks in term of biocompatibility<sup>5</sup>. Amongst, glutaraldehyde is the most widely used chemical, due to its high efficiency in stabilizing mats<sup>17</sup>. Glutaraldehyde-based

crosslinking structures significantly reduce biodegradation, while preserving biological integrity, strength and flexibility. Glutaraldehyde is also easily available, inexpensive and capable of accomplishing the crosslinking in a relatively short time period<sup>17</sup>. The risk of cytotoxicity can be reduced by lowering the concentration of glutaraldehyde solutions, reducing crosslinking time or through adequate post-treatment prior to usage<sup>7</sup>.

A push forward in the use of gelatin as a material for ES is the possibility to form blends of biopolymers with the intention to modulate some physico-chemical properties of the final outcome<sup>18-19</sup>. In this regard, elastin and hyaluronic acid appear particularly interesting; they are two of the main ECM components of connective tissues, and numerous studies have demonstrated the advantages related to the use of these biopolymers for tissue engineering applications. For example, the presence of elastin in collagen-based scaffolds (non-electrospun) was shown to decrease scaffold stiffness<sup>20</sup>, and enhance angiogenesis and elastic fiber formation<sup>21</sup>. Hyaluronic acid has unique viscoelastic properties, high water retention capacity, good biocompatibility and biodegradability<sup>22</sup>, thus resulting extremely interesting in a wide range of applications, including as components of cosmetics, as drug delivery systems, for wound dressing, and as tissue engineering scaffolds<sup>23</sup>. Electrospun membranes made of gelatin-elastin-hyaluronic acid blend can mimic the complexity of ECM better than most of the electrospun scaffolds studied in literature; furthermore, by tuning the relative amount of the three biopolymers it is also possible to produce scaffolds with tailorable composition and chemical properties for the specific engineering tissue.

## **2. Materials and methods**

The biopolymers used in this work were purchased from Sigma-Aldrich and used with no further purification. For each of them, molecular weight from the data sheet is reported (Table 2.1), as this is an important parameter for ES and can greatly affect the process and the result:

Table 2.2: Molecular weight of the biopolymers used.

<b>Material</b>	<b>Molecular weight [kDa]</b>
Collagen type I from bovine achille tendon (C4387 and C9879)*	300
Gelatin A from porcine skin (G1890)	50 – 100
Elastin from bovine neck ligament (E1625)	<i>not indicated</i>
Sodium hyaluronate from <i>Streptococcus equi</i> (53747)	1500 – 1800

\* C4387: batch #1 collagen; C9879: batch #2 collagen.

For ES technique, the polymer needs to be in solution form; the choice of solvent plays a vital role, since the properties of solution (e.g. viscosity, evaporation rate) strongly affect fiber formation<sup>24</sup>. Therefore, suitable solvents for ES have initially to allow polymer dissolution with adequate concentration that permits fiber formation without defects, and then they should possess high vapor pressure and low surface tension in order to favor the process. All the solvents tested in this work are purchased from Sigma Aldrich; their main properties are described in Table 2.2:

Table 2.3: Values of vapor pressure and surface tension of the solvents considered for ES.

<b>Solvent</b>	<b>Vapor pressure [atm]</b>	<b>Surface tension [mN/m]</b>
Phosphate buffer saline (PBS)	0.0231 (20°C)-0.0313 °	71.99 °
Hexafluoroisopropanol (HFIP)	0.158 *	16.4 °
Trifluoroacetic acid (TFA)	0.128 *	0.9 °
Ethanol (EtOH)	0.059 °	21.9 °
Formic acid (FA)	0.052 °	37.6 *
Acetic acid (AA)	0.026 #	27.6 *

\* measured at 20°C; ° measured at 25°C; # measured at 30°C.



## 2.1 Solubility tests

In order to investigate good solvents for the biopolymers chosen, preliminary solubility tests have been carried out: the concentration used for all the tests was 2% w/v and homogeneity of the solution was evaluated simply by looking at it after 2 days of stirring at room temperature.

## 2.2 Electrospinning apparatus

The conventional setup used in this thesis consists of three parts: 1) high voltage, 2) solution flow rate control, and 3) collector. Each part is described below:

- 1) DC high voltage power supply (Enrico Pesatori Costruzioni Elettriche) used for applying a positive (to the needle) and negative (to the collector) voltage up to 30 kV (maximum electrical current: 0.1 mA).
- 2) Syringe pump (100 model, KD Scientific) used to control the flow rate of solution. Syringes used were 20ml PP/PE syringes (I.D. of 20 mm, Sigma Aldrich); they were connected to a PTFE tube (I.D. of 16G, Supelco), which at the end was finished in a stainless steel iron needle (I.D. of 0.030", Supelco).
- 3) The collector was an easily removable metal plate (15 x 10 cm) covered with aluminum foil.

In order to limit unwanted dripping of the solution on the collector, the ES experimental setup used was always with horizontal configuration. Temperature and relative humidity were monitored during the process, and it was possible to partially decrease humidity value by using a de-humidicator (Trotec TTR 56 E).

The experimental procedure to optimize ES process consists of the following steps:

1. Load the solution to be tested into a plastic syringe, which is connected to a metal needle through a PTFE tube in order to protect the syringe pump from the high voltage;
2. select the desired solution flow rate by using a syringe pump;
3. adjust the distance between the needle and collector according to the chosen distance value;
4. place an aluminum foil over the collector plate to collect fibers for characterizations;

5. apply a positive high voltage to the needle and a negative voltage to the collector plate;
6. optimize ES parameters, i.e. applied voltage, flow rate, distance between the needle and collector, according to the solution.

Table 2.3 summarizes the different solutions used in this work, and the parameter ranges tested to optimize ES process; if ES of the solution had been previously optimized in literature studies, the reference is reported.

### **2.3 Evaluation of process stability**

In order to check Taylor cone formation and stability of ES process, a specific imaging system has been used. In particular, a laser light ( $\lambda = 656 \text{ nm}$ , SY Lasiris SNF501L, StockerYale) was used to illuminate the tip of the spinneret (where the Taylor cone is formed); the transmitted light then passed through a lens ( $f = 300 \text{ mm}$ ), that magnified the image and focused the beam, and arrived to a camera (EoSens CL, Mikrotron) for recording. The camera was connected to a computer, where the images were visible thanks to a specific software (MotionBLitz Director). This method permitted real-time control over jet formation related to process parameters, and it allowed also the identification of eventual problems during ES (e.g. solution gelification, process instability).

### **2.4 Morphological analysis**

With the intention of evaluating the optimal process parameters, the morphology of each sample for all the solutions electrospun was examined via scanning electron microscopy (SEM, Cambridge Stereoscan 360). Dry, as-spun samples were mounted onto aluminum stubs, sputter coated with gold, and imaged with a 10 kV accelerating voltage. After determining the optimal set of parameters for each solution, fiber diameter of these samples was measured by image analysis with ImageJ software, measuring 100 fibers per type of sample. Fiber diameter is reported as average  $\pm$  standard deviation.

Table 2.4: Polymeric solutions and range of parameters tested for ES.

Material	Solvent	Concentration [% w/v]	Time of stirring [days]	Voltage [ $\Delta V$ , kV]	Flow rate [q, ml/h]	Distance [d, cm]	Temperature [°C]	Relative humidity [%]	Ref.
Collagen, #1	FA	5-8-10-13-15	1-2	20 – 36	0.1 – 0.5	10 – 16	20 – 24	29 – 40	/
Collagen, #2		15-20-25-30	5-9						
Gelatin	AA/H <sub>2</sub> O (9/1)	10	< 1	12 – 21	0.5 – 1	10 – 14	22 – 25	26 – 40	25
	H <sub>2</sub> O/EtOH/FA (3/1/1)	20	< 1	14 – 24	0.5 – 1	10 – 14	22 – 25	30 – 40	26
	FA	10-15-20	< 1	10 – 21	0.1 – 0.5	10 – 14	20 – 25	20 – 40	3
Gelatin/elastin (9/1 and 7/3)	FA	8-10-15-20-22-25	2	12 – 21	0.1 – 0.3	10 – 14	19 – 24	< 40	/
Gelatin/elastin/HA (% of HA = 5-8-10)	FA	10-13-18	2	21 – 36	0.1 – 0.3	10 – 14	17 – 22	< 40	/

## 2.5 SDS-PAGE analysis

SDS-PAGE is a useful technique in biochemistry field which separates proteins depending on their molecular weight, based on their differential rates of migration through a sieving matrix (a gel) under the influence of an applied electrical field. In their native state proteins in an electrical field would migrate at different speeds depending not only to their molecular weight, but also on their charge and tridimensional shape. In order to be able to separate proteins based on their molecular weight only, it is necessary to destroy the tertiary structure and reducing the protein to a linear molecule; moreover, the intrinsic net charge of the protein has to be masked. To achieve this aim, sodium dodecyl sulfate (SDS) is used: it is a detergent present in the SDS-PAGE sample buffer where, along with thermal denaturation and a reducing agent (normally dithiothreitol or  $\beta$ -mercaptoethanol which are able to break protein disulphide bonds), it disrupts the tertiary structure of proteins, reducing the folded proteins to linear molecules. Moreover, SDS binds uniformly to linear protein, thus coating it with a negative charge which masks the intrinsic charges of the protein: therefore, protein charge becomes proportional only to its molecular weight.

The gel matrix used for SDS-PAGE is polyacrylamide, a chemically inert polymer that allows the production of gel with different concentrations. Tailoring the concentration of polyacrylamide allows the production of different pore size gels, thus resulting in a variety of separating conditions that can be changed depending on the size of the protein of interest. When the proteins are in the gel, separation occurred because higher molecular weight proteins move more slowly through the porous acrylamide gel than lower molecular weight proteins.

In this work, investigation of protein molecular weight distribution was carried out for both the batches of collagen in order to find possible explanations to the different behavior during ES. Therefore, SDS-PAGE of #1 and #2 batches of collagen before and after solubilisation in formic acid was carried out. SDS-PAGE analyses were similarly performed on fibrinogen as control, because its migration pattern had been previously verified. Samples consisted of "raw" fibrinogen and collagen powder dissolved in Laemmli buffer,

or of acid-treated collagen. In particular, collagen was dissolved in formic acid ( $c = 10\%$  w/v), and then solvent casted films were obtained. Because this analysis technique is highly sensitive to the pH and to small amount of solvent residues that can affect the results, solvent traces in collagen films have been completely removed by use of a vacuum pump before analysis. SDS-PAGE electrophoresis was carried out with PowerPacHC using 4-15% gradient gel (Mini-PROTEAN TGX Gel), both purchased from BIORAD. Each sample was submitted to reducing treatment with Laemmli buffer and  $\beta$ -mercaptoethanol (1 mg protein/1ml solution 0.375 M Laemmli + 5% v/v  $\beta$ -mercaptoethanol) at 95°C for 5 minutes. After brief centrifugation, two different amounts of collagen (or fibrinogen) for each sample were loaded in the gel (i.e. 5 and 10  $\mu$ g); the gel was then submitted to electrophoretic run (90-140 V) using two different protein standards, Kaleidoscope and Dual Color (BIORAD). At the end of the run, SDS-PAGE slide was treated with a fix solution composed by 50% v/v of methanol and 10% v/v of acetic acid for protein fixing, and then colored with Coomassie Brilliant Blue (BIORAD, 0.2% w/v in the same solution used for fixing).

## **2.6 Crosslinking methods**

As gelatin and collagen after ES are soluble in aqueous media, different crosslinking methods, both physical and chemical, extensively studied in literature have been investigated and compared in order to determine the most suitable ones. For each method, parameters reported in literature have been used as reference. Gelatin electrospun samples in formic acid ( $c = 10\%$  w/v) have been used during this optimization phase, as gelatin was the main component of the blends, and also the cheapest and easiest material to be electrospun. Circular samples ( $\varnothing = 13$  mm) were punched from the membrane and used for the following crosslinking tests. The efficacy of crosslinking processes was evaluated taking into considerations two parameters: the abilities to preserve fiber morphology (investigated by SEM analyses) and to increase sample stability (investigated by degradation test in PBS at 37°C).

## **Physical methods**

### a. Dehydrothermal (DHT) treatment:

Numerous studies have been performed that utilize DHT for stabilization of collagenous natural materials and gelatin scaffolds. Samples to be crosslinked are put in oven at high temperature ( $> 98^{\circ}\text{C}$ ) and usually at very low pressure for few days, in order to favour condensation reactions. According to works in literature, two values of temperature (110 and  $140^{\circ}\text{C}$ ) and three different crosslinking times (1, 3, and 5 days) have been tested<sup>27-29</sup>.

### b. Ultraviolet (UV) radiation:

This physical method is commonly used for gelatin, and it is sometimes preferred over DHT because it is faster, with duration limited to few hours. Energy related to UV radiation allows the formation of free radicals on the aromatic residues, which subsequently can bind to each other. Important parameters for this method are sample exposure time, their distance from the lamp, and energy of the radiation. In particular, crosslinking time has to be carefully optimized, because prolonged exposure to UV irradiation can cause denaturation, while limited exposure results in membranes with no adequate stability<sup>28,30</sup>. In this work, circular samples were irradiated by UV lamp (Philips Lyvia,  $\lambda = 254\text{nm}$ , 8W) at a distance of 5 cm, in a close and dark environment, for 40 or 90 minutes.

## **Chemical methods**

### a. Glutaraldehyde (GA) vapour:

Amongst chemical methods, GA is the most widely used, due to its high efficiency in stabilizing collagenous materials. Crosslinking reaction occurs between aldehyde groups of GA and amino groups of lysine residues<sup>7, 31-32</sup>. In this work, the process was carried out by placing gelatin circular samples in a sealed desiccator containing 2 or 5 ml of aqueous GA solution (Sigma Aldrich, 340855) with different concentrations (i.e. 5, 25, or 50%) in a Petri dish. Samples were placed on a holed ceramic shelf in the desiccator and crosslinked at room temperature for different times, ranging from 30

minutes to 24 hours. After crosslinking, the samples were exposed in a fume hood for 5 hours to remove residual GA.

b. Genipin (GP) crosslinking:

Among the chemical crosslinking agents genipin has been reported to provide materials with higher biocompatibility and less cytotoxicity. This naturally occurring molecule has been investigated as crosslinker for electrospun gelatin, because of its ability to react with primary amino groups. However, up to now results in literature are controversial, as often crosslinked gelatin membranes did not maintain electrospun morphology<sup>32-34</sup>. Genipin (Sigma, G4796) crosslinking was performed using ethanol as solvent. Two experimental parameters were varied: genipin concentration (1.25 and 2.5% w/v) and reaction time (1, 2, 3 and 4 days). Electrospun gelatin samples were put in a 24well plate, then 1 ml of the crosslinking solution was added to each well. Finally, the plate was placed in a 37°C incubator to speed up the reaction for the defined period.

c. Ethyl-3-(3-dimethylaminopropyl)carbodiimide (EDC) crosslinking:

There is great interest in carbodiimides, and in particular EDC, because these molecules are zero-length cross-linking agents (i.e. the agent itself is not incorporated into the macromolecule). In fact, EDC molecule reacts with the carboxylic groups of aspartic and glutamic residues of gelatin molecule and forms an intermediate (O-isoacylurea) that then undergoes nucleophilic attack by the amine functional groups of lysine residues on adjacent peptidic chains<sup>35-36</sup>. Different concentrations of EDC hydrochloride (Sigma Aldrich, E1769) solution in ethanol have been evaluated for crosslinking process: 0.5, 1, 2, 2.5, 5% w/v. Circular electrospun gelatin samples have been immersed in 1 ml of EDC solution and placed in a 37°C incubator for different crosslinking time: 1, 2, 3, and 4 days.

### 3. Results and discussion

ECM is a very complex structure, and its composition can vary not only from tissue to tissue, but also within the same one. In fact, chemical composition is strictly related to the function the matrix has to fulfil. In order to partially reproduce ECM structural complexity, blends of natural polymers (i.e. collagen/gelatin, elastin and hyaluronic acid) with different compositions have been here prepared and the respective ES parameters optimized.

#### 3.1 Electrospinning of collagen

Traditionally, collagen has been electrospun in literature using HFIP or TFE as solvent, because they allow effective solubilisation of the protein and they rapidly evaporate during fiber formation process<sup>37-38</sup>. However, in latest years several conflicting results have been reported with regards to collagen molecular structure after ES process. In fact, numerous studies have demonstrated that collagen completely unfolds in fluorinated solvents and, therefore, researchers have started to investigate different solvent systems in order to obtain collagen e-spun fibers with preserved molecular structure<sup>39-40</sup>. A typical alternative to fluorinated solvents for ES are organic acids, as they are usually able to solubilise the polymer without causing extensive denaturation. In particular, collagen has been successfully electrospun in acetic acid aqueous solution, and also in mixture of PBS and ethanol<sup>41-42</sup>. With the aim to determine the adequate solvent system for collagen ES, in this work initially protein solubility in several solvents has been investigated.

##### **Solubility tests**

Table 2.4 reports the results of the solubility tests of collagen in different solvents. Solvents commonly used in literature for collagen ES, such as HFIP, PBS and EtOH, in this work proved to be ineffective to solubilize collagen and this is probably due to the great variation related to the source, the extraction process, but also to the batch.



Table 2.5: Results of collagen solubility tests.

<b>Solvent</b>	<b>Solubility</b>
PBS	×
HFIP	×
TFA	✓
EtOH	×
Formic acid	✓
Acetic acid	×
Citric acid 1M	×
Hydrochloric acid 1M	×
NaOH	×

Different types of organic acid aqueous solutions with the same pH and also a basic solution were investigated as solvents for collagen, in order to separate the effect due the pH from that due to the intrinsic chemical structure of the solvents. The only solvents useful for collagen solubilisation were TFA and formic acid; therefore, it appears clear that collagen solubility is related to the ability of formic acid and TFA to break intra- and inter-molecular hydrogen bonds, and not only to the acidic pH. Even if in formic acid is necessary to wait 2/3 days in order to obtain homogeneous solutions, this solvent was chosen for ES in order to avoid fluorinated solvents, more toxic and expensive.

### **Electrospinning parameter optimization**

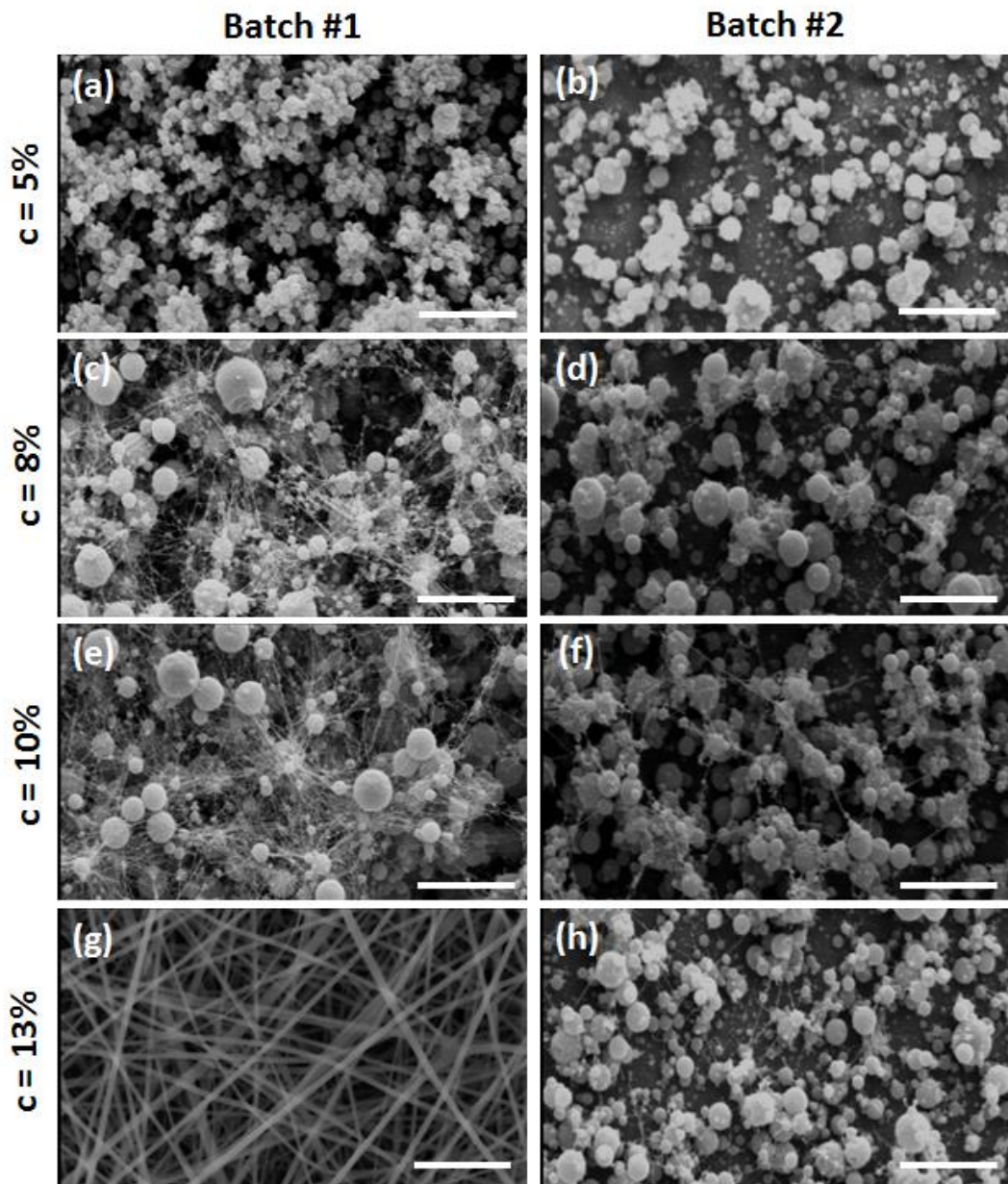
ES experiments were performed on two different batches, #1 and #2, of the same collagen type, in order to investigate the reproducibility of the process with respect to the biopolymer source, which is known to be a common problem in case of natural polymers. For each batch, concentration of collagen in formic acid and process parameters, i.e. applied voltage, flow rate and distance between the needle and the collector, were varied in order to find optimal conditions for ES. Even if it was not possible to control relative humidity and temperature values, all the tests were performed with similar environmental conditions (T= 20-24°C, RH = 29-40 %): therefore, it is possible to assume that the small differences in temperature and humidity did not dramatically affect ES results obtained.

Table 2.5 shows the results of ES of the two collagen batches, at various concentrations. For 5% w/v concentration, in both cases the solutions could not be electrospun and only beads were formed, because molecule concentration was too low and did not allow adequate entanglement formation, necessary to obtain fibers (Tab. 2.5a, b). By increasing the concentration, it was possible to notice differences in the ES results between the two batches: in particular, for batch #1 solutions at 8% and 10% w/v concentrations, a mixture of beads and fibers were obtained, while for batch #2 only beads were visible (Tab. 2.5c-f). In case of batch #1, for 13% w/v concentration the process was stable and good fiber morphology was obtained (fiber diameter =  $140 \pm 40$  nm, Fig. 2.1g); therefore, this value was adequate to obtain entanglement of the polymer chains. By further increasing solution concentration to 15% w/v, the formation of continuous fibers was hindered probably because of the high viscosity, and fibers with beads were observed (Tab. 2.5i). Above 15% concentration, for batch #1 no deposition could be obtained because of the high solution viscosity.

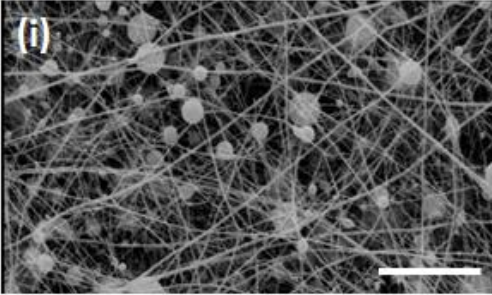
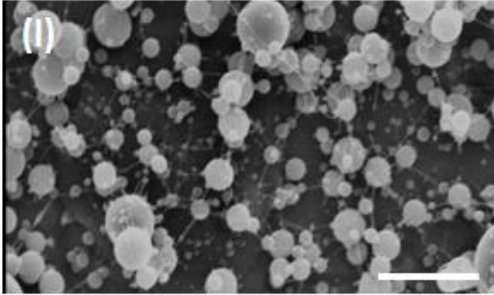
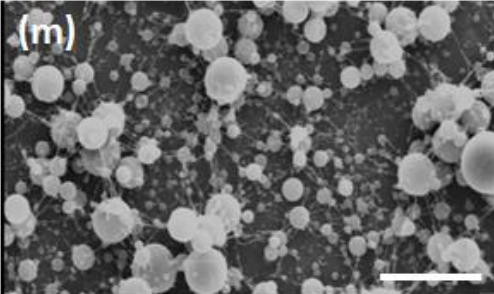
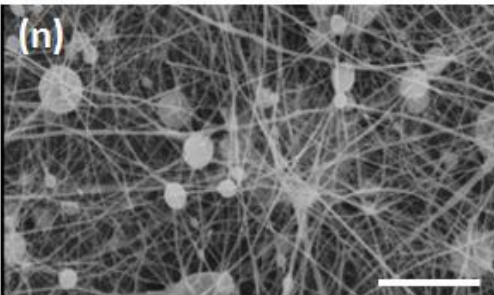
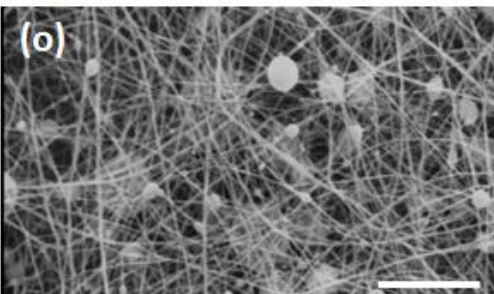
The behavior of batch #2 collagen solution was completely different: in fact, in order to obtain a homogeneous solution at the same concentration values than batch #1, it was necessary to stir it for longer time, i.e. 5 days instead of 2. Moreover, no fibers were obtained by ES of 13% and 15% solutions (Tab. 2.5h, l). Therefore, solution concentration was further increased to 20%, 25%, and 30% w/v: SEM images showed that fiber formation occurred for 25% and 30% concentration, even if few beads were present (Tab. 2.5n, o). However, an important drawback for such high concentrations was the stirring time necessary for the solution to be homogeneous; in fact, solutions were electrospun after 9 days of stirring.

This is the first report of collagen ES in formic acid; the results obtained showed that ES of biopolymers, and in particular of collagen, is trickier than ES of synthetic polymers; in fact, process stability and adequate fiber morphology are achieved only for a narrow range of collagen solution concentration. Moreover, it was clear that ES process optimization was significantly different for the two lots of the same collagen type, thus confirming the great batch-to-batch variability of collagen materials.

Table 2.6: SEM images of electrospun collagen solutions for both the batches used and for different concentrations. Scale bar: 5  $\mu$ m.



Continue Table 2.5:

<b>c = 15%</b>		
<b>c = 20%</b>	<p>Solution viscosity too high → no deposition on the collector</p>	
<b>c = 25%</b>	<p>Solution viscosity too high → no deposition on the collector</p>	
<b>c = 30%</b>	<p>Solution viscosity too high → no deposition on the collector</p>	

### **SDS-PAGE of collagen**

In order to evaluate if the different behavior of the two lots of collagen solutions was related to differences in protein molecular structure between the two batches and to investigate possible structure modifications caused by the acidic environment, SDS-PAGE assay was carried out on both the batches of collagen after solubilisation in formic acid.

Fig. 2.1 shows the results obtained after sample migration; fibrinogen was used as control to demonstrate that the process was correctly carried out (lanes 1 and 2). Batch #1 and #2 collagen after solubilisation in formic acid were loaded in lanes 4-5 and 6-7 respectively; lanes 8-9 contained "raw" batch #1 collagen. Theoretically, SDS-PAGE of collagen under reducing conditions should show molecular bands around 120 and 240 kDa, which correspond to  $\alpha_1(I)$  and  $\alpha_2(I)$  chains of type I collagen and their dimers, respectively<sup>40</sup>. However, in this case the bands were not present: in fact, for batch #1 and #2 the majority of the samples could not penetrate the gel and stacked at the top, and it happened independently to collagen solubilisation in formic acid. Probably this was caused by the bare solubility of the samples in the Laemmli buffer used: despite the strong reducing conditions, collagen molecules were not adequately solubilized and, therefore, they were too large to penetrate the gel.

Even if SDS-PAGE assay was not helpful in understanding the differences in collagen molecular structure between the two batches tested, we supposed that the huge difference in ES process of collagen solutions was related to differences in molecular weight distribution.

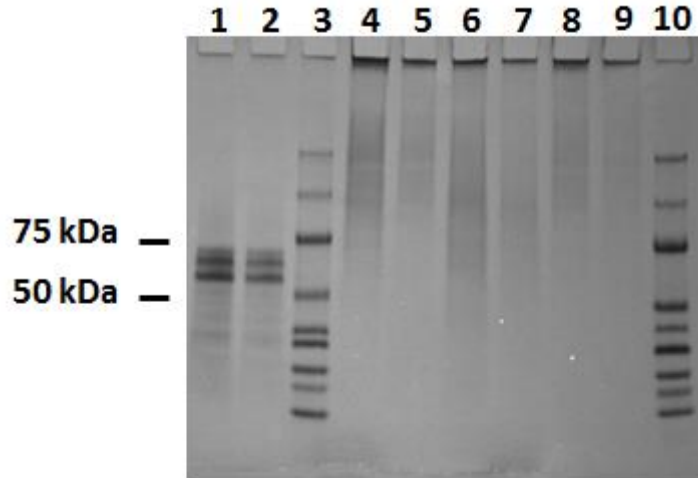


Fig. 2.4: SDS-PAGE analysis of collagen and fibrinogen used as control: fibrinogen (lanes 1-2), batch #1 collagen after solubilisation in formic acid (lanes 4-5), batch #2 collagen after solubilisation in formic acid (Lanes 7-8), "raw" batch #1 collagen (lanes 8-9). Lanes 3 and 10 contain molecular weight standards. Lanes 1, 4, 6, 8 were loaded with 10  $\mu$ g of fibrinogen; Lanes 2, 5, 7, 9 with 5 $\mu$ g.

### 3.2 Electrospinning of gelatin

Because of the big variability issue of collagen material and its high cost, a more convenient alternative to collagen could be gelatin. In fact, gelatin has proven to be an excellent material for ES, as it is easily soluble in several solvents and possesses the viscoelastic properties necessary to have a stable and continuous jet<sup>3,26</sup>. In fact, as gelatin is denatured collagen, it has lost stable intra-molecular forces responsible for secondary and tertiary structure maintenance, thus allowing easier molecular unravelling in the direction of the flow during ES process.

#### Solubility tests

Table 2.6 reports the results of the solubility tests of gelatin in the solvents previously tested for collagen.

Table 2.7: Results of gelatin solubility tests.

Solvent	Solubility
PBS	✓
HFIP	✓
TFA	✓
EtOH	✓
Formic acid	✓
Acetic acid	✓
Citric acid 1M	✓
Hydrochloric acid 1M	✓
NaOH	✓

Gelatin proved to be soluble in all the solvents tested, as can be deduced from its chemical structure, more flexible and with less intra-molecular bonds with respect to collagen. For the same reasons explained above for collagen (i.e. toxicity and cost), fluorinated solvents were not considered for ES of gelatin; instead, three different solvent systems already present in the literature for gelatin ES were selected and morphology of the fibers obtained was compared, in order to choose the most suitable solvent system which allows stable process for subsequently ES of gelatin-based blends.

### Electrospinning parameter optimization

- Gelatin 10% w/v in acetic acid/water (9/1)

Starting from ES parameters reported in literature<sup>25</sup>, flow rate, distance and voltage were shortly optimized with respect to the set-up used in this work; optimal parameters are:  $q = 0.5 \text{ ml/h}$ ;  $d = 13 \text{ cm}$ ;  $\Delta V = 18 \text{ kV}$ .

ES process of gelatin in acetic acid/water mixture was stable and continuous. Fiber morphology confirmed this macroscopic observation, as as random distribution and homogeneous dimensions were observable (diameter:  $268.3 \pm 17.7 \text{ nm}$ , Fig. 2.2).

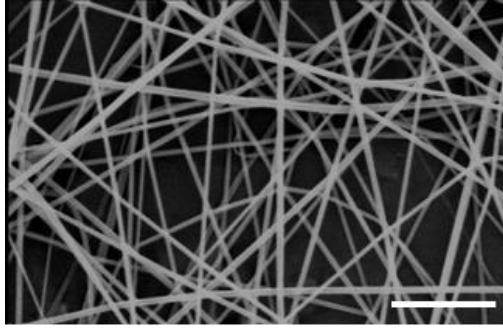


Fig. 2.5: SEM image of electrospun gelatin in acetic acid/water (9/1). Scale bar: 5  $\mu$ m.

- Gelatin 20% w/v in water/ethanol/formic acid

Fig. 2.3 shows the fiber morphology for 20% gelatin solution in water/ethanol/formic acid: fibers are homogeneous and randomly distributed, with bigger dimensions than in the previous solvent system, as the diameter is  $974.5 \pm 180.0$  nm. This can be related to the higher concentration of gelatin used in this case, and to the lower volatility of the solvent system, as here it is mainly composed of water. Within the range of parameters tested, fiber morphology did not significantly change: therefore, ES process proved to be stable.

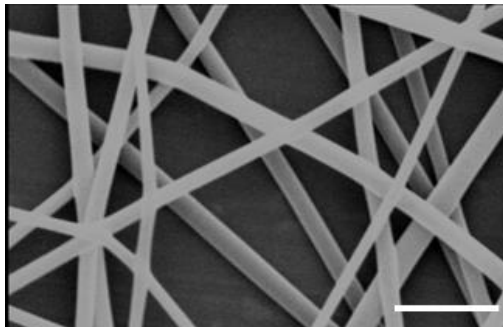


Fig. 2.6: SEM image of electrospun gelatin in water/ethanol/formic acid (3/1/1).  
Scale bar: 5  $\mu$ m.

- Gelatin 10-20% w/v in formic acid

Using pure formic acid as solvent it was possible to electrospin solutions with very different gelatin concentrations, from 10% to 20% w/v, and therefore obtain fiber with a wide range of fiber diameters ( $109.4 \pm 19.2$  nm and  $283.5 \pm 20.9$  nm, Fig.



2.4a, b, respectively). In both cases, the process was stable and efficient for the range of parameters used, and homogeneous fibers could be obtained.

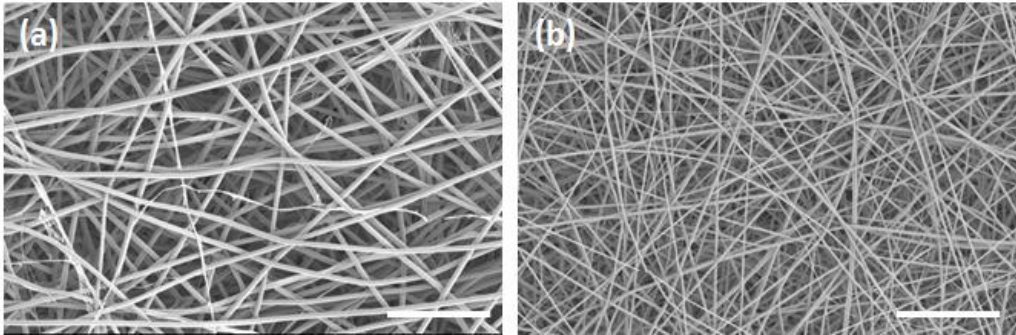


Fig. 2.7: SEM image of electrospun gelatin in formic acid at different concentrations: (a)  $c = 20\%$  w/v; (b)  $10\%$  w/v.

### 3.3 Electrospinning of elastin

Elastin purified from animal tissues is extensively crosslinked, making it insoluble and consequentially difficult to manipulate as a biomaterial. Fragmented elastin, obtained by elastin partial hydrolysis, is easier to solubilize; however, elastin fragmentation can lead to loss of structural integrity and cell signaling properties<sup>43</sup>. Electrospun elastin is extremely interesting as scaffold for tissue regeneration, but because of its solubility issues and unusual solution viscoelastic properties, few works in literature managed to successfully electrospin elastin, and only in its precursor form, i.e. tropoelastin; the only solvent used for tropoelastin ES is HFIP because of its peculiar properties that have already been discussed<sup>44-45</sup>.

#### Solubility tests

The same solvents tested for collagen and gelatin were used to find a proper solvent for elastin ES (Table 2.7).

Table 2.8: Results of elastin solubility tests.

<b>Solvent</b>	<b>Solubility</b>
PBS	✘
HFIP	✘
TFA	✓
EtOH	✘
Formic acid	✓
Acetic acid	✘
Citric acid 1M	✘
Hydrochloric acid 1M	✘
NaOH	✘

As shown in Table 2.7, HFIP, the solvent used in literature for tropoelastin ES, was not able to solubilize elastin because of its high degree of crosslinking. The only solvents for elastin were TFA and formic acid; for the same reasons described above, it was preferable to work with formic acid instead of TFA. Moreover, considering that our final aim was the ES of gelatin-based blends, formic acid appeared extremely useful as previously optimization of ES parameters of gelatin solution in this solvent was carried out. The only limitation using formic acid was that it took 1-2 days in order to have a homogeneous elastin solution.

#### **Electrospinning parameter optimization**

Elastin solution in formic acid with different concentrations were tested for ES; however, even for a wide range of process parameters, it was not possible to obtain a stable jet and no significant deposition on the collector was visible. As we were more interested in obtaining electrospun membranes from a combination of ECM biopolymers, we were confident that the addition of gelatin to elastin solution would have improved its processing ability.

### 3.4 Electrospinning of gelatin/elastin blends

As previously said, the solvent chosen for gelatin-based blend ES was formic acid, because it is a good solvent for the two biopolymers and it has low toxicity compared to fluorinated solvents.

It was demonstrated that gelatin in formic acid could be electrospun with different solution concentrations, from 10 to 20% w/v. As elastin has a higher molecular weight with respect to gelatin and we did not know the effect of blending the two polymers, different gelatin/elastin ratios were considered for ES, starting with low total concentration of the polymeric phase (i.e. 8%), and gradually increasing it in order to obtain a stable ES process and find the maximum concentration limit of solution that can still be electrospun.

Different gelatin/elastin ratio solutions were prepared, i.e. 9/1, 7/3, and 5/5. The first one, 9/1, was chosen in order to have the slightest difference in solution with respect to pure gelatin, and therefore favoring a stable ES process of the blend. 7/3 and 5/5 ratios were selected to evaluate the maximum amount of elastin that could be used in the blend, while keeping the solution spinnable.

Even if it was not possible to have a fine control over temperature and humidity values, samples were electrospun only when RH was lower than 40%, as experimental tests showed that higher humidity values can negatively affect ES of proteins. Temperature varied between 19 and 24°C.

#### Electrospinning parameter optimization

ES process parameters were initially varied around the optimized parameters for gelatin ES in formic acid. The results obtained for gelatin/elastin blend ES are here reported with respect to the total polymer concentration of the solutions used.

- **c = 8% w/v**

Two different gelatin/elastin ratios were initially electrospun: 9/1 and 7/3. During the ES process, it was clearly visible that the jet was not stable and dripping at the tip of the spinneret occurred, even for lower flow rates and higher values of voltage applied, thus suggesting that solution concentration was too low. SEM

images of the electrospun samples confirmed this hypothesis, as fibers with a lot of beads were present for both the solutions (Fig. 2.5). Therefore, it was necessary to increase total concentration of the solution.

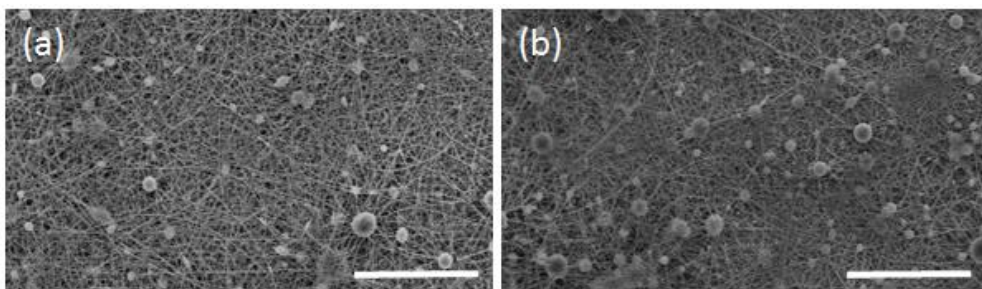


Fig. 2.8: SEM images of electrospun gelatin/elastin blend,  $c = 8\%$  w/v, at different ratios: (a) 9/1; (b) 7/3. Scale bar:  $20\ \mu\text{m}$ .

▪  **$c = 10\%$  w/v**

Increasing in solution concentration effectively reduced solution dripping and increased process stability (Fig. 2.6); however, especially for 7/3 ratio solution, the problem was still not completely solved. As elastin is supposed to have higher Mw than gelatin, we wanted to investigate if an increase of elastin percentage in the blend could solve the dripping problem; therefore, we prepared and electrospun a 5/5 ratio solution. Unfortunately, instead of solving the problem, the higher amount of elastin in solution completely hindered ES process. In fact, as it was possible to see from Taylor cone images captured during pure gelatin ES and during 5/5 gelatin/elastin ES (Fig. 2.7), viscoelastic properties of the blend solution were not adequate in order to have a stable jet: the elastin present greatly increased the elasticity of the solution, and the electric field could only stretch the cone and cause it to assume a very elongate shape, until rupture occurred, without any fiber deposition. For this reason, 5/5 ratio was no longer considered in following optimization experiments.

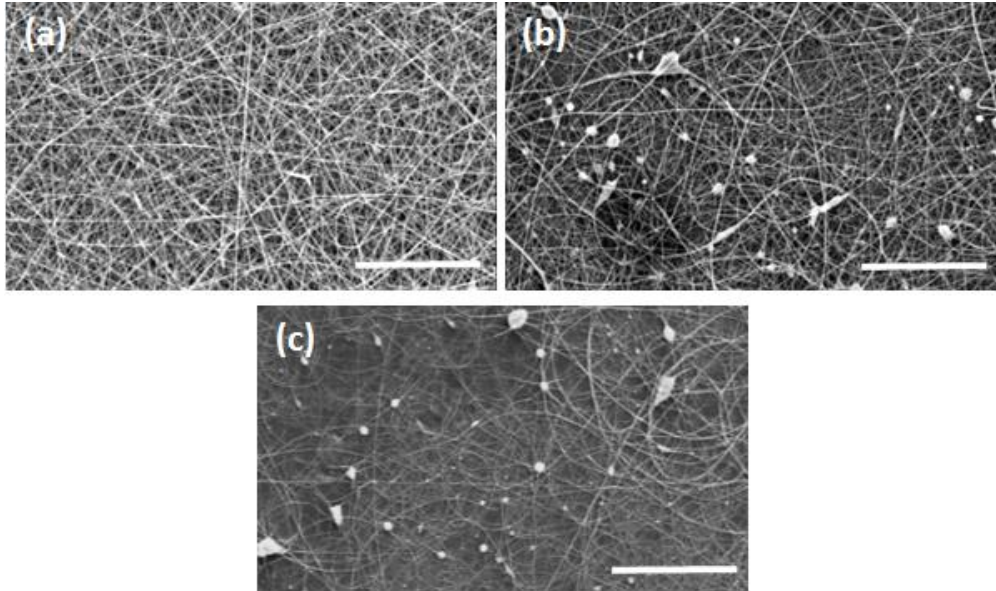


Fig. 2.9: SEM images of electrospun gelatin/elastin blend,  $c = 10\%$  w/v, at different ratios: (a) 9/1; (b) 7/3; (c) 5/5. Scale bar:  $20\ \mu\text{m}$ .

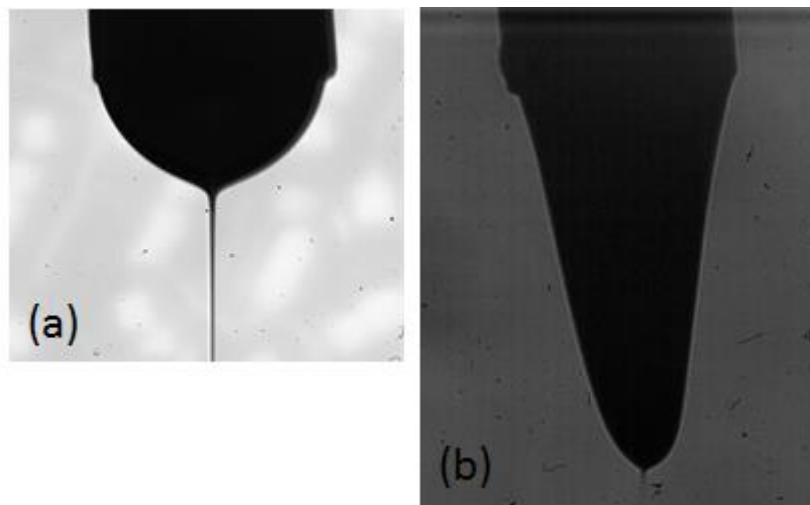


Fig. 2.10: Images of the Taylor cone during ES process of gelatin (a) and 5/5 gelatin/elastin blend (b); in both cases, total concentration was  $10\%$  w/v.

- **c = 15% w/v**

By further increasing the concentration up to 15%, both for 9/1 and 7/3 ratios, it was possible to find proper process parameters in order to obtain stable ES with only minor dripping, that rarely occurred. In fact, for low flow rate (0.1 ml/h) and higher electric field values (1.2-1.5 kV/cm), collected fibers had a good morphology, with randomly oriented distribution and homogeneous dimensions (Fig. 2.8). Within the range of values tested, needle-to-collector distance proved not to influence process stability nor fiber morphology.

In order to determine the maximum concentration value of the solutions that allowed stable ES process, total polymer concentration was further increased and these solutions were tested with ES.

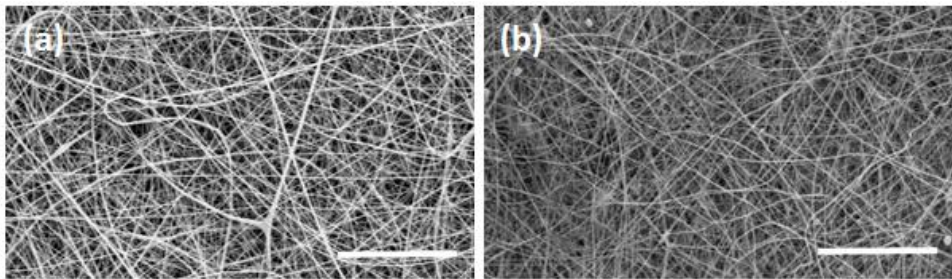


Fig. 2.11: SEM images of electrospun gelatin/elastin blend, c = 15% w/v, at different ratios: (a) 9/1; (b) 7/3. Scale bar: 20  $\mu\text{m}$ .

- **c = 20% w/v**

SEM images (Fig. 2.9) show fiber morphology obtained for the two gelatin/elastin blend ratios, 9/1 and 7/3: fibers are homogeneous and no defects are visible. Using parameters optimized for 15% solution, the process was stable and continuous.

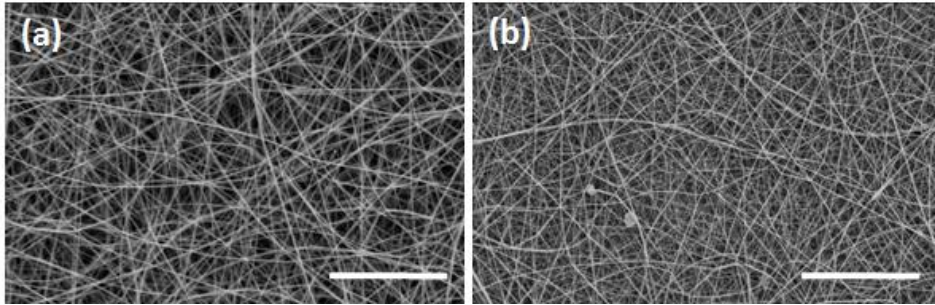


Fig. 2.12: SEM images of electrospun gelatin/elastin blend,  $c = 20\% \text{ w/v}$ , at different ratios: (a) 9/1; (b) 7/3. Scale bar:  $20\mu\text{m}$ .

- **$c = 22\% \text{ w/v}$**

For this concentration value, a quiet different behavior for 9/1 and 7/3 solutions occurred: in fact, 9/1 solution ES was stable and fiber still had adequate morphology without any defect (Fig. 2.10). On the contrary, 7/3 solution was not spinnable because of its very high viscosity: in fact, at the end of the spinneret the solution was extruded like a gel. Therefore, maximum solution concentration for 7/3 blend ratio that allows ES process was  $20\% \text{ w/v}$  (fiber diameter:  $296.3 \pm 56.7 \text{ nm}$ ).

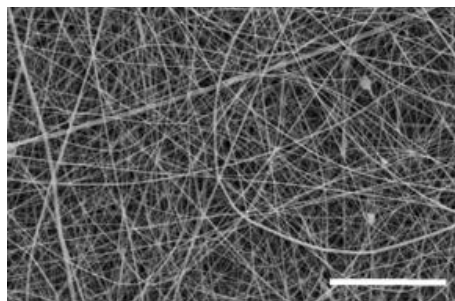


Fig. 2.13: SEM image of electrospun 9/1 gelatin/elastin blend,  $c = 20\% \text{ w/v}$ . Scale bar:  $20\mu\text{m}$ .

- **$c = 25\% \text{ w/v}$**

Because of the results described before for 7/3 ratio solution, only 9/1 blend was prepared for this high concentration value. As it happened for  $22\% - 7/3$  ratio

blend, also in this case solution ES was hindered by the very high solution viscosity, since the prepared blend looked more like a gel than like a solution to be electrospun. Consequently, for 9/1 blend ratio, the maximum concentration allowed for ES was 22% w/v (fiber diameter:  $374.3 \pm 78.7$  nm).

For stable ES process of gelatin/elastin blend, it was important to use low flow rate values (0.1 ml/h) in order to avoid solution dripping; therefore, the possibility to use high concentration solutions could increase process efficiency and reduce the time necessary to obtain a matrix with adequate thickness for tissue engineering applications. ES process of high concentration solutions proved to be stable and continuous, and fibers exhibited the typical non-woven morphology, that was reproducible within a certain range of process parameters, such as voltage (i.e. 1.2-1.5 kV/cm) and distance (10-14 cm) values.

### **3.5 Electrospinning of gelatin/elastin/hyaluronic acid blends**

Hyaluronic acid (HA) is a polysaccharide and one of the main components of the ECM of connective tissues; because of its many unique biological functions, it is a very promising material for tissue engineering applications. However, HA is a polyanionic polymer difficult to electrospin because of its electrical characteristics and high viscosity in aqueous solvent<sup>46-47</sup>. In fact, gelation of HA solution usually occurs at very low polymer concentrations, so that the insufficient entanglement of polymer chains and high viscosity of the solution impede the generation of stable fibers. The idea of blending it in a stable gelatin-based solution can overcome its spinnability limitations, and in the same time allowing the fabrication of tri-component nanofibers constituted by the main biopolymers present in the physiological ECM.

The solvent used is still formic acid, as it proved to be a good solvent not only for gelatin/elastin blends, but also for HA (Table 2.8).



Table 2.9: Results of HA solubility tests.

Solvent	Solubility
PBS	✓
HFIP	✗
TFA	✗
EtOH	✗
Formic acid	✓
Acetic acid	✗
Citric acid 1M	✓
Hydrochloric acid 1M	✓
NaOH	✓

To obtain gelatin/elastin/HA nanofibers, the influence of different solution composition, i.e. polymeric total content, ratio of gelatin/elastin and percentage of HA, were investigated for ES. However, to better understand the effect of each single parameter of the solution, initially gelatin/elastin ratio was kept constant to 9/1 while the other parameters were varied. As HA used in this work has very high Mw (1.5-1.8 x 10<sup>6</sup> Da) and, therefore, can greatly increase solution viscosity even for small concentrations, we decided to start with much lower total concentration, i.e. 10% w/v, with respect to the optimized bi-component blend solution. Process parameters used as reference were the one previously optimized for gelatin/elastin blend; however, it was necessary to adjust them because of the different composition, and therefore different properties, of the solution to be spun.

As for bi-component optimization process, it was not possible to control temperature and humidity values during ES process; however, samples were always electrospun for RH lower than 40% and temperature in the range of 17-22°C.

- **c = 10% w/v**

Three different percentage of HA with respect to total polymer concentration were tested: 5%, 8% and 10% w/w. For the first two HA relative concentrations, it was possible to obtain fiber deposition even if some defects were present and fibers did not always have homogeneous dimensions (Fig. 2.11); the parameters used in

this case were the same than bi-component blend (i.e. 0.1 ml/h and 10-14 cm), except for the voltage (30-36 kV). In fact, real-time observation of the process and SEM analyses of the electrospun samples revealed that it was necessary to increase the applied voltage up to 30 kV (or more) in order to promote formation and deposition of fibers. This could be explained by the macroscopic increase in solution viscosity due to HA contribution; furthermore, HA is known for increasing solution surface tension. Therefore, increasing the electric force (i.e. the applied voltage) was necessary in order to win the greater surface tension of the drop and forming the electrified jet.

As for the bi-component blend, even in this case we wanted to investigate the maximum solution concentration that could be electrospun, so we further increased solution total concentration, keeping the HA percentage constant (5% and 8% w/w).

For HA concentration of 10% w/w, solution viscosity was too high, and solution appeared like a gel, thus making not possible to spin it. Therefore, this concentration was not considered for further ES process.

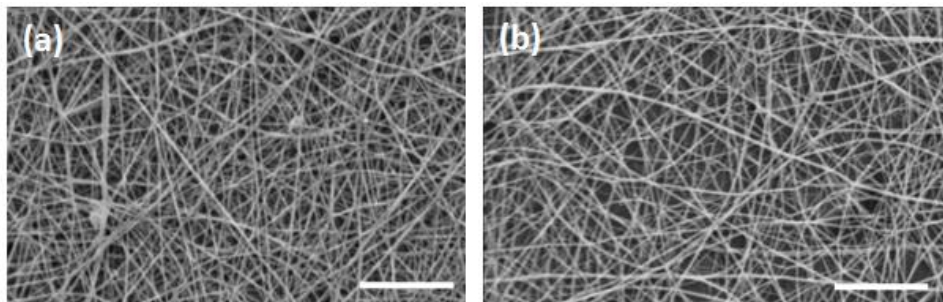


Fig. 2.14: SEM images of electrospun gelatin/elastin/HA blend,  $c = 10\%$  w/v, with different HA amount: (a)  $c_{HA} = 5\%$  w/w; (b)  $c_{HA} = 8\%$  w/w. Scale bar: 5  $\mu\text{m}$ .

- **$c = 13\%$  w/v**

For HA content of 5% w/w, sample morphology was more homogeneous and with less defects than the same sample with 10% w/w total concentration (same ES parameters used, fiber diameter:  $180.0 \pm 32.4$  nm; Fig. 2.12). By increasing HA content to 8%, however, it was no longer possible to spin the solution, as the higher

amount of the glycosaminoglycan caused the solution to be extremely viscous, eventually resulting in solution gelification at the tip of the spinneret. Therefore, maximum polymer solution concentration with 8% w/w HA that allowed ES process was 10% w/v (fiber diameter:  $157.3 \pm 36.9$  nm).

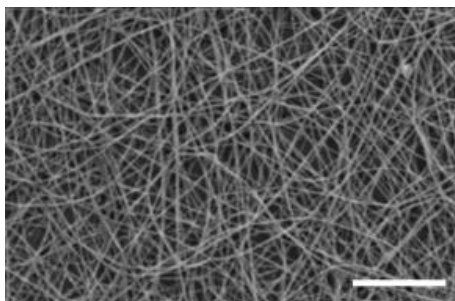


Fig. 2.15: SEM image of electrospun gelatin/elastin/HA blend,  $c = 13\%$  w/v,  $c_{HA} = 5\%$  w/w. Scale bar: 5  $\mu\text{m}$ .

- **$c = 18\%$  w/v**

Given the results obtained with the previous concentration value, only 5% w/w HA solution was tested: unfortunately, ES process was interrupted after few minutes because of solution gelification that occurred also in this case.

From the results obtained, it was clear that the presence of HA greatly influenced the properties of the solution, thus affecting ES; small differences in HA concentration could have huge effect on solution behavior and even completely hinder the process. However, it was possible to successfully electrospin tri-component blends of natural polymers with different compositions, and in particular by varying total solution concentration it was possible to obtain fibers with different percentage of HA: 5% w/w of HA in 13% w/v solution and 8% w/w of HA in 10% w/v solution.

As explained before, in the initial phase of parameter optimization gelatin/elastin ratio was kept constant; however, it was then possible to electrospin solution with same total protein concentration and same HA percentage, but different gelatin/elastin proportion previously optimized, i.e. 7/3. ES process of these solutions proved to be stable and fiber morphology was not different from the one obtained for 9/1 ratio.

### 3.6 Crosslinking strategies

As electrospun membranes are immediately soluble in aqueous media, it is necessary for application as scaffold to enhance their stability by crosslinking treatment. Several methods for the crosslinking of gelatin are investigated in literature, therefore in this work the most promising and common crosslinking strategies were compared. In particular, considering electrospun membranes for biomedical applications three requirements have to be fulfilled by crosslinking treatment: preserve fiber morphology, increase membrane stability in aqueous environment at human body temperature and do not cause cytotoxic effects.

The results showed refer to pure gelatin electrospun membranes, used as reference to compare different crosslinking strategies and eventually optimized crosslinking parameters.

#### Physical methods

a. Dehydrothermal treatment (DHT): this method is widely studied for gelatin crosslinking as it is very simple and cheap. Temperature values used in literature vary from 110°C to 140°C, as for lower temperature there is no significant increase in membrane stability, while for higher values denaturation of gelatin (or collagen) may occur. Fig. 2.13 shows the morphology of the electrospun samples after crosslinking, which proved not to be affected by the DHT. In our case, treatment at 110°C carried out from 1 to 5 days showed no beneficial effect on membrane stability; in fact, membranes dissolved in water after only one hour. At higher temperature, i.e. 140°C, DHT for 3 days proved to be efficient, as samples were stable in PBS up to 7 days, and fiber morphology was perfectly maintained. Moreover, the absence of any chemical agents involved in the crosslinking reaction guarantees the cytocompatibility of the membranes.

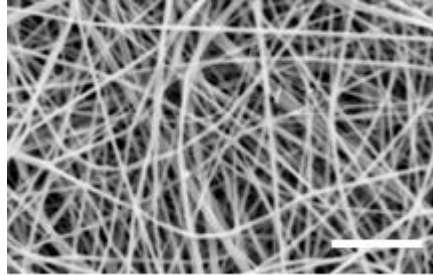


Fig. 2.16: Electrospun gelatin fibers after DHT treatment. Scale bar: 5  $\mu\text{m}$ .

b. Ultra-violet radiation (UV): this method is frequently used in literature because of its simplicity and time-efficiency. Typically, parameters used in literature vary from 30 minutes to 3 hours for the crosslinking time, and from 10 to 15 cm for sample to lamp distance. As for energy, or intensity, of the radiation, this value is very seldom reported in literature, so it was difficult to find a reference for it.

Even if we varied the parameters in the range of those optimized in literature, UV treatment did not prove to be suitable to increase gelatin membrane stability, as samples dissolved in PBS after 2h. A possible explanation can be related to the different UV light source used, which in our case has probably lower power than lamps used in literature<sup>30</sup>.

### **Chemical methods**

a. Glutaraldehyde (GA) vapor: this method is, probably, the most used for biopolymer crosslinking, as it is easy to carry out, not expensive, fast and very efficient. However, an initial careful phase of parameter optimization is necessary in order to obtain stable membranes with adequate fiber morphology. Fundamental parameters of the process are the volume of glutaraldehyde solution used and its concentration, the crosslinking time, and the volume of the desiccator where the reaction takes place. In particular, as one of the main problems related to vapor phase crosslinkers is process reproducibility, small desiccators are preferable, as they allow more homogeneous GA vapor distribution, thus resulting in better control over the process. In literature, a wide range of parameters for electrospun gelatin fiber

crosslinking is used: in fact, GA concentration can vary from 0.5% to 50%, and duration of the treatment from 30 minutes to 4 days. However, no detailed information on volume of the solution used and on desiccator dimensions are reported. Therefore, to optimize GA crosslinking process in this work a huge set of parameters were considered, i.e. GA concentration in solution of 5%, 25%, and 50%, solution volume of 2 and 5ml, crosslinking time from 30 minutes to 24 hours.

SEM images of gelatin samples after crosslinking treatment show that for too high degree of crosslinking, i.e. high GA solution volume or long crosslinking duration, fiber morphology was gradually lost until an almost flat film was obtained (Fig. 2.14). However, up to 3 hours of crosslinking with GA, the treatment did not have any detrimental effect on fibers and the morphology was perfectly preserved (Fig. 2.14a, b), for both the solution volumes (i.e. 2 and 5 ml) and for the three GA concentrations (i.e. 5, 25 and 50%) used (not all the samples are showed to avoid not useful repetition). Then, degradation tests were carried out on crosslinked samples with adequate fiber morphology in order to evaluate the efficacy of the treatment: the only samples that proved to be stable for more than 1 day were those crosslinked with 5 ml of 50% GA solution for 2 and 3 hours. Therefore, these sets of parameters are adequate to enhance gelatin membranes stability in aqueous environment, contemporary preserving the fibrous structure. For more detailed characterization of GA crosslinked samples see Chapter 4.

b. Genipin (GP) crosslinking: as GP is a naturally-derived crosslinking agent, it is extremely interesting for biomedical applications for its intrinsic low cytotoxicity. Usually, gelatin samples to be crosslinked are put in GP solution (with concentrations of 1 to 2% w/v) for different durations, typically from 1 to 5 days. However, the solvent commonly used for GP is ethanol, and debate is still open about its ability to alter electrospun morphology during the treatment.

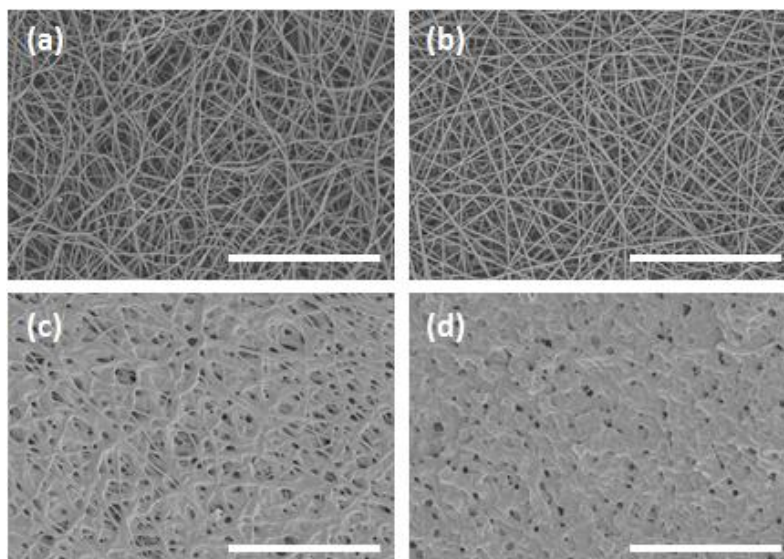


Fig. 2.17: SEM images of electrospun gelatin samples after GA crosslinking ( $c_{GA} = 50\%$ ,  $V = 5$  ml) for different times: (a) 2 hours; (b) 3 hours; (c) 4 hours; (d) 6 hours. Scale bar: 10  $\mu\text{m}$ .

In fact, results in literature showed that it is difficult to completely preserve fiber structure of the sample, and often even the optimal parameters affect sample morphology, which show partially fused fibers and decrease in porosity.

As volume of the solution used for crosslinking is usually not reported, for our tests we decided to use the smallest amount of solution that could completely cover the sample for all the duration of the treatment. In fact, GP major drawback is the high cost, and in this way we could limit the amount of GP necessary. GP concentrations and crosslinking time tested in this work were taken from literature. SEM images show that samples, for all the combination of parameters used, completely lost their morphology, resulting in films completely flat or where few fibers were still visible (Fig. 2.15). These results confirmed the problem related to the use of ethanol as solvent that had been highlighted in other works in literature<sup>32-33</sup>. Further process optimization would have been necessary; in particular, the investigation on a medium alternative to ethanol, that is a good solvent for GP but it is also able to preserve electrospun sample structure, is necessary. However, mainly because of the

high cost of GP, we decided not to go on in process optimization, and we focused more on the use of carbodiimides as crosslinking agents.

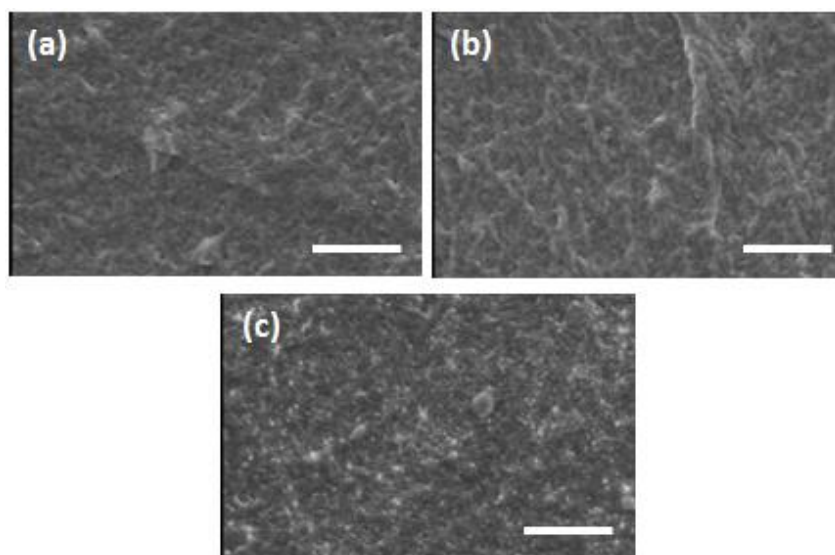


Fig. 2.18: SEM images of electrospun gelatin samples after immersion in 2.5% w/v GP crosslinking solution after different time: (a) 1 day; (b) 2 days; (c) 3 days. Scale bar = 20  $\mu\text{m}$ .

c. Dimethylaminopropyl ethyl carbodiimide (EDC) crosslinking: this molecule is widely studied for natural polymer crosslinking as it is a zero-length crosslinker, i.e. it favors new bond formation between specific functional groups of the protein, but it does not remain inside the molecular chains after the reaction occurred, thus avoiding any potential toxic effect for cells. As for GP, also EDC is solved in ethanol; the samples are then dipped in the solution in order for the reaction to take place. Therefore, the problem related to ethanol affecting fiber morphology remains; however, if EDC crosslinking reaction is more efficient than GP, it can preserve fiber morphology and better results can be obtained. Results reported in literature are not uniform, as in some cases fiber morphology is completely lost and a film is formed, while in some other works fibers swell, but the porous morphology is preserved<sup>18, 35, 48</sup>.

In this work, different solution concentrations and crosslinking time were considered, using literature parameters as reference. However, even for the wide



range of parameters investigated, no suitable morphology of the samples was obtained, as scaffolds did not retain their electrospun structure as a consequence of fiber swelling and pore occlusion; as example, SEM images after 2 days of crosslinking at different EDC concentrations are reported (Fig. 2.16). As in the case of GP, this can be caused by ethanol, used as medium to solve EDC and carry out the reaction, which evidently affect fiber morphology during the treatment. Therefore, in future studies it would be interesting to investigate alternative solvents for EDC crosslinking method.

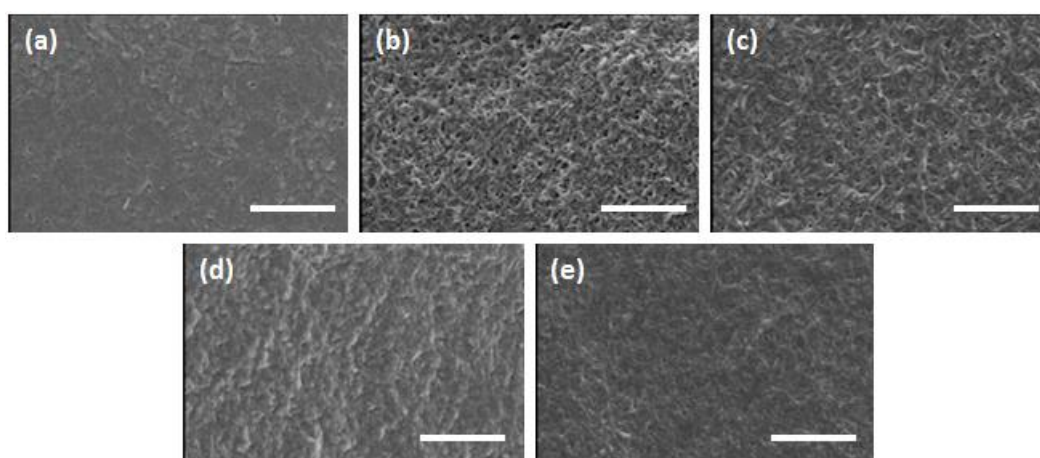


Fig. 2.19: SEM images of electrospun gelatin samples after 2 days of immersion in EDC crosslinking solution at different concentrations: (a) 0.5% w/v; (b) 1% w/v; (c) 2% w/v; (d) 2.5% w/v; (e) 5% w/v. Scale bar = 20  $\mu\text{m}$ .

## 4. Conclusions

Blends of gelatin/elastin and gelatin/elastin/HA with different compositions were electrospun using formic acid as only solvent (Table 2.9). The possibility to tune chemical composition of electrospun membranes according to the application intended is extremely useful in tissue engineering field, as these scaffolds can better mimic the complex chemical structure of ECM in different tissues and can have tailorable mechanical properties according to their composition. Moreover, a non-fluorinated, less toxic and less expensive solvent with respect to the one used in literature for collagen-elastin ES (i.e. HFIP) was used, thus proposing gelatin/elastin blend as an interesting alternative to collagen/elastin ones.

Another advantage in employing gelatin instead of collagen is related to the great batch-to-batch variability of collagen: in fact, optimization of collagen ES process carried out in this work demonstrated that solutions prepared from different collagen batches can be properly electrospun using quite different parameters, specific for each batch. Gelatin, instead, did not show any significant variability depending on the different batches used during the work.

Different crosslinking methods, both physical and chemical, have been investigated in order to improve electrospun membrane stability; however, some of them demonstrated not to be adequate for this aim. In particular, UV irradiation was not effective in prolong degradation kinetics, while GP and EDC crosslinking significantly affected electrospun fiber morphology. Therefore, the methods that proved to be the most suitable are DHT treatment and GA crosslinking, as they were both able to preserve fiber morphology while increasing gelatin membrane stability up to some days.

Table 2.10: composition of gelatin/elastin and gelatin/elastin/HA solutions optimized for ES process.

<b>Total polymer concentration [% w/v]</b>	<b>Gelatin/elastin ratio</b>	<b>Amount of HA with respect to total concentration [% w/w]</b>
20	7/3	-
22	9/1	-
10	9/1 7/3	8
13	9/1 7/3	5

In future it would be interesting to characterize the membranes produced and compare their properties, in particular by mechanical and biological tests, in order to evaluate the effect of different chemical compositions and determine the appropriate blend for different soft tissue applications (e.g. skin, adipose tissue, nerves, connective tissue).

## References

1. Catalina, M.; Attenburrow, G. E.; Cot, J.; Covington, A. D.; Antunes, A. P. M., Influence of crosslinkers and crosslinking method on the properties of gelatin films extracted from leather solid waste. *J Appl Polym Sci* **2011**, *119* (4), 2105-2111.
2. Hoch, E.; Schuh, C.; Hirth, T.; Tovar, G. E.; Borchers, K., Stiff gelatin hydrogels can be photo-chemically synthesized from low viscous gelatin solutions using molecularly functionalized gelatin with a high degree of methacrylation. *Journal of Materials Science: Materials in Medicine* **2012**, *23* (11), 2607-2617.
3. Ki, C. S.; Baek, D. H.; Gang, K. D.; Lee, K. H.; Um, I. C.; Park, Y. H., Characterization of gelatin nanofiber prepared from gelatin–formic acid solution. *Polymer* **2005**, *46* (14), 5094-5102.
4. Kretlow, J. D.; Klouda, L.; Mikos, A. G., Injectable matrices and scaffolds for drug delivery in tissue engineering. *Adv Drug Deliver Rev* **2007**, *59* (4-5), 263-273.
5. Madaghiele, M.; Piccinno, A.; Saponaro, M.; Maffezzoli, A.; Sannino, A., Collagen- and gelatine-based films sealing vascular prostheses: evaluation of the degree of crosslinking for optimal blood impermeability. *J Mater Sci-Mater M* **2009**, *20* (10), 1979-1989.
6. Powell, H.; Boyce, S., Fiber density of electrospun gelatin scaffolds regulates morphogenesis of dermal–epidermal skin substitutes. *J Biomed Mater Res A* **2008**, *84* (4), 1078-1086.
7. Zhang, Y.; Venugopal, J.; Huang, Z.-M.; Lim, C.; Ramakrishna, S., Crosslinking of the electrospun gelatin nanofibers. *Polymer* **2006**, *47* (8), 2911-2917.
8. Heydarkhan-Hagvall, S.; Schenke-Layland, K.; Dhanasopon, A. P.; Rofail, F.; Smith, H.; Wu, B. M.; Shemin, R.; Beygui, R. E.; MacLellan, W. R., Three-dimensional electrospun ECM-based hybrid scaffolds for cardiovascular tissue engineering. *Biomaterials* **2008**, *29* (19), 2907-2914.
9. Huang, Z.-M.; Zhang, Y.; Ramakrishna, S.; Lim, C., Electrospinning and mechanical characterization of gelatin nanofibers. *Polymer* **2004**, *45* (15), 5361-5368.
10. Choktaweessap, N.; Arayanarakul, K.; Aht-Ong, D.; Meechaisue, C.; Supaphol, P., Electrospun gelatin fibers: effect of solvent system on morphology and fiber diameters. *Polymer journal* **2007**, *39* (6), 622-631.
11. Kuijpers, A. J.; Engbers, G. H. M.; Krijgsveld, J.; Zaat, S. A. J.; Dankert, J.; Feijen, J., Cross-linking and characterisation of gelatin matrices for biomedical applications. *J Biomat Sci-Polym E* **2000**, *11* (3), 225-243.
12. Lee, K. Y.; Mooney, D. J., Hydrogels for tissue engineering. *Chem Rev* **2001**, *101* (7), 1869-1879.
13. Ozeki, M.; Tabata, Y., In vivo degradability of hydrogels prepared from different gelatins by various cross-linking methods. *Journal of Biomaterials Science, Polymer Edition* **2005**, *16* (5), 549-561.
14. Liu, H. C.; Yao, C. H.; Sun, J. S.; Lee, C. J.; Huang, C. W.; Lin, F. H., Osteogenic evaluation of glutaraldehyde crosslinked gelatin composite with fetal rat calvarial culture model. *Artificial organs* **2001**, *25* (8), 644-654.

15. Lau, T. T.; Lee, L. Q. P.; Leong, W.; Wang, D.-A., Formation of model hepatocellular aggregates in a hydrogel scaffold using degradable genipin crosslinked gelatin microspheres as cell carriers. *Biomedical Materials* **2012**, *7* (6), 065003.
16. Grover, C. N.; Gwynne, J. H.; Pugh, N.; Hamaia, S.; Farndale, R. W.; Best, S. M.; Cameron, R. E., Crosslinking and composition influence the surface properties, mechanical stiffness and cell reactivity of collagen-based films. *Acta Biomater* **2012**, *8* (8), 3080-3090.
17. Gomes, S.; Rodrigues, G.; Martins, G.; Henriques, C.; Silva, J., In vitro evaluation of crosslinked electrospun fish gelatin scaffolds. *Materials Science and Engineering: C* **2013**, *33* (3), 1219-1227.
18. Lian, Y.; Yuan, L.; Ji, L.; Zhang, K., Gelatin/hyaluronic acid nanofibrous scaffolds: biomimetics of extracellular matrix. *Acta biochimica et biophysica Sinica* **2013**, gmt032.
19. Balasubramanian, P.; Prabhakaran, M. P.; Kai, D.; Ramakrishna, S., Human cardiomyocyte interaction with electrospun fibrinogen/gelatin nanofibers for myocardial regeneration. *Journal of Biomaterials Science, Polymer Edition* **2013**, *24* (14), 1660-1675.
20. Daamen, W.; Van Moerkerk, H. T. B.; Hafmans, T.; Buttafoco, L.; Poot, A.; Veerkamp, J.; Van Kuppevelt, T., Preparation and evaluation of molecularly-defined collagen–elastin–glycosaminoglycan scaffolds for tissue engineering. *Biomaterials* **2003**, *24* (22), 4001-4009.
21. Daamen, W. F.; Nillesen, S. T.; Wismans, R. G.; Reinhardt, D. P.; Hafmans, T.; Veerkamp, J. H.; Van Kuppevelt, T. H., A biomaterial composed of collagen and solubilized elastin enhances angiogenesis and elastic fiber formation without calcification. *Tissue Eng Pt A* **2008**, *14* (3), 349-360.
22. Hsu, F.-Y.; Hung, Y.-S.; Liou, H.-M.; Shen, C.-H., Electrospun hyaluronate–collagen nanofibrous matrix and the effects of varying the concentration of hyaluronate on the characteristics of foreskin fibroblast cells. *Acta Biomater* **2010**, *6* (6), 2140-2147.
23. Fischer, R. L.; McCoy, M. G.; Grant, S. A., Electrospinning collagen and hyaluronic acid nanofiber meshes. *J Mater Sci-Mater M* **2012**, *23* (7), 1645-1654.
24. Pham, Q. P.; Sharma, U.; Mikos, A. G., Electrospinning of polymeric nanofibers for tissue engineering applications: a review. *Tissue Eng* **2006**, *12* (5), 1197-1211.
25. Song, J.-H.; Kim, H.-E.; Kim, H.-W., Production of electrospun gelatin nanofiber by water-based co-solvent approach. *Journal of Materials Science: Materials in Medicine* **2008**, *19* (1), 95-102.
26. Chen, H. C.; Jao, W. C.; Yang, M. C., Characterization of gelatin nanofibers electrospun using ethanol/formic acid/water as a solvent. *Polym Advan Technol* **2009**, *20* (2), 98-103.
27. Ratanavaraporn, J.; Rangkupan, R.; Jeeratawatchai, H.; Kanokpanont, S.; Damrongsakkul, S., Influences of physical and chemical crosslinking techniques on electrospun type A and B gelatin fiber mats. *Int J Biol Macromol* **2010**, *47* (4), 431-438.
28. Weadock, K. S.; Miller, E. J.; Bellincampi, L. D.; Zawadsky, J. P.; Dunn, M. G., Physical crosslinking of collagen fibers: comparison of ultraviolet irradiation and dehydrothermal treatment. *J Biomed Mater Res* **1995**, *29* (11), 1373-1379.
29. Wang, X.; Um, I. C.; Fang, D.; Okamoto, A.; Hsiao, B. S.; Chu, B., Formation of water-resistant hyaluronic acid nanofibers by blowing-assisted electro-spinning and non-toxic post treatments. *Polymer* **2005**, *46* (13), 4853-4867.

30. Ohan, M. P.; Weadock, K. S.; Dunn, M. G., Synergistic effects of glucose and ultraviolet irradiation on the physical properties of collagen. *J Biomed Mater Res* **2002**, *60* (3), 384-391.
31. Lin, W.-H.; Tsai, W.-B., In situ UV-crosslinking gelatin electrospun fibers for tissue engineering applications. *Biofabrication* **2013**, *5* (3), 035008.
32. Sisson, K.; Zhang, C.; Farach-Carson, M. C.; Chase, D. B.; Rabolt, J. F., Evaluation of cross-linking methods for electrospun gelatin on cell growth and viability. *Biomacromolecules* **2009**, *10* (7), 1675-1680.
33. Panzavolta, S.; Giofrè, M.; Focarete, M. L.; Gualandi, C.; Foroni, L.; Bigi, A., Electrospun gelatin nanofibers: optimization of genipin cross-linking to preserve fiber morphology after exposure to water. *Acta Biomater* **2011**, *7* (4), 1702-1709.
34. Mekhail, M.; Wong, K. K. H.; Padavan, D. T.; Wu, Y.; O'Gorman, D. B.; Wan, W., Genipin-cross-linked electrospun collagen fibers. *Journal of Biomaterials Science, Polymer Edition* **2011**, *22* (17), 2241-2259.
35. Fiorani, A.; Gualandi, C.; Panseri, S.; Montesi, M.; Marcacci, M.; Focarete, M. L.; Bigi, A., Comparative performance of collagen nanofibers electrospun from different solvents and stabilized by different crosslinkers. *Journal of Materials Science: Materials in Medicine* **2014**, *25* (10), 2313-2321.
36. Barnes, C. P.; Pemble IV, C. W.; Brand, D. D.; Simpson, D. G.; Bowlin, G. L., Cross-linking electrospun type II collagen tissue engineering scaffolds with carbodiimide in ethanol. *Tissue Eng* **2007**, *13* (7), 1593-1605.
37. Jha, B. S.; Ayres, C. E.; Bowman, J. R.; Telemeco, T. A.; Sell, S. A.; Bowlin, G. L.; Simpson, D. G., Electrospun collagen: a tissue engineering scaffold with unique functional properties in a wide variety of applications. *Journal of Nanomaterials* **2011**, *2011*, 7.
38. Rho, K. S.; Jeong, L.; Lee, G.; Seo, B.-M.; Park, Y. J.; Hong, S.-D.; Roh, S.; Cho, J. J.; Park, W. H.; Min, B.-M., Electrospinning of collagen nanofibers: effects on the behavior of normal human keratinocytes and early-stage wound healing. *Biomaterials* **2006**, *27* (8), 1452-1461.
39. Jiang, Q.; Reddy, N.; Zhang, S.; Roscioli, N.; Yang, Y., Water-stable electrospun collagen fibers from a non-toxic solvent and crosslinking system. *J Biomed Mater Res A* **2013**, *101* (5), 1237-1247.
40. Foltran, I.; Foresti, E.; Parma, B.; Sabatino, P.; Roveri, N. In *Novel biologically inspired collagen nanofibers reconstituted by electrospinning method*, Macromolecular symposia, Wiley Online Library: 2008; pp 111-118.
41. Bürck, J.; Heissler, S.; Geckle, U.; Ardakani, M. F.; Schneider, R.; Ulrich, A. S.; Kazanci, M., Resemblance of electrospun collagen nanofibers to their native structure. *Langmuir* **2013**, *29* (5), 1562-1572.
42. Dong, B.; Arnoult, O.; Smith, M. E.; Wnek, G. E., Electrospinning of collagen nanofiber scaffolds from benign solvents. *Macromolecular rapid communications* **2009**, *30* (7), 539-542.
43. Nivison-Smith, L.; Rnjak, J.; Weiss, A. S., Synthetic human elastin microfibers: stable cross-linked tropoelastin and cell interactive constructs for tissue engineering applications. *Acta Biomater* **2010**, *6* (2), 354-359.

44. McKenna, K. A.; Gregory, K. W.; Sarao, R. C.; Maslen, C. L.; Glanville, R. W.; Hinds, M. T., Structural and cellular characterization of electrospun recombinant human tropoelastin biomaterials. *J Biomater Appl* **2012**, *27* (2), 219-230.
45. Rnjak-Kovacina, J.; Wise, S. G.; Li, Z.; Maitz, P. K.; Young, C. J.; Wang, Y.; Weiss, A. S., Tailoring the porosity and pore size of electrospun synthetic human elastin scaffolds for dermal tissue engineering. *Biomaterials* **2011**, *32* (28), 6729-6736.
46. Brenner, E. K.; Schiffman, J. D.; Thompson, E. A.; Toth, L. J.; Schauer, C. L., Electrospinning of hyaluronic acid nanofibers from aqueous ammonium solutions. *Carbohydrate Polymers* **2012**, *87* (1), 926-929.
47. Yao, S.; Wang, X.; Liu, X.; Wang, R.; Deng, C.; Cui, F., Effects of ambient relative humidity and solvent properties on the electrospinning of pure hyaluronic acid nanofibers. *J Nanosci Nanotechnol* **2013**, *13* (7), 4752-4758.
48. Kim, T. G.; Chung, H. J.; Park, T. G., Macroporous and nanofibrous hyaluronic acid/collagen hybrid scaffold fabricated by concurrent electrospinning and deposition/leaching of salt particles. *Acta Biomater* **2008**, *4* (6), 1611-1619.

## Chapter 3 – Study on fibrinogen stability at acidic pH and electrospinning of fibrinogen/gelatin blend

---

---

*Blends of fibrinogen and gelatin were electrospun using formic acid as solvent. Effect of the acidic solvent used on fibrinogen structure was investigated by both experimental (SDS-PAGE, circular dichroism spectroscopy, rheology, photon correlation imaging) and computational (molecular dynamics simulations) techniques. The membranes were stable in aqueous environment up to 7-10 days.*

---

# 1. Introduction

The fabrication of biomimetic scaffolds with tailored architecture made from natural polymers is an active area of research in tissue engineering field. In this regard, one of the major goal is to reach the complexity of the extracellular matrix (ECM) which is characterized by a dynamic network composed by polysaccharide and protein fibers with diameters between 50 and 500 nm<sup>1-6</sup>. Interactions between cells and ECM, that are fundamental for tissue homeostasis and repair, are mediated by cell surface receptors, integrins being the most important family of these receptors, that recognize RGD aminoacid sequence<sup>7-8</sup>.

Therefore, an ideal scaffolding should not only define the three-dimensional organization of the tissue-engineered space and offer structural support for cells, but it should also mimic the biological (i.e. surface chemistry) and morphological (i.e. nanometer sized fibers) properties of the ECM to favor cell-matrix adhesion and influence their behavior by specific signal sequences<sup>8-10</sup>. Other fundamental properties of scaffolds are the high surface-to-volume ratio and open porosity for better cell migration and perfusion, the biodegradability with adequate degradation kinetics, the mechanical properties similar to those of the native tissue, and the ability not to elicit an inflammatory response<sup>2, 11-12</sup>.

Natural polymers are widely studied as scaffold materials due to their similarities with the ECM, their good biological performances and the reduced inflammatory host response<sup>13</sup>. Among them, fibrinogen is of particular interest for tissue engineering. Fibrinogen is a globular protein present in the blood plasma; after thrombin cleavage it is converted into fibrin, which acts as the most important structural molecule in clot formation and forms a physiological provisional scaffold for cell adhesion and proliferation during tissue repair and wound healing<sup>14-15</sup>. In addition, fibrinogen and fibrin contain integrin binding sites (i.e. RGD domains) which commonly bind fibroblasts and endothelial cells, and have also high affinity towards some growth factors (i.e. fibroblast growth factor and vascular endothelial growth factor) and several other cytokines<sup>16-17</sup>. Thanks to its capacity to bind a wide variety of cells and molecules, fibrinogen can be used in biomedical applications not only as a



hemostatic agent or wound dressing material, but also as scaffold for tissue engineering<sup>6</sup>. In fact, it has been reported that fibrinogen based scaffolds induce better cell interaction and matrix remodeling compared to synthetic scaffolds<sup>18</sup>. Furthermore, fibrinogen has low immunogenicity and does not cause inflammatory response; it also offers the possibility to be autologously harvested from patient blood, thus eliminating any possible immune reaction<sup>15, 19</sup>. Moreover, fibrinogen scaffolds are resistant to hydrolysis degradation, but they are degraded by proteinases found in serum.

Different fabrication techniques that allow the production of nanofibrous scaffolds are on studies: drawing, template synthesis, phase separation, self-assembly, and electrospinning<sup>20</sup>. Among them, electrospinning (ES) process presents many unique advantages: it is a versatile technique, as for example it can also be applied to natural polymers, the set-up is simple and not expensive, and finally it offers the possibility to tune scaffold shape and fiber morphology and orientation by easily adjusting process parameters<sup>21-22</sup>. Due to their unique structure, electrospun matrices present a high surface-to-volume ratio and interconnected porosity: these features, as already said, are important to favor cell attachment and allow efficient mass transport of nutrients, oxygen and waste products<sup>22</sup>.

Despite the promising features of electrospun fibrinogen nanofibers for tissue engineering applications, ES of fibrinogen remains a challenging process, as for the vast majority of natural polymers. The stability of fibrinogen tertiary structure reduces its capacity to unravel in an extensional flow field, and, as a consequence, solution viscoelasticity is not adequate for jet stabilization<sup>23</sup>. Moreover, it is difficult to find a suitable solvent for fibrinogen ES; solvent is a key factor in this process, as it should solubilize the protein, hence breaking intra- and inter-molecular bonds, solvate polymer molecules, and it should evaporate quickly to allow the formation of dry fibers on the collector<sup>7</sup>. Electrospun fibrinogen fibers have been usually produced from hexafluoro iso-propanol (HFIP) or trifluoro ethanol (TFE) solution, as these solvents cause protein denaturation due to their strong interaction with both polar and non-polar amino acid side groups<sup>19, 24-25</sup>. However, HFIP and TFE have been reported to be corrosive and highly toxic other than expensive<sup>26</sup>.

We recently tested a less expensive and less toxic solvent system composed by formic and acetic acids<sup>27</sup>. Results showed a fibrous mat with fibers random or aligned (according to the collector used), and diameters in physiological range. *In vitro* tests demonstrated good cytocompatibility of the electrospun membranes, as cells well adhered and proliferate on fibrinogen matrices. Nonetheless, during ES process solution gelification at the tip of the spinneret occurred hence resulting in a non-continuous jet. Moreover, there was evidence that after solubilisation in acids fibrinogen was no longer soluble in PBS, both in electrospun form and also as solvent-casted film, thus suggesting that the solvents, and not the process, had a major role in inducing this effect.

Because of the promising applications of fibrinogen matrices electrospun from acidic solvent system, in this work solution gelification phenomenon has been investigated in details, by means of analysis techniques ranging from nano- to macro-scale, in order to find possible solutions to this problematic behavior during ES process.

## 2. Materials and methods

### 2.1 Electrospinning of fibrinogen and fibrinogen/gelatin blends

The biopolymers used in this work, i.e. fibrinogen and gelatin, were purchased from Sigma-Aldrich and used with no further purification; material information are reported in Table 3.1:

Table 3.11: Product information of fibrinogen and gelatin used with indication of their molecular weight.

Material	Molecular weight [kDa]
Fibrinogen from bovine plasma (F8630)	340
Gelatin A from porcine skin (G1890)	50 – 100

In order to investigate the optimal solution for fibrinogen ES, some solvents commonly used for ES process were considered; they were all purchased from Sigma Aldrich: phosphate buffer saline (PBS), hexafluoroisopropanol (HFIP), trifluoroacetic acid (TFA),

ethanol (EtOH), formic acid (FA), acetic acid (AA). The main properties of these solvents are reported in Chapter 2, Table 2.2. Moreover, 1M solutions of citric acid and hydrochloric acid were prepared and used for solubility test.

### **Solubility tests**

In order to investigate good solvents for fibrinogen, preliminary solubility tests were carried out: the concentration used for all the tests was 2% w/v and homogeneity of the solution was evaluated simply by looking at it after 2 days of stirring at room temperature.

### **Electrospinning of fibrinogen and fibrinogen/gelatin blends**

The setup described in Chapter 2.2 was used. Despite the successful ES of fibrinogen obtained in previous works in terms of fiber morphology<sup>27</sup> derived from a systematic and extensive experimental campaign to optimize process parameter, ES process was not continuous because solution gelification at the tip of the spinneret occurred; in order to eliminate this problem, different strategies were considered, concerning the variation of solution or process parameters. In particular, small amounts of water (i.e. 10% and 20% v/v) or salts (NaCl, KHPO<sub>4</sub>) were added to the solution; in fact, water molecules and salts have the possibility to form hydrogen or ionic bonds with fibrinogen molecules, thus reducing inter-molecular interactions and possibly hindering gelification. Another approach was to decrease fibrinogen concentration from 12 to 6% w/v, as usually gelification kinetics is dependent on molecule concentration. Also process parameters were varied: in particular, flow rate was doubled with the intention of maintain a bigger and liquid drop of solution at the end of the spinneret, thus lowering gelification rate. For ES of fibrinogen/gelatin blend, both solution and process parameters were taken from pure fibrinogen ES. In particular, solvent system and polymer total concentration were kept fixed, while different fibrinogen/gelatin ratios were tested. Solution and process parameters are summarized in Table 3.2.

Table 3.12: Solution, process and ambient parameters used for electrospinning of fibrinogen/gelatin blends.

Solvent	Total concentration [% w/v]	Fibrinogen/gelatin ratio	Voltage [kV]	Flow rate [ml/h]	Distance [cm]	Temperature [°C]	Relative humidity [%]
FA/AA (3/2)	12	5/1, 3/1, 2/1, 1/1	24	0.3	12	20 – 26	25 – 45

### Evaluation of process stability

In order to check Taylor cone formation and stability of ES process, with specific attention to solution gelification at the tip of the spinneret, a custom-designed optical imaging system was used. In particular, this instrument allowed to observe the kinetics of solution gelification for the different blend compositions, thus helping in determining the optimal solution for stable and continuous ES. The description of imaging system and its detailed information are reported in Chapter 2, paragraph 2.3.

### Morphological analysis

Morphology of the samples obtained by ES of different fibrinogen/gelatin blends was examined via scanning electron microscopy (SEM, Cambridge Stereoscan 360). Dry samples were mounted onto aluminum stubs, sputter coated with gold, and imaged with a 10 kV accelerating voltage. Fiber diameter was measured by image analysis with ImageJ software, measuring 100 fibers per type of sample. Fiber diameter is reported as average  $\pm$  standard deviation.

### Degradation tests

In order to evaluate stability of electrospun matrices in aqueous environment, circular samples ( $\varnothing = 13$  mm) were punched from electrospun membranes of pure fibrinogen or fibrinogen/gelatin blend, and were immersed in 1 ml of PBS. Then, they were put in an oven at 37°C until dissolution occurred. As fibrinogen after ES is no more rapidly soluble in PBS, we wanted to investigate if this effect was related to the acidic solvent system or to ES process. For this purpose, films of fibrinogen in acid solvent were used: a 12% w/v

solution of fibrinogen in FA/AA (3/2) was prepared, and then films were obtained by solvent casting of 500  $\mu$ l drops. Films were left under the hood overnight to allow solvent evaporation. Finally, degradation tests were carried out as explained for electrospun samples.

## **2.2 Study of fibrinogen molecular structure and investigation on gelification process**

### **SDS-PAGE analysis**

The theoretical basis of this technique are reported in Chapter 2, paragraph 2.5. In this work, SDS-PAGE of fibrinogen after solubilisation in formic acid was carried out, in order to investigate the formation of new covalent bonds, resulting in longer molecular chains, that could explain solution gelification. Possible hydrolysis of molecules due to the solvent effect could also be studied. SDS-PAGE analyses were similarly performed on fibrinogen dissolved in formic acid aqueous solution at pH 4 to evaluate the influence of a slight acidic pH, in HFIP to compare the effect on protein molecules due to the fluorinated solvent commonly used in literature for fibrinogen ES, and in PBS as control. Fibrinogen was dissolved in all the solvents considered ( $c = 12\%$  w/v), and then solvent casted films were obtained as previously reported. Because this technique is highly sensitive to the pH and to small amount of solvent residues that can affect the results, solvent traces in fibrinogen films were completely removed by use of a vacuum pump before analysis. SDS-PAGE electrophoresis was carried out with PowerPacHC using 4-15% gradient gel (Mini-PROTEAN TGX Gel), both purchased from BIORAD. Each sample was submitted to reducing treatment with Laemmli buffer and  $\beta$ -mercaptoethanol (1 mg fibrinogen/1ml solution 0.375 M Laemmli + 5% v/v  $\beta$ -mercaptoethanol) at 95°C for 5 minutes. This treatment allowed the break of disulphide bonds which are naturally present between different peptidic chains of the protein; formation of disulphide bonds as a consequence of the acidic treatment could be excluded as an oxidizing environment and complex biochemical phenomena are involved in S-S bond formation.

After brief centrifugation, two different amounts of fibrinogen for each sample were loaded in the gel (i.e. 5 and 10  $\mu\text{g}$ ); the gel was then submitted to electrophoretic run (90-140 V) using two different protein standards, Kaleidoscope and Dual Color (BIORAD). At the end of the run, SDS-PAGE slide was treated with a fix solution composed by 50% v/v of methanol and 10% v/v of acetic acid for protein fixing, and then colored with Coomassie Brilliant Blue (BIORAD, 0.2% w/v in the same solution used for fixing).

### **Molecular Dynamics simulations**

The aim of Molecular Dynamics (MD) simulations is understanding the properties (of assemblies) of molecules at the nanoscale level, in terms of structures, properties and microscopic interactions between them. Usually it is extremely difficult and sometimes even impossible to obtain this information in other, experimental, ways.

MD simulation is a computer simulation method which uses mathematical models to simulate atomic and molecular systems. In particular, it consists of the numerical, step-by-step, solution of the classical equations of motion, which for a simple atomic system may be written as:

$$m_i \ddot{r}_i = f_i \quad f_i = -\partial U / \partial r_i$$

where  $r_i$  is representative of the geometrical information of the  $i$ -atom and  $f_i$  is the force acting on the  $i$ -atom. For this purpose, we need to calculate the forces  $f_i$ , which are usually derived from a force field defined by the potential energy function  $U(r^N)$ , (where  $r^N = (r_1; r_2, \dots, r_N)$  represents the complete set of  $3N$  atomic coordinates). This mathematical function depends on the positions of the atoms composing the system and on the interactions between these atoms. The interaction energies composing the potential function can be divided in bond and non-bond terms. In particular, bond energy term includes covalent bond, angle, and dihedral angle energies; non-bond energy term consists of electrostatic and Van der Waals energy, hydrogen bonds, and hydrophobic interactions.

To limit the computational cost of calculating all the terms of the potential function, different simplifications are usually applied to the models. To mimic real physiological conditions of biological molecules, these cannot be simulated into a void ambient; usually

they are simulated in water. The most common method to reproduce a water ambient with an acceptable computational cost is to use a water box. To avoid side effects, the box dimensions should be too big to be computationally acceptable; for this reason, a finite box is used, treated as an elementary cell and replicated periodically in all directions. This periodic repetition simulates an infinite ambient where every time a molecule exits the box another one enters it. To further reduce computational cost, it is possible to mimic biological environment using an implicit solvent characterized by its dielectric constant.

To speed up the computation, simplifications are applied also on computation of non-bonded interactions among atoms. The simplest one consists in imposing a cut-off distance (usually between 8 to 14Å) beyond which all the non-bonded interaction are ignored. However, the abruptly knocking down of the interactions may still cause high energy fluctuations and several different functions to terminate the interaction between two atoms have been developed over the years. These functions usually gently bring interactions values to zero (e.g. *shift* method and *switch* method).

The initial configuration of the built system is usually characterized by atom displacements which are not energetically acceptable because of unfavorable interactions. Therefore, before the starting of the dynamic it is necessary to apply an energy minimization. Minimization process uses algorithms which provide energy to the system so that it is able to explore the space and find configuration of energy minima (which depend on positions of the atoms composing the system). These algorithms are able to find only the local minimum close to the starting point and not the point of global equilibrium of the system. After the minimization process, it is possible to start the real dynamic, which is, as previously explained, a determinist process governed by the Newton's law equation. By integrating the equation step-by-step it is possible to compute the position of each *i*-atom in time, obtaining the time dependent behavior of the molecular system. All the positions collected result in a time series of conformations; this is called trajectory followed by each atom in accordance with Newton's laws of motion. However, an analytical solution of the equation is not possible and it has to be solved numerically. Starting from initial velocities given by the temperature imposed on the system, numerical integrators, which apply finite

different schemes to compute velocity, acceleration and position of each atom at each time step, are used to solve the equation: Verlet algorithm, Leap-frog algorithm, velocity Verlet, Beeman algorithm. The time step determines the frequency of velocity and position calculation. This parameter has to be chosen smaller than the fastest oscillation period of the atoms in the system, usually the vibration of C-H bonds. It is generally in the order of femtoseconds. Different kind of simulations, called *ensembles*, can be developed depending on the imposed conditions: *ensemble* NVT (constant number of molecules, temperature and volume), *ensemble* NPT (constant number of molecules, pressure and temperature), *ensemble* NVE (constant number of molecule, volume and energy). Most used *ensembles* are NVT and NPT, which involved the use of a thermostat or a thermostat and a barostat, respectively. Once the dynamic reaches the equilibrium state, it is possible to collect average properties of the system. The achievement of equilibrium state is usually identified by monitoring RMSD (root mean square deviation) mediated on all atoms of the molecule; when its variation reduced significantly, its plot in time reaches a plateau-like shape, and the system is considered at equilibrium<sup>28</sup>.

In this work, MD simulations were carried out in order to investigate more in details the effect of acidic pH on fibrinogen conformation and configuration. In fact, simulations allow to study fibrinogen molecule at different pH on a nanometric scale, that otherwise would require very complex and extremely time-expensive experimental analyses. The crystal structures of human fibrinogen were taken from the PDB entry 3GHG. The crystallographic data on fibrinogen structure are incomplete because there are missing unstructured portions; accordingly, these portions were not included in the virtual structures. As previously explained, fibrinogen is a dimer of three peptidic chains ( $\alpha$ ,  $\beta$  and  $\gamma$ ) linked by disulphide bonds (Fig. 3.1). Focusing only on a single monomer, it is possible to identify two regions, the first (named head) consists of residues 138 to 200 of chain  $\alpha$ , and residues 197 to 458 of chain  $\beta$ ; the second (named tail) consists of residues 27 to 137 of chain  $\alpha$ , residues 58 to 196 of chain  $\beta$ , and the whole chain  $\gamma$ .

Its crystal structure is composed of almost two thousand aminoacids; therefore, MD simulations of the whole molecule appear extremely time consuming. For this reason, we



decided to exploit protein symmetry and consider only the monomer for MD simulations; furthermore, implicit solvent was employed to simulate the aqueous environment. MD simulations used CHARMM22 force field; the system was minimized and equilibrated using the NAMD code (Nelson) under constant volume and temperature (NVT) conditions. The temperature was set to 310 K, while using a time step of 2 fs, a non-bonded cut-off of 14 Å, rigid bonds and particle-mesh Ewald long-range electrostatics. Finally, the production run was performed using NAMD on a NVIDIA GeForce GT 640 GPU for a total time of about 100 ns, depending on molecular stability.

In order to simulate different pH values (i.e. 1, 4, and 7), protonation states of amino acid residues were changed. The side chain groups that can vary within this pH range are those of histidine, glutamic acid and aspartic acid: in fact, their pKa values are about 6, 4.2 and 3.8 respectively. Therefore, at physiological pH none of these residues are protonated. For simulations at pH 4 histidine and glutamic acid were protonated ( $\text{pH} < \text{pKa}$ ), and for pH 1 also aspartic acid residues were protonated. Topology and parameter files used for running the simulations already included information and parameters of the protonated residues, and they were referred to as HSP, GLUP, and ASPP. Therefore, for pH 4 and pH 1 simulations, instructions indicating the use of the parametrized protonated residue instead of the “classic” one were included in the tcl-script used to generate the file with protein structural information (i.e. psf file). Even if the topology file used for the simulations is optimized for environment at pH 7, it has been previously used in literature for non-physiological pH simulations<sup>29-33</sup>, as in general topology parameters are obtained in mild conditions very close to neutral pH.

The stability of the system was checked by monitoring the convergence of the Root Mean Square Deviation (RMSD) of the protein. In order to evaluate the effect of acidic pH on fibrinogen molecule, we analyzed protein secondary structure, solvent accessible surface area, and intra-molecular H bonds. The timeline VMD tool was used to determine fibrinogen secondary structure, and a tcl-script was employed to determine the percentage of  $\alpha$ -helix and random coil in the protein. Solvent accessible surface area (SASA) is the surface area of a biomolecule that is accessible to a solvent; therefore, it gives information

about the folding/unfolding of a protein and its three dimensional shape. SASA for fibrinogen at different pH values was calculated by means of a tcl-script in VMD. Another parameter that can be related to molecular unfolding is the number of intra-molecular hydrogen bonds; in this work, hydrogen bonds were calculated by means of a tcl-scripts in VMD on a geometric basis (donor-acceptor distance  $< 3.2 \text{ \AA}$  and donor-hydrogen-acceptor angle  $< 40^\circ$ ).

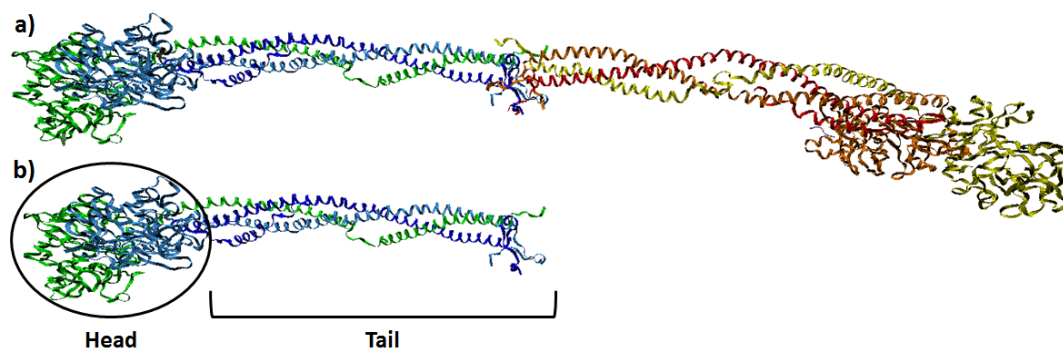


Fig. 3.20: Crystal structure of a) human fibrinogen and b) fibrinogen monomer considered for the MD simulations in this Chapter, with indication of head and tail regions.

### CD spectroscopy

Circular dichroism (CD) is the difference in the absorption by a chiral molecule of the two components, left-handed and right-handed, of circularly polarized light; the same term is used to refer to the spectroscopic technique based on this principle. Circularly polarized light is an electro-magnetic radiation whose electric field oscillates describing a helix; the helices can be either right-handed (R-CPL) or left-handed (L-CPL). Physical and chemical properties of a pair of enantiomers, i.e. mirror-image isomers not superimposable, are identical with two exceptions: the way they interact with polarized light and the way they interact with other chiral molecules. In fact, enantiomers absorb differently R-CPL and L-CPL (circular birefringence property); the resultant electric field vector coming out from the sample will have elliptical trajectory, i.e. light will be elliptically polarized. This phenomenon is CD. CD spectroscopy is used to study a wide range of chiral molecules, but it is in the study of large biological molecules where it finds its most important applications

(e.g. configurational assignment, conformational studies of proteins). In fact, CD spectrum is greatly influenced by the three dimensional structure of the macromolecules, and each structure has a specific CD signature. Therefore, CD spectra of proteins with different secondary or tertiary structure are different. In particular, CD spectrum in far-UV region (180 - 250 nm) is sensitive to secondary structure change, because the chromophore in this range is the peptidic bond, and different secondary structures cause a different interaction between adjacent peptidic bonds, thus greatly influencing CD spectrum. The types of secondary structure which give different contribution to CD spectrum are  $\alpha$ -helices,  $\beta$ -sheets and random coil (Fig.3.2).

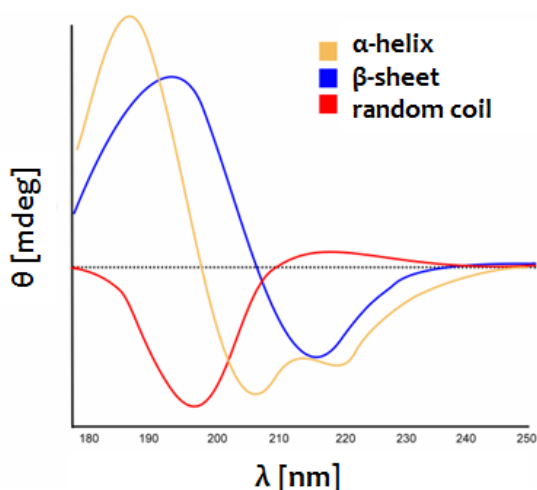


Fig. 3.21: Representative CD spectra in far-UV region for different types of secondary structure.

In this work, we used CD spectroscopy in order to investigate the possible denaturation effect of the solvent used for fibrinogen ES in the literature and in this work (HFIP and formic acid respectively). As for this latter, to understand the influence of the acidic pH alone on fibrinogen folding, we also used aqueous solutions of formic acid at pHs 4 and 1. CD spectra were acquired using a Jasco-J810 spectropolarimeter and analyzed by means of Jasco software, using a quartz rectangular cuvette (110-QS, Hellma Italia) with path length of 0.1 cm.

Fibrinogen was dissolved at a concentration of 1 mg/ml in the solvents tested. The final concentration of all CD samples was adjusted to 0.1 mg/ml by diluting the prepared stock solutions with an appropriate amount of the corresponding solvent and subsequently mixing. Solution of fibrinogen in PBS was prepared in the same way as control. CD spectra were recorded at 15°C over the wavelength interval of 190 – 260 nm. The spectra of the pure solvents were used as baseline and subtracted from the correspondent sample spectrum. The final sample spectra were obtained by averaging results from five scans for each sample.

### **Rheological measurements**

To investigate the rheological behavior of fibrinogen solution used for ES, a rheometer (Paar Physica MCR 300, Austria) equipped with a plate–cone system was used. Viscosity was measured at 20 °C in oscillation mode (frequency and angular) with controlled shear rate: flow curves of viscosity and shear stress as function of shear rate, varying from 0.001 – 1000 1/s, are reported.

Important information about the solution behavior can be achieved also by measuring the storage modulus,  $G'$ , the loss modulus,  $G''$ , and  $\tan \delta$ . In fact, the storage modulus is related to the elastic solid-like behavior of the material, and to its ability to store energy, while the loss modulus is the viscous response and gives information about the ability of the material to dissipate energy; moreover,  $\tan \delta = G''/G'$  is a measure of material damping. In particular, if  $G'$  is larger than  $G''$ , then the material has some capacity to store energy and it behaves as an elastic solid, although not ideal as some of the mechanical energy is dissipated. On the contrary, if  $G''$  is larger than  $G'$ , it means that the mechanical energy given to the material is dissipated, and the material flows like a fluid. For monitoring  $G'$ ,  $G''$ , and  $\tan \delta$  a controlled-strain mode was selected, and their curves are reported as function of strain.

### **Photon correlation imaging and polarized light microscopy**

A novel and interesting technique to study gelation kinetics is Photon Correlation Imaging (PCI), as it allows to investigate the microscopic dynamics of spatially heterogeneous systems (e.g. a biopolymer solution undergoing gelation process) by means of light scattering. In fact, PCI is an optical correlation technique that, similarly to standard Dynamic Light Scattering (DLS), provides detailed information on the microscopic Brownian dynamics of colloidal systems and gels, while retaining the spatial resolution of an imaging system by investigating the local dynamics at distinct points within the scattering volume. Moreover, it allows to identify collective motion within the sample, i.e. to evaluate the presence of large-scale restructuring effects. A more detailed description of the technique has been furnished by L. Cipelletti and coworkers<sup>34</sup>. Basically, an image of the scattered volume is formed on a multi-pixel camera, observed at a given scattering angle  $\vartheta$  through a suitably stopped-down optics. A partially closed iris diaphragm is placed in the focal plane of the lens that, besides fixing the scattering wave-vector

$$q = (4\pi n/\lambda) \sin(\vartheta/2)$$

where  $\lambda$  is the incident wavelength and  $n$  is the sample refractive index, causes the image to become “speckled” because the intensity at each given point on the image plane originates from the interference of the field scattered by a finite-size region in the sample plane. In particular, the intensity on each speckle fluctuates in time according to the Brownian dynamics of the sample, but relative to the specific spatial location of the sample mapped on the image plane. This allows us to detect spatially-inhomogeneous dynamics. As the dynamics are slow, the time-dependence scattered intensity can be simultaneously measured over a large number of independent speckles using a multi-pixel detector (e.g. a CMOS camera), obtaining the ensemble-averaged correlation function via software analysis. The analysis of the images collected by the CMOS camera at first consists in grouping together a suitable block of adjacent pixels (also called a “region of interest”, ROI), over which the signal average and standard deviation are calculated. Then, the so-called “correlation index” (or “degree of correlation”)

$c_I(\tau; t, \mathbf{r})$  between two images taken at times  $t$  and  $t + \tau$  is introduced in order to have a general picture of the local dynamics:

$$c_I(\tau; t, \mathbf{r}) = \frac{\langle I_p(t)I_p(t + \tau) \rangle_r}{\langle I_p(t) \rangle_r \langle I_p(t + \tau) \rangle_r} - 1$$

where  $I_p$  is the scattered intensity measured by the  $p^{\text{th}}$  pixel and  $\langle \dots \rangle_r$  denotes an average over all the pixels within a ROI centered around  $\mathbf{r}$ . Therefore, the correlation index is related to the covariance between the intensity measured on the same speckle at two different times, sampled over the given ROI. This time-dependence yields the basic features of the gelation process. Provided that the investigated kinetics is sufficiently slow, the statistical accuracy can be enhanced by time-averaging  $c_I(\tau; t, \mathbf{r})$  over a time window  $\delta t$  that is much shorter than the characteristic evolution time of the investigated kinetics, which allows reduction of statistical noise due to finite sampling on the limited number of pixels in a ROI. The local dynamics can then be quantified by defining:

$$g_2(\tau) - 1 = \langle c_I(\tau; t, \mathbf{r}) \rangle_{\delta t}$$

This ‘coarse-grained’ correlation index bears the same information of the ensemble-averaged correlation function measured in a standard DLS experiment, but with better statistical accuracy due to pre-averaging over the speckles in a ROI<sup>35-36</sup>.

In this study, PCI technique was used simply to see the speckle pattern dynamics and the rearrangement of fibrinogen molecules in the solution during gelification, without any quantitative analysis of the data, in order to understand the effect on the whole solution related to protein denaturation caused by formic acid. The same fibrinogen solution optimized for ES process (i.e.  $c = 12\%$  w/v in formic acid-based solvent) was prepared for the analysis and placed in a cuvette (VWR International). Initially, we closed the cuvette and looked at the sample; however, as convective motion was observable, thus indicating the liquid nature of the solution, we decided to carry out the analysis on the open cuvette in order to allow solvent evaporation and (probably) faster gelification kinetics.

The sample was illuminated by a horizontal laser at  $\lambda = 656$  nm (SY Lasiris SNF501L, StockerYale), and imaged by a lens ( $f = 300$  mm) on a CMOS camera sensor (uEye 3370CP,

Imaging Development Systems GmbH) set at  $\vartheta = 90^\circ$  with respect to the illumination plane, with a diaphragm placed in the focal plane of the imaging lens.

After 3 days of analysis, the sample was also examined by an optical microscope (Prosilica GX1050) at a magnification 10x, and in polarized light in order to determine eventual orientation of fibrinogen molecules. In fact, the transmission of a polarized light passing through a sample can be influenced by the orientation of the molecules (e.g. highly order structuration) within the sample.

The same analysis was conducted on a drop of fibrinogen solution placed on a glass slide, in order to better simulate the environmental conditions during ES (i.e. high surface-to-volume ratio of the drop at the tip of the spinneret), where gelification occurs.

### **3. Results and discussion**

#### **3.1 Electrospinning of fibrinogen: effect of solution and process parameters on morphology and gelification kinetics**

In literature fibrinogen has always been electrospun using a 9/1 mixture of HFIP/minimal essential medium (MEM): this solvent system allows rapid solubilisation of the protein and rapid evaporation during fiber formation, so that adequate electrospun morphology with dry and homogeneous fibers can be obtained<sup>14, 25, 37-38</sup>. However, HFIP has a toxic and corrosive nature, and it is reported to induce change in fibrinogen secondary structure<sup>19</sup>. For this reason, my research group focused its attention on finding an alternative solvent, less cytotoxic and cheaper, for fibrinogen ES.

##### **Solubility tests**

Initially, fibrinogen solubility in different solvents was evaluated (Table 3.3). Results show that the protein was soluble in PBS, in fluorinated solvents and in formic acid, which proved to be the only good solvent among the acids tested, because of its ability to break molecular H-bonds. In order to avoid the use of fluorinated solvent, which is toxic, corrosive, and expensive, formic acid was chosen as main solvent for fibrinogen ES.





Table 3.13: Results of fibrinogen solubility tests.

Solvent	Solubility
PBS	✓
HFIP	✓
TFA	✓
EtOH	×
Formic acid	✓
Acetic acid	×
Citric acid 1M	×
Hydrochloric acid 1M	×

### Electrospinning of fibrinogen in acidic solvent system

In our group, we were able to optimize solution and process parameters in order to obtain electrospun fibrinogen fibers from formic acid-based solvent system: SEM images show adequate fiber morphology, with no defects and homogeneous fiber dimensions (fiber diameter =  $202 \pm 41$  nm, Fig. 3.3). However, the real-time imaging system revealed that ES process was not stable nor continuous: in fact, solution gelification at the tip of the spinneret occurred after 10-20 minutes, thus completely hindering jet formation and fiber spinning.

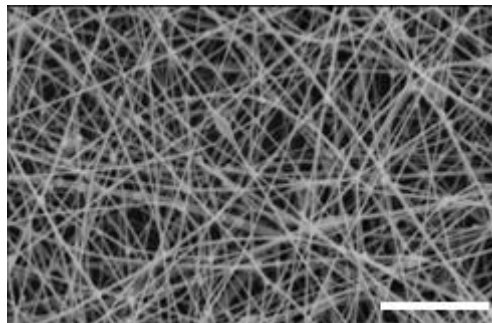


Fig. 3.22: SEM image of electrospun fibrinogen from acidic solvent system. Scale bar: 5  $\mu$ m.

Degradation tests in PBS at 37°C revealed that electrospun fibrinogen matrices were able to maintain their morphology up to two weeks, while raw fibrinogen was immediately soluble at the same conditions. In order to investigate if this effect was due to acidic solvent

or to ES process, we carried out the same degradation tests on fibrinogen films obtained by solvent casting of acidic fibrinogen solution: results showed that also fibrinogen films were stable in aqueous environment up to 20 days, thus suggesting that the solvent had major influence. Some works in literature<sup>25,37</sup> also report that fibrinogen becomes insoluble during ES, using HFIP as solvent. These studies speculate that ES conditions unfold fibrinogen molecule, hence exposing regions usually hidden that can interact by non-covalent forces (e.g. van der Waals) thus increasing membrane stability. Unluckily, no one of these studies reported the problem related to solution gelification during ES.

Changes in ES solution or process parameters were not effective in solving the question. For example, addition of salts or small amount of water in fibrinogen solution did not slow down gelification kinetics, while negatively affecting fiber morphology. Decreasing of fibrinogen concentration effectively improved solution processability by ES; however, such a low concentration was not sufficient to obtain adequate morphology and a lot of defects were present (Fig. 3.4). Even variations in process parameters did not succeed in solving the problem. In particular, the only parameter which seemed to have an effect on gelification kinetics was flow rate; in fact, by doubling it the solution gelled after 30-40 minutes. However, this value of flow rate was too high for fibrinogen ES, resulting in formation of big drops on the collector and beaded fibers (Fig. 3.5).

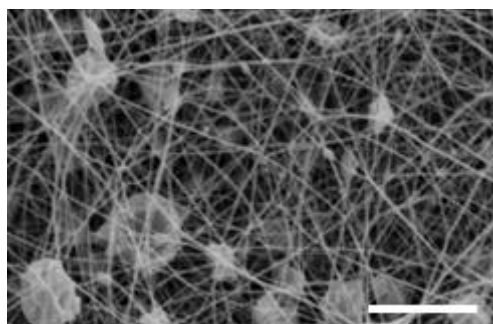


Fig. 3.23: SEM image of electrospun fibrinogen from 100 mg/mL solution concentration.  
Scale bar: 5  $\mu$ m.

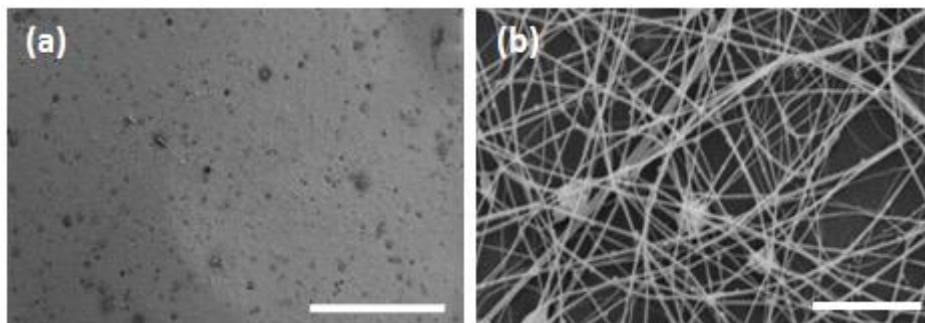


Fig. 3.24: SEM images of electrospun fibrinogen for high flow rate values. In particular, (a) shows the presence of drops of solution on the electrospun sample. Scale bar: (a) 1 mm, (b) 5  $\mu\text{m}$ .

### 3.2 Study of fibrinogen molecular structure and investigation on gelification process

Gelification of fibrinogen solution is a peculiar phenomenon that has never been reported nor studied in literature; therefore, we decided to further investigate the process with the idea of better elucidate the physical and molecular phenomena underneath it. Initially we conducted experiments to characterize how different solvents, in particular formic acid and HFIP that are used for ES, impact fibrinogen molecular structure eventually causing its denaturation.

#### SDS-PAGE

For SDS-PAGE analysis, fibrinogen was solved in different media and subsequently analyzed in order to evaluate formation or break (typically due to hydrolysis) of the peptidic bonds as a consequence of the solvent effect. In particular, PBS at physiological pH was employed to obtain fibrinogen native sample, used as comparison for the other samples. In fact, under reducing condition, fibrinogen exhibits a typical profile, with three bands representing the three different chains that form the molecule:  $\alpha$ ,  $\beta$ , and  $\gamma$ , with different molecular weights in the range of 50 to 70 kDa<sup>39</sup>. The solvents investigated were formic acid, as it is the one used in this work for fibrinogen ES and causing gelification, an aqueous solution of formic acid with intermediate pH (i.e. pH = 4), and HFIP, that is the solvent employed in literature for fibrinogen ES, as comparison. SDS-PAGE analysis showed that, under reducing conditions (Fig 3.6), all fibrinogen samples appeared as three predominant

bands that correspond to the  $\alpha$ ,  $\beta$ , and  $\gamma$  chains of fibrinogen; no detectable changes in the protein banding patterns present on the SDS gels were visible in the samples subjected to different solvent treatment, thus indicating no change in the molecular weight and no degradation products. These profiles indicated that prior to the SDS treatment, all fibrinogen samples comprised complete fibrinogen molecules. Therefore, we demonstrated that both the solvents used for ES (formic acid and HFIP) did not cause changes in molecular configuration, i.e. they did not induce rupture of the peptidic chains nor formation of new covalent bonds.

These results proved that gelification of fibrinogen solution in formic acid was not related to formation of covalent bonds between fibrinogen molecular chains; evidently, formation of the gel was related to the presence of numerous weak bonds that cause solution structuration and gelification.

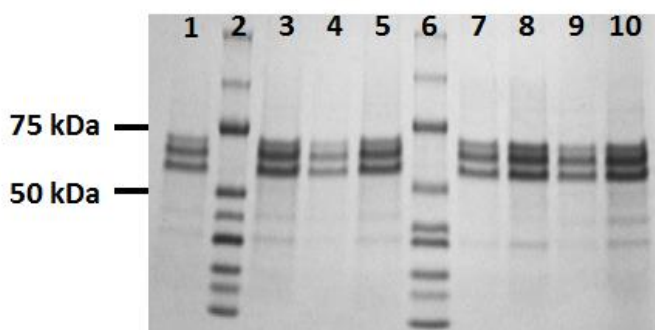


Fig. 3.25: SDS-PAGE analysis of fibrinogen after treatment with different solvents: formic acid (pH = 1, Lanes 1,3), HFIP (Lanes 4-5), formic acid aqueous solution pH = 4 (Lanes 7-8), PBS (pH = 7, Lanes 9-10). Lanes 2 and 6 contain molecular weight standards. Lanes 1, 4, 7, 9 were loaded with 10  $\mu$ g of fibrinogen; Lanes 3, 5, 8, 10 with 15 $\mu$ g.

### MD simulations

For all the pH values, stable trajectories were obtained, RMSD plot of pH 1 fibrinogen is reported in Fig. 3.7 as an example. In particular, it was necessary to increase the simulation time for the tail domain in order to obtain stable conformation. The major result of MD simulation was a rearrangement of fibrinogen tertiary structure: if in the neutral condition

fibrinogen monomer remained open, increasing the pH value produced a scissoring motion of the tail towards the head, as depicted in Fig. 3.8.

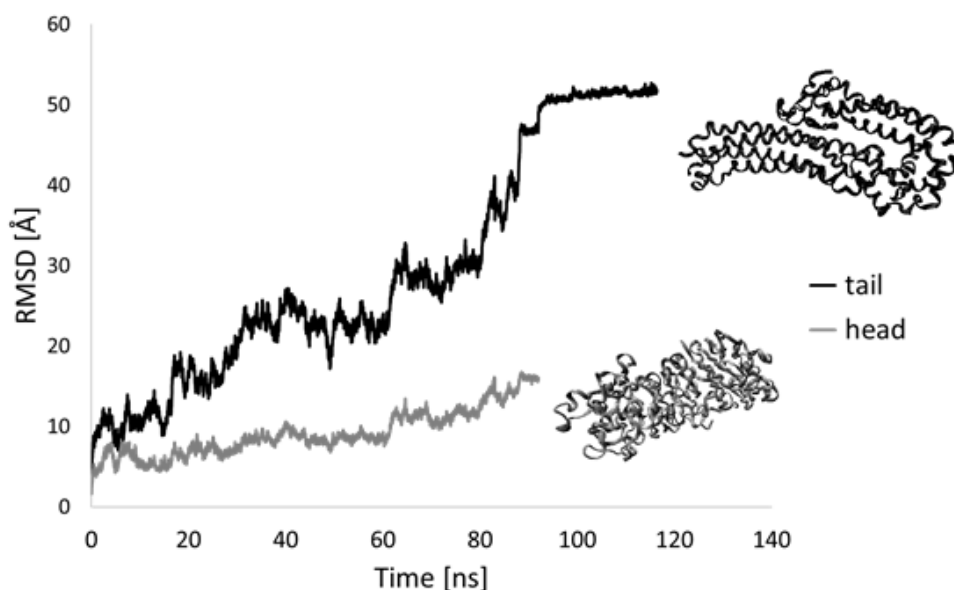


Fig. 3.26: RMSD plot of tail and head regions of fibrinogen at pH 1.

Further analysis regarded SASA values for the whole protein, the head, and the tail: pH conditions did not have any effect on protein SASA value, which remained stable in the three cases (Table 3.4). The same was true also for the other parameter investigated, that was the H-bond number. Here again, the number remained constant for the whole protein (Table 3.4). Finally, the secondary structure timeline was evaluated, but in this case it was not possible to define a trend for the protein at different pH values; in particular, the  $\alpha$ -helix and random coil structures analyzed remained stable (Table 3.4).

MD simulation allowed to capture an important rearrangement within a monomer, but to fully characterize this behavior further *in silico* analyses are mandatory. In fact, the use of an implicit solvent did not allow to study the influence of the environment on the molecule. Indeed, in order to solvate completely the molecule, it would have been necessary to construct a box containing about 1 million of solvating molecules, thus making this study unfeasible also for the most powerful hardware architectures.

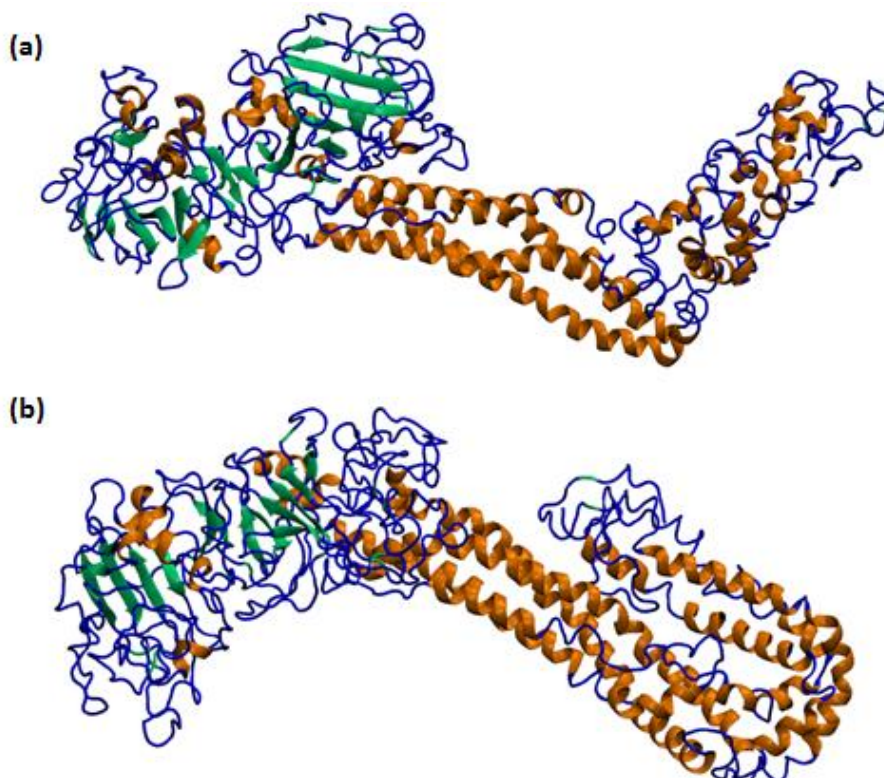


Fig. 3.27: Fibrinogen monomer conformation and secondary structure at different pH values: (a) pH = 7, and (b) pH = 1. Images were obtained using VMD software; in particular,  $\alpha$ -helices are depicted in orange,  $\beta$ -sheets in green, random coil and turn in blue.

Table 3.14: SASA value, number of H-bonds, and percentage of  $\alpha$ -helix and random coil in fibrinogen secondary structure for the different pH values tested.

	pH = 7	pH = 4	pH = 1
SASA [ $\text{\AA}^2$ ]	36'060 $\pm$ 268	38'981 $\pm$ 271	36'051 $\pm$ 305
H-bonds [ ]	192 $\pm$ 11	209 $\pm$ 12	211 $\pm$ 11
Sec. structure:			
$\alpha$ -helix [%]	28 $\pm$ 1	33 $\pm$ 1	29 $\pm$ 1
random coil [%]	24 $\pm$ 1	20 $\pm$ 1	22 $\pm$ 1

With the aim of overcome this limitations, experimental analyses of protein secondary structure can be performed, and in this regard CD spectroscopy was employed.

### **CD spectroscopy**

In order to evaluate the effects of ES solvents on fibrinogen folding, and in particular on its secondary structure (i.e. local organization of protein domains), CD spectra of fibrinogen in different solutions were obtained (Fig. 3.9). The same solvents used for SDS-PAGE analyses were considered (i.e. PBS, formic acid, aqueous formic acid solution at pH 4, HFIP), and in addition an aqueous solution of formic acid at pH 1 was introduced for CD analysis, with the intention of separate the effect related to acidic environment (comparing spectra in PBS at pH 7, and in formic acid aqueous solutions at pHs 4 and 1), and the influence of pure formic acid solvent (comparing spectra measured in pure and aqueous formic acid solutions at pH 1).

The main feature of the spectra was the decreasing values of the ellipticity (more negative) over the wavelength range 206-235 nm for aqueous formic acid solutions with decreasing pH or for HFIP solvent: this indicates that  $\alpha$ -helix content of the molecules increased with decrease in pH or in the fluorinated solvent. In particular, fibrinogen spectrum recorded in HFIP had the highest  $\alpha$ -helix amount; this effect is in accordance with results reported in literature which showed that HFIP induces  $\alpha$ -helical structure in proteins<sup>19</sup>.

As for pH influence on fibrinogen secondary structure, acidic environments proved to cause an increase in  $\alpha$ -helix content of fibrinogen. In fact, on decreasing the pH from neutrality to pH 1 the protein became maximally positively charged, since the pK of most carboxylic groups is greater or around 3. The resulting intramolecular repulsion between the positively charged groups led to unfolding, and apparently helices were formed during this process.

Finally, based on the intensity of the two characteristic bands of 205-210 and 220-225 nm, CD spectrum of fibrinogen in pure formic acid shows that the protein was transformed to a random coil conformation, and not to  $\alpha$ -helical structure as for pH 1 of aqueous formic acid solution. Therefore, the effect of pure formic acid was not only related to the acidic

pH: in fact, it affected the conformational change of fibrinogen causing a structural transition towards a completely unfolded conformation. This phenomenon was already reported in literature for gelatin in formic acid<sup>40</sup>; it could be explained from the fact that the inter- and intramolecular hydrogen bonds among amide groups, carboxyl groups and hydroxyl groups, which are the major contributing of the  $\alpha$ -helix structure of molecules, are disrupted to a certain extent by reconstructing hydrogen bonds with formic acid molecules<sup>41</sup>. Therefore, the chain conformation of fibrinogen might be changed from the rigid helical structure to the coil conformation. In case of aqueous formic acid solution at pH 1, this effect was not important as the amount of formic acid in solution was very low (about 0.1% v/v).

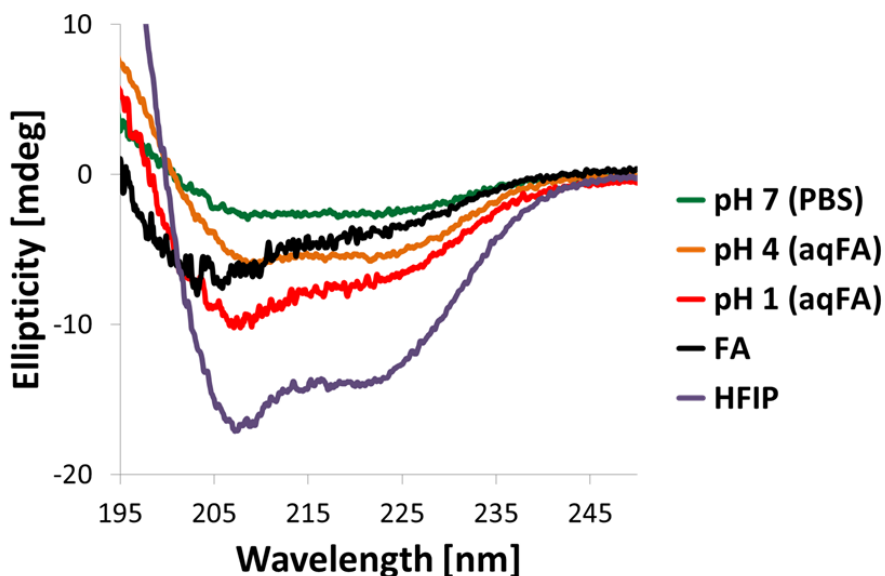


Fig. 3.28: CD spectra of fibrinogen in different solvents: PBS (pH 7), aqueous solutions of formic acid at pHs 4 and 1, pure formic acid, and HFIP.

In conclusion, both the solvents that can be used for fibrinogen ES, i.e. HFIP and formic acid, caused extensive protein denaturation: in HFIP fibrinogen was almost completely transformed in a rigid  $\alpha$ -helical structure, while in formic acid the molecule was unfolded and assumes random coil conformation. The open and flexible structure adopted by fibrinogen in the organic acid could encourage formation of weak/non-covalent inter-



molecular bonds, thus resulting in a denser molecule structuration and finally in the solution gelification.

In order to evaluate the effect of fibrinogen molecule unfolding on the behavior of the solution and, in particular, on the transition from fluid to gelled system, rheological analyses and photon correlation imaging were employed.

### Rheological analyses

Fibrinogen solution in acidic solvent displayed typical pseudoplastic behavior of polymeric solutions; in fact, material flew instantaneously upon load application, and then viscosity decreased (shear-thinning) until a plateau was reached (Fig. 3.10a). This effect is due to alignment of fibrinogen molecules towards the direction of the applied stress for increasing shear rates, that therefore decreases the internal resistance to flow and viscosity value.

The strain dependence of storage ( $G'$ , blue) and loss ( $G''$ , red) moduli is showed in Fig. 3.10b. Fibrinogen solution exhibited a gel-type mechanical behavior; that is,  $G' > G''$  in the entire strain range tested, thus suggesting that the material was highly structured and the component of elastic solid overcame that of viscous solution<sup>42</sup>. Both  $G'$  and  $G''$  values increased with increasing strain applied up to about 500%, where gel fracture happened. These results demonstrate that fibrinogen solution has a rheological behavior typical of gels, thus confirming the macroscopic observations conducted during ES process.

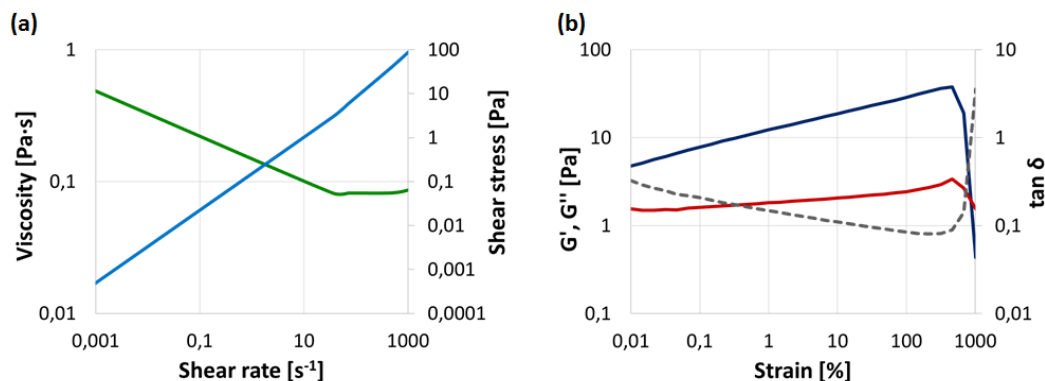


Fig. 3.29: Results of rheological measurements of fibrinogen solution: (a) viscosity (green) and shear stress (blue) as a function of shear rate; (b) strain-dependence of elastic modulus ( $G'$ , blue), viscous modulus ( $G''$ , red), and  $\tan \delta$  (grey).

### **Gelation kinetics - Photon correlation imaging and polarized light microscopy**

The powerful PCI technique was used in this work only with the aim of obtaining qualitative (not quantitative) information about the structural changes occurring in fibrinogen solution and leading to gelification. We were not interested in studying the details of gelification front in the cuvette, as what happens during ES process is a phenomenon with completely different conditions. Initially, solution in a close environment (i.e. close cuvette) was examined: the speckle pattern showed a convective motion within the solution, which is typical of fluid system. In order to accelerate gelification process, we therefore decided to open the cuvette and continued the analysis by looking at the free surface of the solution exposed to air, as we were interested in determine the effect of solvent evaporation on solution gelification phenomenon.

With this set-up configuration it was possible to observe solvent redistribution through a convective motion: in fact, it looked like the solvent was coming up in order to balance the local increase of concentration at the free surface due to solvent evaporation. Therefore, gelification kinetics was slowed down by this redistribution process. However, after 3 days significant solvent evaporation occurred, and it was possible to see transition from a fluid to a gelled system. After 6 days, the gel structure was almost dynamically arrested, but residual dynamic effects persisted in the gel. Moreover, solvent evaporation generated strong stresses within the gel network, which subsequently caused the macroscopic break of the sample. This preliminary analysis by PCI confirmed that gelification rate of fibrinogen solution was dependent on evaporation rate, which increases solution concentration thus favoring gel formation; in fact, the same fibrinogen solution kept in a close vial gelled after about 10 days.

After 3 days of solvent evaporation, the solution in the open cuvette was also examined at the optical microscope: as shown in Fig. 3.11a, fibril-like structure were observable, both within the gel and on the cuvette border where the solvent had evaporated. In order to better simulate solution gelification conditions during ES process (i.e. high surface-to-volume ratio), we also observed a drop of solution placed on a glass slide: micrographs showed the formation of crystal-like structures (Fig. 3.11c), which likely originated from

protein agglomeration and precipitation. By examining the two samples, i.e. the solution in the cuvette and on the glass slide, with polarized light, the fibrillary and crystal structures resulted formed by highly ordered molecules (Fig. 3.11b, d).

Taken together, these results indicate that fibrinogen solution gelification is not a stable or regular process, as molecules structuration is affected by environmental conditions (in particular evaporation rate), and the system is extremely complex. Therefore, at the moment it is not possible to comprehensively describe what really happens at the tip of the spinneret during ES process, as this situation is further complicated by the presence of the electric field which imposes a shear stress on the drop of solution.

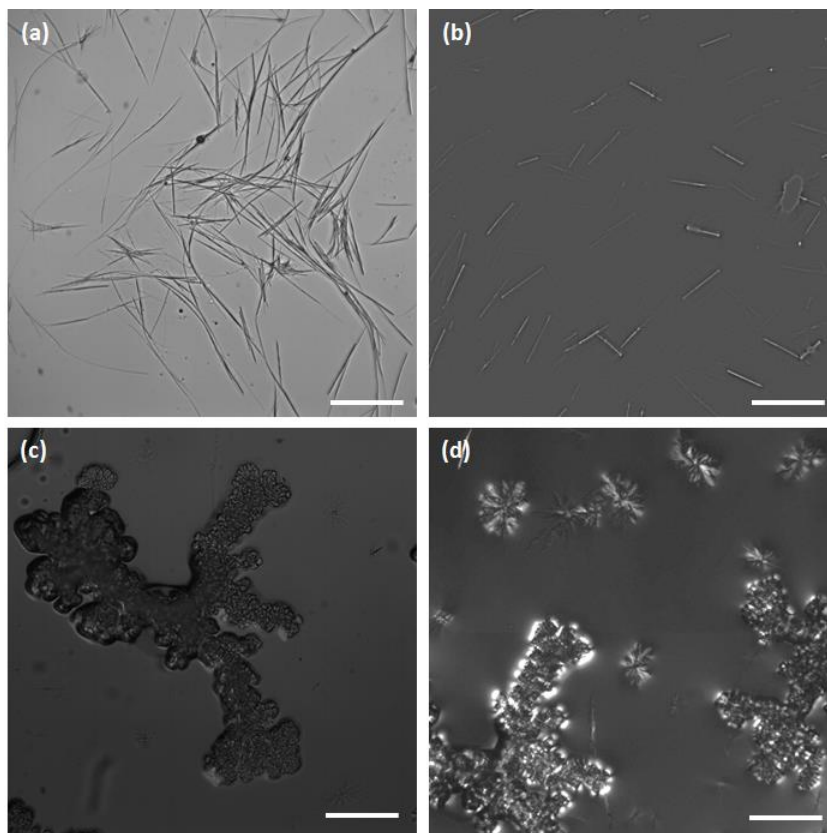


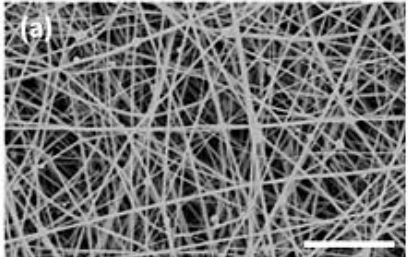
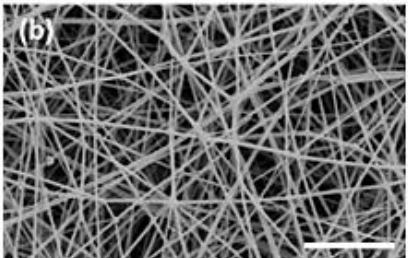
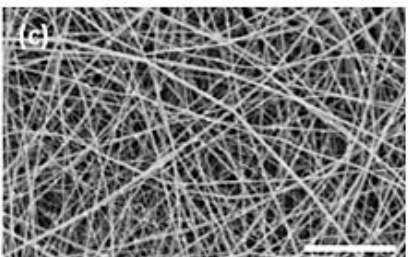
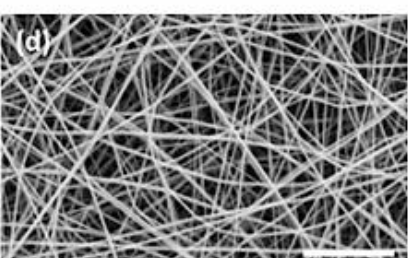
Fig. 3.30: Images of structures formed by fibrinogen in acidic solution at different conditions: (a-b) higher evaporation rate (glass coverslip); (c-d) lower evaporation rate (cuvette). (b-d) show light depolarization due to molecular organization at nanometric scale. Scale bar: 100  $\mu\text{m}$ .

### **3.3 Electrospinning of fibrinogen/gelatin blend: solution and parameters optimization**

The detailed study on fibrinogen acidic solution behavior allowed to better characterize and understand gelification phenomenon, and it was clear that the problem was related to the solvent employed. Unluckily, the solvent system used for ES derived from a vast analysis and optimization process conducted with many different solvents, and therefore it was not possible to change it without greatly affected ES outcome. Consequently, it was necessary to find alternative strategies that could increase fibrinogen solution processability and in the same time preserve the excellent biocompatibility of the electrospun scaffold. An important parameter affecting solution gelification was the concentration; in fact, for low concentration values the solution did not gel or, at least, gelled for longer times. Therefore, a possible strategy could be to decrease fibrinogen concentration in solution, while keeping constant the total concentration in order to obtain good electrospun fibers without defects; to reach this aim, fibrinogen could be blended with a different polymer in the ES solution. However, the polymer to be added had to fulfill some requirements: it should have been miscible with fibrinogen and soluble in formic acid, compatible with ES process, and cytocompatible for the application intended for the electrospun membrane. A good candidate which satisfied all these specifications was gelatin, as it had already proved to be easily soluble and spinnable in formic acid, and it is well known for its good cell interaction properties<sup>13, 40</sup>. Therefore, blends of fibrinogen and gelatin with different ratios were prepared and electrospun using the same process parameters previously optimized for fibrinogen ES: the real-time imaging system allowed to evaluate gelification kinetics for all the blends during ES.

Table 3.5 summarizes the results obtained for different fibrinogen/gelatin blend compositions: SEM morphology proved to be adequate for all the solutions used, as homogeneous fibers without defects were observable. However, for 5/1, 3/1, and 2/1 ratios the process was not continuous, as solution gelification still occurred with only lower frequency. Only by increasing fibrinogen/gelatin ratio up to 1/1, it was possible to achieve a stable and continuous process; in this case, fiber average diameter was  $213.7 \pm 33.0$  nm.

Table 3.15: SEM images and indication of gelification rate during ES for different fibrinogen/gelatin blend compositions. Scale bar: 5  $\mu$ m.

Fibrinogen/gelatin ratio	SEM image	Gelification rate
5/1		20 – 25 minutes
3/1		20 – 25 minutes
2/1		40 – 45 minutes
1/1		/

Electrospun fibrinogen membranes proved to be stable in aqueous environment at 37°C up to 14 days, while gelatin membranes immediately solved upon water contact; therefore, it was important to investigate whether electrospun blend sample stability was more similar to pure fibrinogen or to pure gelatin matrices. Degradation tests in PBS at 37°C revealed

that the samples could maintain their shape up to 7-10 days. In order to verify morphology stability, samples after 24 hours in PBS were analyzed by SEM: images showed that electrospun structure was preserved, and the fibers were swollen in aqueous media (Fig. 3.12, fiber diameter:  $308.7 \pm 45.5$  nm) because of their high hydrophilicity. The presence of gelatin, that is usually immediately solved by water contact, did not cause any visible hole nor pore formation: therefore, the two biopolymers were perfectly mixed in the solution and no changes in fiber structure after immersion in PBS were noticeable at the microscale.

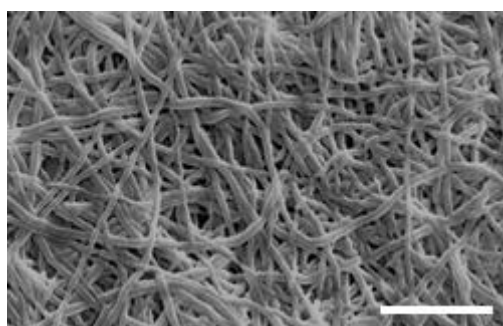


Fig. 3.31: SEM image of fibrinogen/gelatin electrospun sample after immersion in PBS at 37°C for 24 hours. Scale bar: 5  $\mu$ m.

Intrinsic stability of electrospun fibrinogen/gelatin membranes is an important advantage with respect to other matrices composed of biomolecules or natural polymers, as it avoids the necessity of post-treatment crosslinking procedures, thus eliminating one further step in scaffold production that can also potentially introduce harmful residues.

To the best of our knowledge, ES of fibrinogen/gelatin blend has been reported only in one work<sup>43</sup>, for applications as myocardial patch or muscle regeneration; fibrinogen/gelatin ratios tested were 1/4 and 1/1, and the solvent used was HFIP. Therefore, the present study shows an attractive alternative for fibrinogen/gelatin blend ES, as it involves the use of acidic solvents instead of fluorinated ones, thus resulting in a less toxic, more environmental friendly and less expensive process. Furthermore, while for membranes electrospun from HFIP solution glutaraldehyde crosslinking was necessary in order to increase stability, the matrices produced in this work do not need any crosslinking post-treatment.

## 4. Conclusions

ES of fibrinogen in acidic solvent system is a novel and promising alternative for biocompatible scaffold production. However, during the process solution gelification at the tip of the spinneret occurred, thus hindering process stability and continuity. In order to investigate the problem and find possible solutions, further analyses on fibrinogen molecular structure and gelification kinetics were carried out. SDS-PAGE results showed that no formation nor break of covalent bonds within fibrinogen chains occurred after solubilisation in formic acid. Investigation of protein secondary and tertiary structure, carried out by means of MD simulations and CD spectroscopy, revealed that acidic environment caused a significant change in fibrinogen conformation and configuration; in particular, formic acid produced a transition of native protein secondary structure to random coils. Therefore, it is possible that formation of weak bonds (i.e. hydrophobic interactions, van der Waals, and H-bonds) between denatured protein molecules occurred, thus causing gelification. The gel behavior of fibrinogen solution was further observed by macroscopic analyses, i.e. rheology and PCI, which also elucidated that gelification kinetics was affected by evaporation rate.

These studies indicated that gelification process was related to the solvent system employed and to fibrinogen concentration; as it was not possible to change the solvent without greatly compromise the ES outcome, the strategy chosen was to decrease the amount of fibrinogen in solution by blend it with another polymer. Gelatin was employed as a cospun means because of its biocompatibility, biodegradability and good spinnability; in fact, gelatin had been already added to natural polymer solutions difficult to spin (i.e. hyaluronic acid) to favor their processability<sup>44</sup>. ES process of fibrinogen/gelatin blend (1/1) in formic acid proved to be a continuous process, and membrane with adequate fiber morphology could be obtained. Moreover, these matrices were stable in aqueous environment up to 7-10 days without need of any crosslinking treatment.

Due to these features, fibrinogen/gelatin electrospun membranes have promising applications as wound dressing or scaffolds for tissue engineering of soft tissues.

## References

1. Boland, E.; Bowlin, G.; Simpson, D.; Wnek, G. In *Electrospinning of tissue engineering scaffolds*, Abstr Pap Am Chem S, AMER CHEMICAL SOC 1155 16TH ST, NW, WASHINGTON, DC 20036 USA: 2001; pp U344-U344.
2. Lannutti, J., Electrospinning of tissue engineering scaffold. *Materials Science and Engineering C* **2007**, *C* (27), 504 - 509.
3. Chen, Z., Intermolecular interactions in electrospun collagen–chitosan complex nanofibers. *Carbohydrate Polymers* **2008**, *72*, 410-418.
4. Wnek, G. E., Electrospinning of Nanofiber Fibrinogen Structures. *Nano Letters* **2003**, *3* (2), 213-216.
5. Dalby, M. J., Fibroblast response to a controlled nanoenvironment produced by colloidal lithography. *J Biomed Mater Res* **2004**, *69A*, 314-322.
6. Sell, S. A., The Use of Natural Polymers in Tissue Engineering: A Focus on Electrospun Extracellular Matrix Analogues. *Polymers* **2010**, *2*, 522-553.
7. Hsu, F.-Y., Electrospun hyaluronate–collagen nanofibrous matrix and the effects of varying the concentration of hyaluronate on the characteristics of foreskin fibroblast cells. *Acta Biomaterialia* **2010**, *6*, 2140-2147.
8. Rho, K. S., Electrospinning of collagen nanofibers: Effects on the behavior of normal human keratinocytes and early-stage wound healing. *Biomaterials* **2006**, *27*, 1452-1461.
9. Huang, Z.-M., A review on polymer nanofibers by electrospinning and their applications in nanocomposites. *Composites Science and Technology* **2003**, *63*, 2223-2253.
10. Xu, C. Y., Aligned biodegradable nanofibrous structure: a potential scaffold for blood vessel engineering. *Biomaterials* **2004**, *25*, 877-886.
11. Zong, X., Electrospun fine-textured scaffolds for heart tissue constructs. *Biomaterials* **2005**, *26*, 5330-5338.
12. Kolacna, L., Biochemical and Biophysical Aspects of Collagen Nanostructure in the Extracellular Matrix. *Physiol. Res. J* **2007**, *56*, S51-S60.
13. Malafaya, P. B., Natural–origin polymers as carriers and scaffolds for biomolecules and cell delivery in tissue engineering applications. *Advanced Drug Delivery Reviews* **2007**, *59*, 207-233.
14. McManus, M. C., Electrospun fibrinogen: Feasibility as a tissue engineering scaffold in rat cell culture model. *J Biomed Mater Res* **2007**, *81A*, 299-309.
15. Makogonenko, E., Interaction of the Fibronectin COOH-Terminal Fib-2 Regions with Fibrin: Further Characterization and Localization of the Fib-2-Binding Sites. *Biochemistry* **2007**, *46*, 5418-5426.
16. Mosesson, M. W., The Structure and Biological Features of Fibrinogen and Fibrin. *ANNALS NEW YORK ACADEMY OF SCIENCES*, 11-30.
17. Rajangam, T., Fibrinogen and fibrin based micro and nano scaffolds incorporated with drugs, proteins, cells and genes for therapeutic biomedical applications. *International Journal of Nanomedicine* **2013**, *8*, 3641-3662.
18. Sell, S. A., Electrospinning of collagen/biopolymers for regenerative medicine and cardiovascular tissue engineering. *Advanced Drug Delivery Reviews* **2009**, 1007-1019.



19. Carlisle, C. R., The mechanical properties of individual, electrospun fibrinogen fibers. *Biomaterials* **2009**, *30*, 1205-1213.
20. Fischer, R. L., Electrospinning collagen and hyaluronic acid nanofiber meshes. *J Mater Sci: Mater Med* **2012**, *23*, 1645-1654.
21. McManus, M., Electrospun nanofibre fibrinogen for urinary tract tissue reconstruction. *Biomed. Mater* **2007**, *2*, 257-262.
22. Lim, S. H., Electrospun scaffolds for stem cell engineering. *Advanced Drug Delivery Reviews* **2009**, *61*, 1084-1096.
23. Burck, J., Resemblance of Electrospun Collagen Nanofibers to Their Native Structure. *Langmuir* **2013**, *29*, 1562-1572.
24. McManus, M., Mechanical properties of electrospun fibrinogen structures. *Acta Biomaterialia* **2006**, *2*, 19-28.
25. Gugutkov, D., Fibrinogen nanofibers for guiding endothelial cell behavior. *Biomaterials Science* **2013**, *1*, 1065-1073.
26. Dong, Z., Thermodynamic Modeling and Investigation of the Formation of Electrospun Collagen Fibers. *Langmuir* **2011**, *27*, 12417-12422.
27. Campiglio, C. Elettrofilatura di matrici allineate in fibrinogeno per la rigenerazione del tessuto nervoso periferico. Politecnico di Milano, 2013.
28. Leach, A. R., *Molecular modelling: principles and applications*. Pearson education: 2001.
29. Cheng, C. J.; Daggett, V., Molecular dynamics simulations capture the misfolding of the bovine prion protein at acidic pH. *Biomolecules* **2014**, *4* (1), 181-201.
30. Sekijima, M.; Motono, C.; Yamasaki, S.; Kaneko, K.; Akiyama, Y., Molecular dynamics simulation of dimeric and monomeric forms of human prion protein: insight into dynamics and properties. *Biophysical journal* **2003**, *85* (2), 1176-1185.
31. Alonso, D. O.; DeArmond, S. J.; Cohen, F. E.; Daggett, V., Mapping the early steps in the pH-induced conformational conversion of the prion protein. *Proceedings of the National Academy of Sciences* **2001**, *98* (6), 2985-2989.
32. Langella, E.; Improta, R.; Barone, V., Checking the pH-induced conformational transition of prion protein by molecular dynamics simulations: effect of protonation of histidine residues. *Biophysical journal* **2004**, *87* (6), 3623-3632.
33. Cao, Z.; Zhang, X.; Liu, L.; Zhao, L.; Li, H.; Wang, J., Effect of pH on the Aggregation of  $\alpha$ -syn12 Dimer in Explicit Water by Replica-Exchange Molecular Dynamics Simulation. *Int J Mol Sci* **2015**, *16* (7), 14291-14304.
34. Cipelletti, L.; Bissig, H.; Trappe, V.; Ballesta, P.; Mazoyer, S., Time-resolved correlation: a new tool for studying temporally heterogeneous dynamics. *Journal of Physics: Condensed Matter* **2002**, *15* (1), S257.
35. Secchi, E.; Munarin, F.; Alaimo, M.; Bosisio, S.; Buzzaccaro, S.; Ciccarella, G.; Vergaro, V.; Petrini, P.; Piazza, R., External and internal gelation of pectin solutions: microscopic dynamics versus macroscopic rheology. *Journal of Physics: Condensed Matter* **2014**, *26* (46), 464106.
36. Secchi, E.; Roversi, T.; Buzzaccaro, S.; Piazza, L.; Piazza, R., Biopolymer gels with "physical" cross-links: gelation kinetics, aging, heterogeneous dynamics, and macroscopic mechanical properties. *Soft Matter* **2013**, *9* (15), 3931-3944.

37. Baker, S.; Sigley, J.; Helms, C. C.; Stitzel, J.; Berry, J.; Bonin, K.; Guthold, M., The mechanical properties of dry, electrospun fibrinogen fibers. *Materials Science and Engineering: C* **2012**, *32* (2), 215-221.
38. McManus, M.; Boland, E.; Sell, S.; Bowen, W.; Koo, H.; Simpson, D.; Bowlin, G., Electrospun nanofibre fibrinogen for urinary tract tissue reconstruction. *Biomedical Materials* **2007**, *2* (4), 257.
39. Gorkun, O. V.; Veklich, Y. I.; Weisel, J. W.; Lord, S. T., The conversion of fibrinogen to fibrin: recombinant fibrinogen typifies plasma fibrinogen. *Blood* **1997**, *89* (12), 4407-4414.
40. Ki, C. S.; Baek, D. H.; Gang, K. D.; Lee, K. H.; Um, I. C.; Park, Y. H., Characterization of gelatin nanofiber prepared from gelatin–formic acid solution. *Polymer* **2005**, *46* (14), 5094-5102.
41. Liu, Y.; Ma, G.; Fang, D.; Xu, J.; Zhang, H.; Nie, J., Effects of solution properties and electric field on the electrospinning of hyaluronic acid. *Carbohydrate Polymers* **2011**, *83* (2), 1011-1015.
42. Ikeda, S.; Nishinari, K., “Weak Gel”-type rheological properties of aqueous dispersions of nonaggregated κ-carrageenan helices. *J Agr Food Chem* **2001**, *49* (9), 4436-4441.
43. Balasubramanian, P.; Prabhakaran, M. P.; Kai, D.; Ramakrishna, S., Human cardiomyocyte interaction with electrospun fibrinogen/gelatin nanofibers for myocardial regeneration. *Journal of Biomaterials Science, Polymer Edition* **2013**, *24* (14), 1660-1675.
44. Li, J.; He, A.; Han, C. C.; Fang, D.; Hsiao, B. S.; Chu, B., Electrospinning of hyaluronic acid (HA) and HA/gelatin blends. *Macromolecular rapid communications* **2006**, *27* (2), 114-120.

## Chapter 4 – Core-shell electrospinning of natural polymers for wound healing applications

---

---

*Gelatin and hyaluronic acid were co-axially electrospun in order to fabricate core-shell fibers. An innovative drug for inhibition of myofibroblast differentiation was loaded in the core (gelatin) solution. In vitro tests demonstrated that electrospun membranes were cytocompatible; moreover, the drug retained its activity after ES process.*

---

# 1. Introduction

As described in Chapter 1, electrospinning (ES) is a fabrication technique extensively studied and employed for the production of nonwoven fiber meshes composed of biopolymeric fibers with diameters ranging from tens of nanometers to micrometers.

The focus of this Chapter is co-axial electrospinning (or co-electrospinning), a new variation of ES which has emerged in latest years, with the intention of preparing nanometric core-shell fibers<sup>1</sup>. The operating principle is the same than for traditional ES, but it typically uses a concentric spinneret in order to prepare core-shell structured fibers in one-step. In fact, core-shell ES is particularly interesting because it allows encapsulation in the core or covering as shell of polymers lacking adequate properties for ES (e.g. mineral oil, olive oil), and even non-polymeric materials (e.g. metal powders, nanoparticle suspensions, catalysts, bioactive molecules)<sup>2</sup>. As it represents an efficient and scalable method, it is considered promising in a variety of applications including the biomedical field (e.g. tissue engineering, drug release systems), filtration, catalysis, and optical applications<sup>3</sup>. Unluckily, the use of a concentric needle does not necessarily result in the formation of core-shell fibers. Several works in literature have tried to describe and investigate the theoretical physics of core-shell ES in order to better understand the process and improve its efficiency<sup>4</sup>. However, there is still no complete understanding of formation and bending instabilities of viscoelastic core-shell jet.

Core-shell jet formed at the tip of the concentric needle undergoes several instabilities: as for the traditional ES process, initially the jet is thinned by bending perturbations. Then, two types<sup>4</sup> of capillary instabilities can occur: the first is the regular capillary instability and happens when the viscoelastic forces are not strong enough to prevent it (e.g. polymer concentration is not sufficiently high). This kind of instability is driven by the surface tension of the shell solution and leads to the rupture of the electrified jet into droplets, as it can happen for traditional ES jet. The second type of capillary instability is specific for core-shell jets, as it regards the interfacial tension between core and shell phases; in this case, the core can break up into separate droplets inside of an intact shell, thus resulting in a compound jet with no intact core. Additional form of instabilities can originate from

relative velocity between core and shell solutions due to different flow rates; this can cause a longitudinal compression force acting on the core, which therefore can buckle. Furthermore, if the solvent used in the core solution is evaporating too fast, a hollow core inside the fiber can be formed: the core is then subjected to lateral compressive pressure from the shell solution, thus making ribbons instead of cylindrical fibers<sup>1</sup>.

In order to favor the successful outcome of the core-shell process, several studies in literature have investigated the role of solution and process parameters on the resulting fiber morphology<sup>1, 5-7</sup>. First of all, certainly a stable, liquid Taylor cone at the tip of the spinneret is necessary in order to have formation of continuous core-shell structure. Then, other fundamental parameters have an important effect on core-shell ES process:

1. solution viscosity: a stable ES process depends on the shell solution driving the core solution through shearing and contact forces, thus keeping inner solution confined to the core during fiber stretching. Therefore, shell solution viscosity should be higher than core solution, so that the viscous force generated by the shell on the core is sufficient to overcome the interfacial tension and drive compound jet formation.

2. interfacial tension and miscibility of the two solutions: it is clear that two immiscible solutions will favor core-shell structure formation, as the two phases will remain separated throughout the spinning process. If the two solutions are miscible, a rapid diffusion may lead to their mixing, thus preventing core-shell fiber formation. However, several works in literature have obtained bicomponent fibers by core-shell ES of pairs of miscible polymer solutions; in this case, the two solutions must have low interfacial tension in order to prevent high stresses at the interface thus hindering Taylor cone stability. In order to reduce interfacial tension, many works in literature have tried to use the same solvent for inner and outer solutions, obtaining successful fiber structuration<sup>8</sup>.

3. solution conductivity: shell solution is usually chosen to possess higher conductivity than the core, so that surface charge density is high enough to cause the elongational force for fiber formation.

4. solvent vapor pressure: vapor pressure of the two solutions should be sufficiently low and comparable, so that they both dry with similar rates to avoid fiber collapsing.

5. degree of protrusion of the core nozzle outside the shell nozzle: core-shell fiber formation is favored by a core nozzle protruding from a coaxial shell nozzle<sup>9</sup>.

6. solution concentration: this parameter affects core and shell thickness. In fact, increasing shell solution concentration has the effect of increasing shell thickness and overall fiber dimension, while increasing core concentration results in an increase of the core fiber diameter and a decrease of shell thickness<sup>10-11</sup>. Therefore, a balance between core and shell solution concentrations is necessary in order to obtain adequate co-axial fiber morphology.

7. flow rate: shell solution usually has higher flow rate than the core, so that viscous drag applied by the outer solution is adequate to confine inner solution within the core. Moreover, thickness of core and shell can be varied by tuning the feed rates; when increasing the inner flow rate an increase of core size and total fiber diameter is observed<sup>12-13</sup>.

Core-shell ES setups are more complicated than the traditional ones, as they need a special co-axial needle and two syringe pumps. However, solutions for co-ES have been studied and core-shell fibers from a normal single nozzle ES setup were also obtained by employing an emulsion of two solutions as working liquid<sup>3, 14-15</sup>. Evidently, in this case specific pairs of polymeric solutions have to be used, as immiscibility is a key factor. Moreover, it is crucial that the emulsion remains stable over the whole time of the process. However, in many cases emulsion ES does not result in core-shell fibers, as often core solution is embedded as separate spots.

Core-shell ES has been studied for many applications as it offers fascinating opportunities in tailoring fiber structure. In particular, it can be used to modify wettability properties of nanofiber surface (for example, using PTFE solution as shell), to improve cytocompatibility of nanofibers used as cell scaffold, or to encapsulate drugs or biologically active agents. In fact, as it is not necessary for the core material to be a polymeric solution, encapsulation by core-shell ES is potentially beneficial for the storage and drug delivery of bioactive agents, and it presents two major advantages: the biological molecule in the core is protected from possible harsh solvents used for shell polymer solution and also from the effect of electric field, as charges are present only on the outer surface of the shell at the beginning of jet formation. In addition, the polymer shell offers the possibility to control

the release rate; in particular, it helps to prevent initial burst release<sup>1,3</sup>. In this regard, the use of core-shell electrospun matrices represents a promising solution for sustained release strategies, with interesting applications in tissue engineering and, in particular, in wound healing where a tunable sustained drug release is an important feature.

As for this latter, wound healing is a complex biological process which naturally takes place in human body and involves several types of cells; it consists of four precisely phases: hemostasis, inflammation, proliferation, and remodeling<sup>16</sup>. These four phases must occur in the proper sequence and time frame in order to have successful outcome.

Many factors can interfere with the healing process of both acute and chronic wounds, thus causing improper or impaired tissue repair: the presence of foreign bodies or infection, oxygenation and venous insufficiency, diseases such as diabetes, fibrosis, and keloids. Non-healing wounds frequently enter a state of pathologic inflammation due to an incomplete healing process. This problem affects about 3 to 6 million people only in the United States, thus resulting in a huge health care expense<sup>16</sup>.

In particular, fibrosis is defined as an excess deposition of collagen and fibronectin, secreted by myofibroblasts, which are activated form of fibroblasts induced by wound local conditions, such as mechanical stress, growth factors (in particular, TGF- $\beta$ ), and cytokines (Fig. 4.1). These cells are highly contractile and usually express  $\alpha$ -smooth muscle actin ( $\alpha$ -SMA). During physiological healing process, fibroblasts are activated and become myofibroblasts in order to favor wound healing; after re-epithelialization, these cells undergo apoptosis. However, in case of pathological conditions, myofibroblasts become resistant to apoptosis and produce extensive amount of collagen, thus leading to scar formation and fibrogenesis<sup>17</sup>.

Wound dressings have become fundamental component of wound treatment, and innovative dressings are constantly available on the wound care market. Wound dressing materials act as physical barriers, permeable for moisture and oxygen, but protecting the wound from pathogenic microorganisms<sup>18</sup>. Among all the classes of biomaterials employed for wound dressings, biopolymers are the most suitable, as they possess properties of excellent cytocompatibility, degradability, and lack of antigenicity. In particular, alginate,

chitosan, collagen and hyaluronic acid are commonly used, and there are several studies demonstrated that these biomaterials can promote wound healing<sup>18-19</sup>.

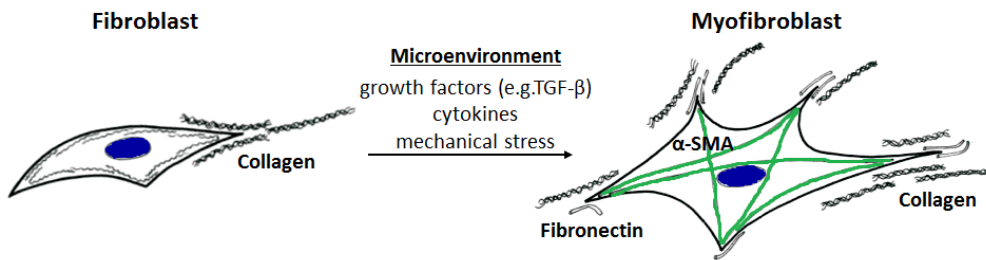


Fig. 4.32: Fibroblast to myofibroblast transition can be caused by microenvironment conditions such as growth factors, cytokines, and mechanical stress.  $\alpha$ -SMA expressing myofibroblasts are responsible for the excess deposition of collagen observed in pathological fibrosis.

Because of the different types of wounds and the complexity of healing process, there is no single dressing suitable for the treatment of all wound types. Generally, modern dressings are fabricated according to several important requirements: they should maintain a moist environment around the wound, allowing the passage of oxygen, promoting epithelial restoration and minimize infection and pain. Moreover, they should have adequate adherence to wound area and must be easy to apply and remove to avoid patient discomfort, as repeated changing of the dressing is necessary until the wound is completely healed. In addition, several dressings are impregnated with bioactive molecules, i.e. drugs or growth factors, in order to actively favor the healing process<sup>18</sup>. In particular, drugs commonly released by wound dressings can be divided into three main categories: antimicrobials, painkillers and anti-inflammatory drugs. Antimicrobials include drugs as gentamycin, ofloxacin, minocycline, and tetracycline; their main function is to prevent or combat infection, and local release is advantageous as it allows lower antibiotic doses thus reducing the risk of systemic toxicity<sup>18, 20</sup>. Painkillers such as ibuprofen and lidocaine provide local pain relief to the patients; finally, anti-inflammatory drugs such as salicylic acid favor wound healing process and help in achieving moderate pain relief<sup>18</sup>.

To the best of author's knowledge, release of drug to prevent excessive scar formation and fibrosis has never been reported. In this Chapter the possibility of local releasing a novel small molecule, namely CCG-203971<sup>21</sup>, from wound dressing has been investigated. In fact,



this drug has been reported to prevent differentiation of fibroblasts into myofibroblasts, thus avoiding excessive deposition of collagen and consequently scar formation and fibrosis; in particular, CCG-203971 inhibits TGF- $\beta$  induced protein expression of  $\alpha$ -SMA<sup>22-23</sup>. Core-shell ES technique was here used to fabricate a natural wound dressing, where gelatin and hyaluronic acid are the inner and outer polymers, respectively. In fact, gelatin has excellent cytocompatibility properties and it is easily processable by ES (see Chapter 2), while hyaluronic acid has been chosen because of its well-established relevance in wound healing, especially in favoring re-epithelialisation<sup>24-26</sup>. However, HA has a very poor processability by ES, because of its high molecular weight (in the order of millions of Da) and charged nature<sup>27</sup>; therefore, co-ES with gelatin can favor its spinnability while allowing the formation of nanofibers with HA on the surface. In recent years, ES has been used to fabricate wound dressing that could promote faster restoration and increase biocompatibility<sup>28</sup>. In fact, nanofiber dressings have high void volumes that can accommodate a greater quantity of exudates, and the dressings can act as scaffolds to favor migration and proliferation of the cells in the wound, while promoting tissue growth and faster wound healing. Moreover, the use of natural polymers allows fast degradation kinetics of the dressing (about 5-7 days), thus eliminating the problem of repeated changing that can destroy the new tissue formed. In addition, incorporation and controlled release of CCG-203971 drug in the electrospun membrane can inhibit myofibroblast differentiation, which is responsible for tissue contraction and scar formation. In particular, the drug has been added to the core solution with the intention of obtaining a sustained drug release, as demonstrated by several works in literature.

## 2. Materials and methods

### 2.1 Core-shell electrospinning optimization

#### Solution preparation

Gelatin (Gel, Gelatin A from porcine skin, G1890), hyaluronic acid (HA, Sodium hyaluronate from *Streptococcus equi*, 53747), and all the solvents used were purchased from Sigma Aldrich.

#### Core solution

Gelatin solutions in different solvents were used as core, in order to investigate how different solvent properties and solution concentrations could affect the formation of core-shell structure. In particular, two of the solvent systems used in this work had been previously optimized for ES in Chapter 2: pure formic acid (FA<sup>29</sup>), and 9/1 acetic acid/water (AA/H<sub>2</sub>O<sup>30</sup>). In addition, another solvent, which had been employed for ES of Gel in literature<sup>31</sup>, was here investigated: hexafluoroisopropanol (HFIP). Pure HFIP and 9/1 HFIP/H<sub>2</sub>O were used as solvent systems for Gel; in fact, a small amount of water was added with the intention to slow down the solvent evaporation rate. Gel concentrations tested for each solvent system are reported in Table 4.1.

Table 4.16: Solvent systems and concentration values of Gel investigated as possible core solutions.

Solvent system	Concentration [% w/v]
FA	5 – 10 – 15
AA/H <sub>2</sub> O (9/1)	5 – 7 – 10
HFIP	5
HFIP/H <sub>2</sub> O (9/1)	3 – 5

#### Shell solution

Because of its high molecular weight (1.5–1.8 x 10<sup>6</sup> Da) and anionic nature, HA is an extremely challenging polymer for ES technique, as HA solutions possess unusually high viscosity and surface tension. Therefore, few works in literature have succeeded in

electrospinning it using standard ES setups; among these, solvent systems and concentration values reported in two studies<sup>32-33</sup> (first two solvents reported in Table 4.2) were chosen, as the HA molecular weights used in these works are similar to that employed in the present study. In addition, the use of the same solvent, namely FA, for both core and shell solutions was investigated, with the aim of reducing surface tension at the interface of the solutions; with this solvent, the effect of stirring time on solution viscosity and processability by ES was also evaluated. The solvent systems and relative HA concentrations tested are summarized in Table 4.2.

Table 4.17: Solvent systems and concentration values of HA investigated as possible shell solutions.

Solvent system	Concentration [% w/v]	Reference
FA/DMF/H <sub>2</sub> O (2/1/1)	1.5 – 2.5	[32]
NH <sub>4</sub> OH/DMF (2/1)	1.5	[33]
FA	2 – 4	-

### Electrospinning: setup and parameter optimization

The electrospinning setup used in this work consisted of a syringe pump (KD scientific), a variable high voltage power source (AIPWild AG Switzerland), and a rectangular metal plate (dimensions 15 x 15 cm) used as collector. Standard or co-axial spinnerets were mounted on the plastic syringes used (1 mL, Braun). Stainless steel needle with inner diameter of 0.8 mm was employed for traditional ES, while stainless steel co-axial spinneret was used for core-shell ES; dimensions of the spinneret were: for the inner nozzle, ID = 0.51 mm, OD = 0.83 mm, and for the outer nozzle, ID = 1.37 mm, OD = 1.83 mm. Positive electric potential was applied to the needle tip and negative potential on the collector. The whole equipment was placed in a grounded Faraday cage located in a fume hood, and voltage values were controlled by LabView software (National Instruments). Where necessary, the ES process was carried out in a climatic chamber which provided stable and controlled environmental conditions during the process (deviations  $\pm 0.5$  °C,  $\pm 5\%$  RH).

A wide set of solutions were tested both as core and shell phases, and numerous combinations of Gel and HA solutions were co-axially electrospun in order to find the

couple of solutions suitable for obtaining core-shell fibers. The range of process and environmental parameters tested for the ES of each solution or combination of core/shell solutions are summarized in Tables 4.3 and 4.4.

In order to fabricate drug-loaded electrospun membranes, CCG-203971 (Sigma, SML1422) was dissolved in pure ethanol, at a concentration of 0.01 mol/L. Immediately before ES process, the desired amount of drug stock solution was mixed to gelatin by vortexing for one minute, in order to obtain homogeneous distribution of the drug within the solution.

### **Characterization techniques**

#### Morphological analysis

Electrospun sample morphology and core-shell structure were investigated by Scanning Transmission Electron Microscope (STEM, Hitachi S-4800, Hitachi High-Technologies). For scanning mode imaging, as-spun samples were mounted onto metal stubs with double sided adhesive tape, sputter coated with gold/palladium (a LEICA EM ACE600 was used as sputter coater), and imaged with a 2 kV accelerating voltage. Average diameter of the core-shell fibers was measured by image analysis with ImageJ software on 100 fibers per type of sample.

In order to investigate the bicomponent structure of the fibers, SEM images of their cross-section were examined; electrospun membranes were cut with a surgical blade in liquid nitrogen, fixed on a sample holder with vertical sample fixation, sputter coated with gold/palladium, and immediately analyzed by SEM.

Table 4.18: Solutions and parameter tested for traditional ES.

<b>Solution</b>	<b>Flow rate [q, mL/h]</b>	<b>Voltage [ΔV, kV]</b>	<b>Distance [d, cm]</b>	<b>Temperature [°C]</b>	<b>Relative humidity [%]</b>
Gel in FA, c = 5–10–15% w/v	0.05 – 0.5	15 – 20	11 – 18	20 – 22	20 – 40
Gel in AA/H <sub>2</sub> O, c = 5–7–10% w/v	0.3 – 1	15 – 20	11 – 18	20 – 22	20 – 40
Gel in HFIP, c = 5% w/v	0.2 – 0.6	15 – 20	10 – 18	20 – 22	20 – 40
Gel in HFIP/H <sub>2</sub> O, c = 3–5% w/v	0.2 – 0.6	15 – 20	10 – 18	20 – 40	20 – 30
HA in FA, c = 2% w/v	0.1 – 0.5	15 – 25	10 – 18	20 – 22	20 – 30

Table 4.19: Combinations of core and shell solutions used for co-axial ES and optimized parameters.

<b>Solution</b>	<b>Flow rate [q, mL/h]</b>	<b>Voltage [ΔV, kV]</b>	<b>Distance [d, cm]</b>	<b>Temperature [°C]</b>	<b>Relative humidity [%]</b>
Core: Gel in FA, c = 10–15% w/v	0.1 – 0.5	15 – 20	11 – 18	20 – 22	20 – 40
Shell: HA in FA/DMF/H <sub>2</sub> O, c = 1.5% w/v	0.1 – 0.5				
Core: Gel in AA/H <sub>2</sub> O, c = 7–10% w/v	0.3 – 1	15 – 20	11 – 18	20 – 22	20 – 40
Shell: HA in FA/DMF/H <sub>2</sub> O, c = 1.5% w/v	0.3 – 1				

Continue Table 4.4:

Core: Gel in HFIP/H <sub>2</sub> O, c = 3–5% w/v	0.2 – 0.6	17 – 20	10 – 14	20 – 40*	20 – 40
Shell: HA in FA/DMF/H <sub>2</sub> O, c = 1.5% w/v	0.2 – 0.6				
Core: Gel in FA, c = 10–15% w/v	0.1 – 0.3	17 – 20	9 – 17	20 – 22	20 – 40
Shell: HA in FA/DMF/H <sub>2</sub> O, c = 2.5% w/v	0.1 – 0.3				
Core: Gel in AA/H <sub>2</sub> O, c = 7–10% w/v	0.1 – 0.3	17 – 20	9 – 17	20 – 22	20 – 40
Shell: HA in FA/DMF/H <sub>2</sub> O, c = 2.5% w/v	0.1 – 0.3				
Core: Gel in HFIP/H <sub>2</sub> O, c = 3–5% w/v	0.1 – 0.5	14 – 20	10 – 14	20 – 40*	20 – 35
Shell: HA in FA/DMF/H <sub>2</sub> O, c = 2.5% w/v	0.1 – 0.5				
Core: Gel in HFIP/H <sub>2</sub> O, c = 3–5% w/v	0.1 – 0.3	17 – 20	8 – 12	20 – 40*	20 – 35
Shell: HA in NH <sub>4</sub> OH/DMF, c = 1.5% w/v	0.1 – 0.3				
Core: Gel in FA, c = 10% w/v	0.1 – 0.5	15 – 20	8 – 16	20 – 25	20 – 40
Shell: HA in FA, c = 2% w/v	0.1 – 0.5				

\*Gel solution was pre-warmed at 40 °C and a heating system, composed of a heating pad wrapped around the syringe and a heater control unit, was used to maintain the solution at 40 °C during ES process.

The samples for observation in transmission mode were prepared by directly electrospinning onto copper grids for about 30 seconds; accelerating voltage used was 30 kV. In order to increase the contrast between the two phases, different concentrations of Bromophenol Blue (B0126, Sigma-Aldrich) were added to the core and shell solutions before ES; in particular, 0.2% w/v in the core and 2% w/v in the shell solution<sup>34</sup>. Then, TEM samples were prepared as previously described and examined with a TEM instrument with higher resolution (Philips CM200 FEG), with 200 kV accelerating voltage.

To investigate the distribution of Gel and HA within the nanofibers, the biopolymers were conjugated to fluorescence probes. HA was labeled with fluorescein isothiocyanate (FITC, F7250, Sigma Aldrich) according to the method reported by Hsu<sup>35</sup>. Practically, 50 mg HA were dissolved in 40 mL formamide. Subsequently, 25 mg FITC and 20 mg dibutyltin dilaurate were added to 25 mL dimethyl sulfoxide and the mixture heated to 100 °C for 30 minutes. The reaction mixture was then dialyzed against distilled water and lyophilized.

For Gel labeling, rhodamine isothiocyanate (RITC, R1755, Sigma Aldrich) was used according to the method reported by Chang et al.<sup>36</sup>, but with some modifications. In particular, 0.25 g of Gel were dissolved in 0.1 M carbonate buffer at 40 °C, and 0.018 g of RITC were dissolved in 4.5 mL DMSO. Then, the two solutions were mixed and stirred for 1 hour at RT, before being incubated at 4 °C for 24 h. The reaction mixture was then dialyzed against distilled water and lyophilized. RITC-Gel and FITC-HA prepared as described were dissolved in FA and used as core and shell solutions; samples for subsequently analysis at the confocal laser scanning microscope (CLSM, Zeiss 780) were prepared by co-axial ES of the two solutions onto glass coverslips, used as collector.

### Chemico-physical analyses

As previously reported, HA solutions are known for their particularly high viscosity, which can prevent stable ES process; therefore, it was important to investigate rheological behavior of HA solutions used for ES. In particular, viscosity as function of shear rate was measured by means of a rheometer (Paar Physica MCR 300, Austria) equipped with a plate–cone system; measurements were carried out at 20 °C in controlled shear rate mode.

A tentative strategy to decrease HA solution viscosity was to use microwave (MW) radiation, in accordance with the procedure reported by Fuentes et al.<sup>37</sup>. In fact, MW radiations can break inter-molecular hydrogen bonds, thus significantly reducing solution viscosity. Therefore, MW irradiation of 1.5% and 2.5% HA in FA/DMF/H<sub>2</sub>O was carried out on a Milestone Microwave (Microwave Laboratory Systems 1200 mega, EM-45/A Exhaust Module), using a power of 200 W for 1 minute. In order to avoid excess heating, the glass vials containing the solution were immersed in cold water during the treatment.

The conductivity of the solutions used for core-shell fiber fabrication, i.e. 10% Gel and 2% HA in FA, was measured on a Metrohm 660 Conductometer from Brinkmann.

In order to investigate the presence of HA on fiber surface, the surface chemistry of the electrospun membranes was analyzed by X-ray Photoelectron Spectroscopy (XPS). XPS measurements were performed on a PHI 5000 VersaProbe II instrument (USA) equipped with a monochromatic AlK $\alpha$  X-ray source. Energy resolution and pass energy used were 0.8 eV/step and 187.85 eV for survey scans and 0.125 eV/step and 29.35 eV for high resolution scans, respectively. Carbon 1s at 284.5 eV was used as a calibration reference to correct for charge effects. Elemental concentrations and chemical shifts within the region scans were determined selecting the photoelectron-transitions C1s, O1s and N1s. For data analysis CasaXP software (Casa Software Ltd, United Kingdom) was used.

## **2.2 Glutaraldehyde crosslinking process**

Electrospun membranes of pure Gel and Gel/HA were crosslinked by glutaraldehyde (GA) vapor. The parameters used for the procedure were those previously optimized for Gel membranes and reported in Chapter 2. Briefly, each electrospun membrane was fixed to a Petri dish and crosslinked for 2 hours in a sealed desiccator containing 5 mL of 50% aqueous GA solution (Sigma Aldrich, 340855). After crosslinking, the samples were exposed in a fume hood overnight to remove residual GA.

In order to investigate possible variation in morphology of the electrospun membranes after glutaraldehyde crosslinking process (GA\_CL), SEM images of the samples were examined and diameter of the crosslinked fibers was measured as previously reported.



Moreover, a capillary flow porometer (Porolux 1000, Porometer) was used to measure the nominal pore size and pore size distribution of membrane samples ( $\varnothing = 13$  mm) before and after GA\_CL, with the help of an Automated Capillary Flow Porometer system software.

In order to demonstrate that crosslinking reaction of the membranes with GA has occurred and to investigate possible differences in biopolymer molecular structure after GA\_CL at different crosslinking times, XPS and Fourier Transform Infrared (FTIR) spectroscopy were employed. In particular, XPS was used to determine the chemical state of nitrogen (N1s) by means of chemical shift and peak fitting. In fact, reaction between amino groups ( $\text{NH}_2$ ) in Gel molecules and GA causes the formation of imino group ( $\text{N}=\text{H}$ )<sup>38</sup>. Therefore, N1s peak of crosslinked Gel should have a shift in binding energy from 399 eV ( $\text{NH}_2$ ) to 398 (N=H). N1s peak fitting for different GA\_CL times was carried out using CasaXPS software.

IR spectroscopy was used to determine the bond types present in the electrospun fibers, thus investigating GA\_CL induced variation in the molecular structure of the biopolymers; a Bruker Tensor 27 with a PIKE technologies GladiATR was employed.

Stability of the crosslinked samples ( $\varnothing = 13$  mm) was assessed by degradation test in PBS at 37 °C. Morphology of the specimen after 24-hour immersion in PBS was evaluated by SEM analysis.

## **2.3 *In vitro* tests**

### **Drug release test**

Gel and Gel/HA membranes loaded with two different amounts of drug, i.e. 0.1% and 0.2% w/w, were punched into circular samples ( $\varnothing = 13$  mm) for *in vitro* drug release study. Four specimens per type of membrane were then weighed, placed in a 24-well plate and covered with 500  $\mu\text{L}$  of medium; both Phosphate Buffered Saline solution (PBS) and Roswell Park Memorial Institute 1640 medium (RMPI, without serum nor phenol red) were used. The experiment was carried out at 37°C and 5%  $\text{CO}_2$  in order to buffer possible pH variations due to sample degradation in the medium. The multiwell plates containing the samples were oscillating at 50 rpm. At specified immersion periods ranging between 0 and 4 days, all the medium was taken out for the analysis and replaced with an equal volume of fresh

PBS or RPMI. The amount of drugs in the withdrawn media was determined by means of a UV-spectrophotometer (BioTek SynergyMx multi-mode microplate reader). Calibration curves were established using known concentrations of CCG-203971 in PBS or RPMI both at 252 nm and 281 nm (corresponding to drug maximum absorption).

From considerations on sample weight and relative amount of drug in the feed solution, the theoretical amount of drug present in the samples was calculated, and then the measured drug released was expressed at each time point as percentage of the theoretical one.

To eliminate the possible absorbance contribution due to degraded sample material, specimens of Gel and Gel/HA without the drug were also tested as control.

#### **Evaluation of CCG-203971 cytotoxicity**

Cells used in this work were primary Human Dermal Fibroblasts (HDFs) harvested from different donors; cell passage number varied between 11 and 17. Cells were cultured in Dulbecco's Modified Eagle Medium (DMEM, Sigma) supplemented with 10% Calf Serum, 1% Penicillin-Streptomycin, and 1% L-Glutamine in a humidified atmosphere with 5% CO<sub>2</sub> at 37 °C. Cells were used for experiments when in exponential growth phase. In order to evaluate cytotoxic effect of the drug of interest, cells were exposed to different drug concentration, from 0.3 to 30 μM, for 3 or 5 days, and their viability was then evaluated by MTS assay. In particular, 1'800 cells were seeded in each well of a 96-well plate, with 100 μL of medium. CCG-203971 stock solution was prepared in DMSO; after 12 hours from seeding, cell medium was changed and drug stock solution was added to DMEM with the proper amount for each concentration value. The volume of DMSO present in the medium was kept constant (0.1% v/v). DMEM and DMEM with 0.1% DMSO were used as controls.

#### **Evaluation of CCG-203971 efficacy: CLSM analysis and FACS test**

The protocol for myofibroblast differentiation employed a starved medium composed of RPMI-1640 supplemented with 1% Horse Serum, 1% Penicillin-Streptomycin, and 1% L-Glutamine for HDFs culture (cell density = 10'000 cells/cm<sup>2</sup>); in addition, TGF-β (c = 2 ng/mL)

was added to the starved medium in order to induce differentiation. After 3 days, expression of  $\alpha$ SMA (marker for myofibroblasts) was evaluated by CLSM examination. To assess the efficacy of CCG-203971, cells were cultured according to the differentiation protocol and exposed to different drug concentrations; in particular, cells were seeded in a 96well plate with 100  $\mu$ L of starved medium. 12 hours after seeding, the medium was changed: starved RPMI with and without TGF- $\beta$  were used as positive and negative control respectively, and starved medium with TGF- $\beta$  containing different drug concentrations, from 0.3 to 30  $\mu$ M, was used to test drug efficacy. After 3 days of incubation, cell possible differentiation was evaluated on a quality level by CLSM examination, or more precisely by means of FACS test. For CLSM imaging, cells were fixed with paraformaldehyde and stained with  $\alpha$ SMA-FITC monoclonal antibody and DAPI before undergoing microscope analysis. For FACS test, cells were detached with accutase, collected and washed in 0.1% Bovine Serum Albumin. They were then stained with  $\alpha$ SMA-FITC antibody and DAPI, and sorted by FACS using a Gallios 3/10 Flow Cytometer (Beckman Coulter). Unspecific binding of the antibody was evaluated by means of an isotype. Cells positive both for  $\alpha$ SMA and DAPI were considered as differentiated (i.e. myofibroblasts). At least 10'000 cells were analyzed for each sample. Results were elaborated and expressed in terms of differentiation inhibition, considering the percentage of cells differentiated in the positive control as reference. FACS test was repeated three times to have valuable statistics data.

#### **Membrane cytocompatibility test: Live/Dead and MTS assays**

Circular sample ( $\varnothing = 13$  mm) were punched from electrospun membranes after GA\_CL. To evaluate sample cytocompatibility, three specimens per type (i.e. Gel and Gel/HA with and without the drug) were used for Live/Dead assay and three for MTS test. As the samples are highly hydrophilic, they swelled and shrunk upon contact with aqueous media; therefore, it was necessary to use smaller glass rings ( $\varnothing = 10$  mm) to keep the samples flat after seeding. In particular, dry samples were put in a 24-well plate, and a glass ring was placed above them. 500  $\mu$ L of HDF suspension in complete DMEM were used for seeding (cell density = 12'000 cells/mL). After 12 hours, 200  $\mu$ L of medium were added to each well.

Three days after seeding, cell viability was evaluated by Live/Dead assay and MTS assay, using cells seeded on tissue culture polystyrene (TCPS) well as control.

### **Effects of drug-loaded membranes on HDF differentiation: indirect and direct cell tests**

In order to evaluate if CCG-203971 incorporated in the electrospun membranes retained its activity after ES process, indirect contact cell tests were initially carried out. Eluates of Gel and Gel/HA samples with or without the drug were prepared by placing three disks ( $\varnothing = 13$  mm) for each material into a 48-well plate with 500 $\mu$ L of starved RPMI with TGF- $\beta$ , and then incubated at 37 °C, 5% CO<sub>2</sub> for 24 hours. Aged RPMI with or without TGF- $\beta$  were used as positive and negative control, respectively. HDFs were seeded at a density 3'350 cells per well and, 12 hours after seeding, they were exposed to eluates for three days at 37°C, 5% CO<sub>2</sub>. Cell differentiation was then evaluated by  $\alpha$ SMA staining and CLSM examination as reported before.

Finally,  $\alpha$ SMA expression of HDFs seeded on electrospun membranes was evaluated. Three specimens for type were placed in a 24-well plate and seeded. Cell suspension (24'000 cells/mL) was prepared in starved RPMI with TGF- $\beta$ . After 3 days from seeding, cells were fixed with paraformaldehyde and stained with  $\alpha$ SMA-FITC monoclonal antibody, DAPI and Alexa Fluor 546 phalloidin, which is an F-actin probe with emission in red-orange field. In order to prevent fluorescence signal from the membranes, before CLSM analysis the samples were treated with 0.3% w/v Black Sudan solution in 70% ethanol for 4 hours, as reported in the article by Jaafar and coworkers<sup>39</sup>.

## **3. Results and discussion**

### **3.1 Core-shell electrospinning optimization**

#### Core solution

In order to obtain a core-shell fiber structure, we initially considered Gel solutions for the core that had already proved to be spinnable alone. In particular, ES of Gel had been

previously optimized in this thesis (see Chapter 2) from parameters found in literature<sup>29-30</sup> using FA (c = 15% w/v) or AA/H<sub>2</sub>O (c = 10% w/v) as solvents. Moreover, a solvent widely used for ES of biopolymers is HFIP, as it can break both hydrophilic and hydrophobic interactions within the molecules and it is highly volatile. Gel solutions in HFIP have been electrospun in literature with concentration of 5%<sup>31</sup>.

The three solvent systems reported for gelatin ES have different properties (e.g. vapor pressure and surface tension, as reported in Table 2.2 of Chapter 2), thus making interesting to investigate the influence of different core solvent systems on the process and on the formation of core-shell fibers; in fact, interfacial tension between the two phases plays a fundamental role in determining the stability of fiber formation process, thus affecting the eventual formation of core-shell structure. Furthermore, as also the concentration ratio between inner and outer solutions is an important factor affecting coaxial ES outcome, ES of different gelatin concentrations for each solvent system was carried out. Figg. 4.2 and 4.3 show SEM images of samples obtained from ES of Gel in FA and AA/H<sub>2</sub>O, respectively, for different concentrations; Table 4.5 reports the optimized parameters for each solution. Gel in FA proved to be spinnable up to 10% concentration (Fig. 4.2a, b), as homogeneous fibers could be obtained. For lower concentration values, i.e. 5%, chain entanglement was no longer sufficient for adequate fiber formation and several beads were present (Fig. 4.2c).

The same trend was observable for AA/H<sub>2</sub>O solvent: for 10% and 7% Gel concentration ES process was stable and homogeneous fibers were produced (Fig. 4.3a, b), while for 5% concentration fibers with beads were formed (Fig. 4.3c).

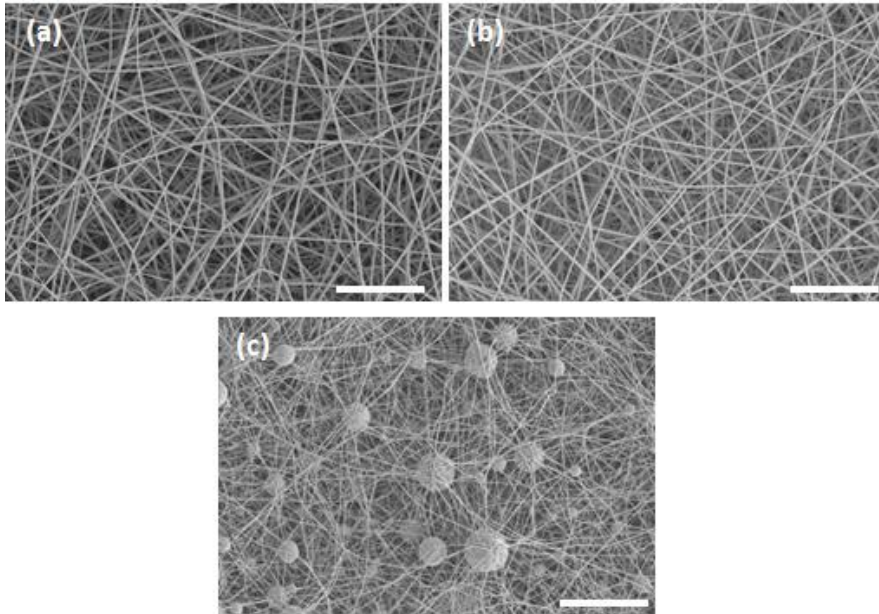


Fig. 4.33: SEM images of gelatin electrospun in FA at different solution concentrations: (a)  $c = 15\% \text{ w/v}$ ; (b)  $c = 10\% \text{ w/v}$ ; (c)  $c = 5\% \text{ w/v}$ . Scale bar:  $5 \mu\text{m}$ .

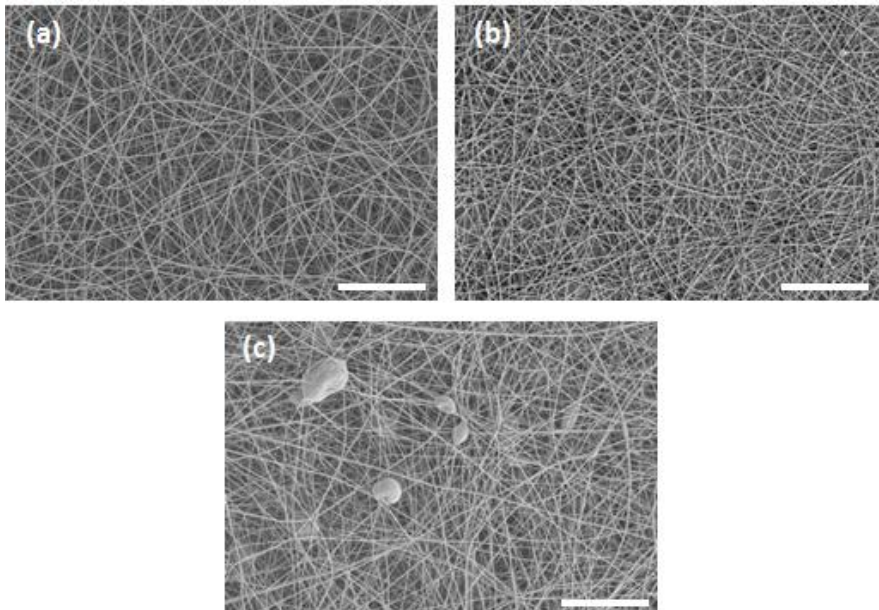


Fig. 4.34: SEM images of gelatin electrospun in AA/H<sub>2</sub>O at different solution concentrations: (a)  $c = 10\% \text{ w/v}$ ; (b)  $c = 7\% \text{ w/v}$ ; (c)  $c = 5\% \text{ w/v}$ . Scale bar:  $5 \mu\text{m}$ .

Table 4.20: Optimized solutions and parameters for traditional ES.

Solution	Flow rate [q, mL/h]	Voltage [ $\Delta V$ , kV]	Distance [d, cm]	Temperature [°C]	Relative humidity [%]
Gel in FA, c = 10–15% w/v	0.2	+12/-5	14	20 – 22	20 – 40
Gel in AA/H <sub>2</sub> O, c = 7–10% w/v	0.6	+12/-5	14	20 – 22	20 – 40
Gel in HFIP/H <sub>2</sub> O, c = 3–5% w/v	0.3	+10/-4	14	40	20 – 30

ES of 5% Gel in HFIP proved not to be a stable process, as needle clog due to fast solvent evaporation occurred, thus leading to gelification of the solution and process interruption after few minutes. In order to lower solvent evaporation rate, we added a small amount (10% v/v) of water to the solution, as water is not a volatile solvent and its vapor pressure is significantly lower than HFIP one. Actually, this expedient improved solution processability, even if solution gelification at the tip of the spinneret still occurred after longer times (20-30 minutes). Moreover, we tried to decrease Gel concentration in solution down to 3% w/v to investigate minimum solution concentration that could be electrospun. Fig. 4.4 shows the morphology of the fibers electrospun from 5% (Fig. 4.4a) and 3% (Fig. 4.4b) Gel solutions in HFIP/H<sub>2</sub>O: in both cases fibers with a lot of beads were obtained. The presence of these defects did not seem related to the low concentration values, as no significant difference between the two solutions was observable in SEM images; most likely, it could be a problem related to non-stability of the process due to spinneret clog. As it is well known that gelatin solutions in water gelled for temperature lower than 30-35 °C but are fluid for higher temperature values, we wanted to investigate the effect of temperature on Gel solution in HFIP/H<sub>2</sub>O to improve ES process stability. In particular, we tried to electrospin 3% Gel solution by warming up the solution immediately before ES and using a heating system wrapped around the syringe during the process; in both the procedures, the temperature was set to 40 °C. The aim was to reduce solution gelification, thus favoring ES process continuity, by means of higher temperature. Fig. 4.4c shows that,

in this case, ES process resulted in formation of homogeneous fibers without any beads; moreover, the temperature increase was effective in preventing solution gelification, thus allowing stable ES process with optimized parameters reported in Table 4.5.

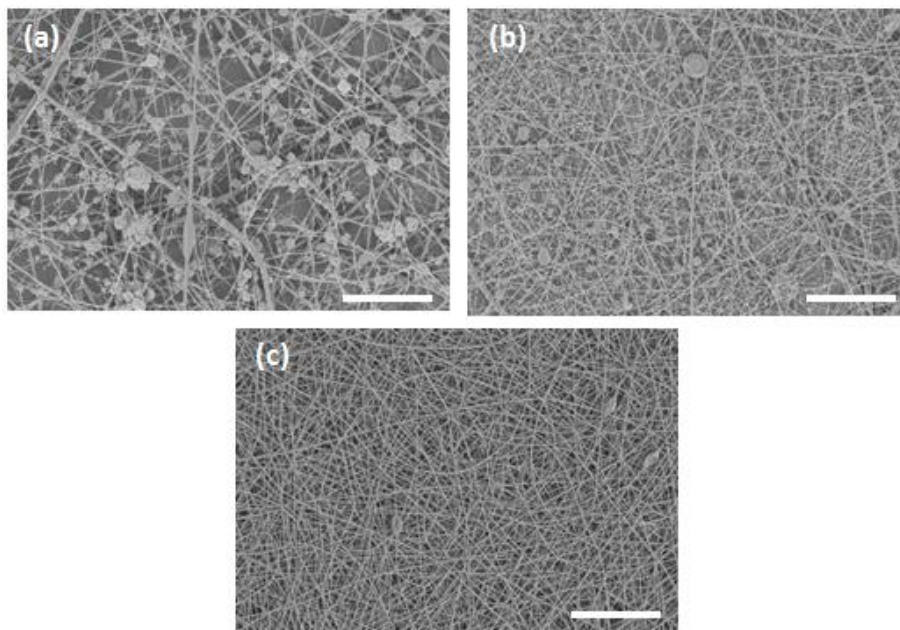


Fig. 4.35: SEM images of gelatin electrospun in HFIP/H<sub>2</sub>O at different solution concentrations and temperature: (a)  $c = 5\%$  w/v,  $T = 20^\circ\text{C}$ ; (b)  $c = 3\%$  w/v,  $T = 20^\circ\text{C}$ ; (c)  $c = 3\%$  w/v,  $T = 40^\circ\text{C}$ . Scale bar:  $5\ \mu\text{m}$ .

In the work by Ki et al.<sup>29</sup> about ES of Gel in FA, a decrease with time of Gel solution viscosity and degradation of molecular structure was reported as consequence of solubilisation in FA of the polymer. Therefore, we investigated the effect of stirring time on rheological behavior of Gel solution in FA ( $c = 10\%$ ). Results showed that Gel solution behaved as a Newtonian fluid, with constant viscosity for increasing shear rate, independently on the stirring time (Fig. 4.5). This behavior is typical of a solution without interconnected network: Gel molecules were probably highly fragmented (because of the intrinsic nature of gelatin, made by relatively short peptides of 50-100 kDa), and FA solvent broke the hydrogen bonds among the molecules, thus eliminating intermolecular interactions. Furthermore, for increasing stirring time solution viscosity decreased: probably, also in this



case cleavage by hydrolysis of Gel molecular chains by FA occurred<sup>29</sup>. Therefore, for ES purposes it was necessary to prepare and spin fresh solutions.

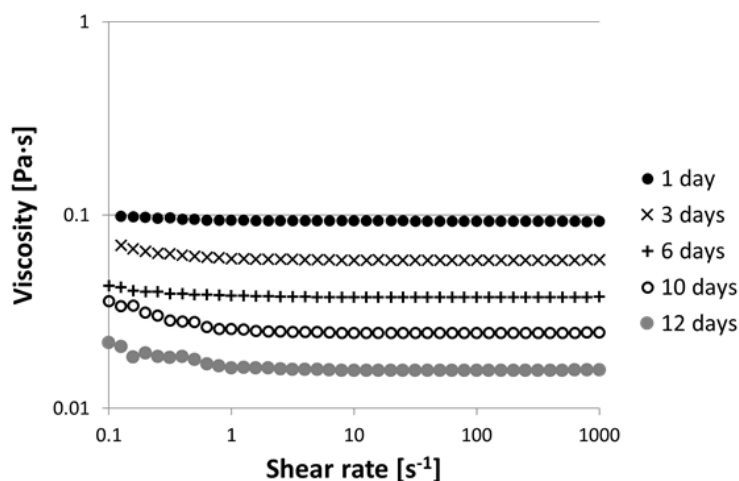


Fig. 4.36: Curves of viscosity as function of shear rate for 10% w/v Gel solution in FA at different stirring time, from 1 to 12 days.

### Shell solution

HA has been successfully electrospun in literature using different solvent system: FA/DMF/H<sub>2</sub>O ( $c = 1-1.5\%$  w/v) and NH<sub>4</sub>OH/DMF ( $c = 1.5\%$  w/v)<sup>32-33</sup>. The concentration values of HA solutions employed in these works were lower than those of Gel solutions which were intended to be used as core material, and this represented a possible limiting factor for co-axial fiber structure achievement, as probably during fiber formation process HA amount could not be sufficient to form a whole sheath around Gel inner fiber. Therefore, HA concentration in FA/DMF/H<sub>2</sub>O, which was the only solvent system compatible with all the three core solvents, was increased from 1.5% to 2.5% w/v. Results of rheological analysis of 1.5% and 2.5% solution concentrations showed that concentration increase had a significant effect on the viscosity; in fact, viscosity value increased of about one order of magnitude, from 10 to 100 Pa·s in the shear rate range of 0.01 to 1 s<sup>-1</sup>, where the solution had almost linear behavior (Fig. 4.6a).

This behavior is related to the high molecular weight of the biopolymer and its polyelectrolyte nature: previous works in literature reported that even a small increase in

HA concentration could remarkably affect solution viscosity<sup>33, 40</sup>. Viscosity of 2.5% HA solution appeared extremely high, thus possibly resulting in a solution difficult to electrospin.

An alternative strategy to maintain solution concentration relatively high, without excessively affecting the viscosity, consists in using MW radiations on the solution. In fact, studies in literature have demonstrated that MW radiations on organic substances disturb the molecule dipoles present in chemical systems stabilized by hydrogen bonds; for example, effects of MW absorption on solution viscosity are reported in literature for chitosan solutions in 5% FA<sup>37</sup>. HA chains in solution are expected to form inter-molecular bonding, and in particular hydrogen bonds, that cause chain stiffness and, consequently, high solution viscosity. MW radiations can disrupt hydrogen bonds among HA chains, thus lowering the viscosity. Rheological analyses of 1.5% and 2.5% HA solutions after MW radiations (200 W, 1 minute) confirmed the expected result (Fig. 4.6a): after MW treatment, viscosity value of both the solutions decreased of about two orders of magnitude, respectively. However, not only viscosity value but also solution rheological behavior was different after MW: in fact, Fig. 4.6a shows that HA solutions before MW radiation, for both the concentrations, had a pseudoplastic behavior, as viscosity decreased for increasing shear rate (shear thinning). This phenomenon is related to the shear-induced disruption of entanglements and intermolecular interactions, and it was already reported by Liu and coworkers<sup>32</sup>. On the contrary, HA solutions after MW radiations behaved almost like Newtonian fluids, with constant viscosity for increasing shear rates; this behavior suggested the possibility that the network made up by polymer chains was no longer present because of molecule breaking. As complete degradation of HA chains was not expected nor desired for the final application, further investigation was carried out in order to evaluate if MW process was affecting only inter-molecular associations or if it was also causing chain degradation.

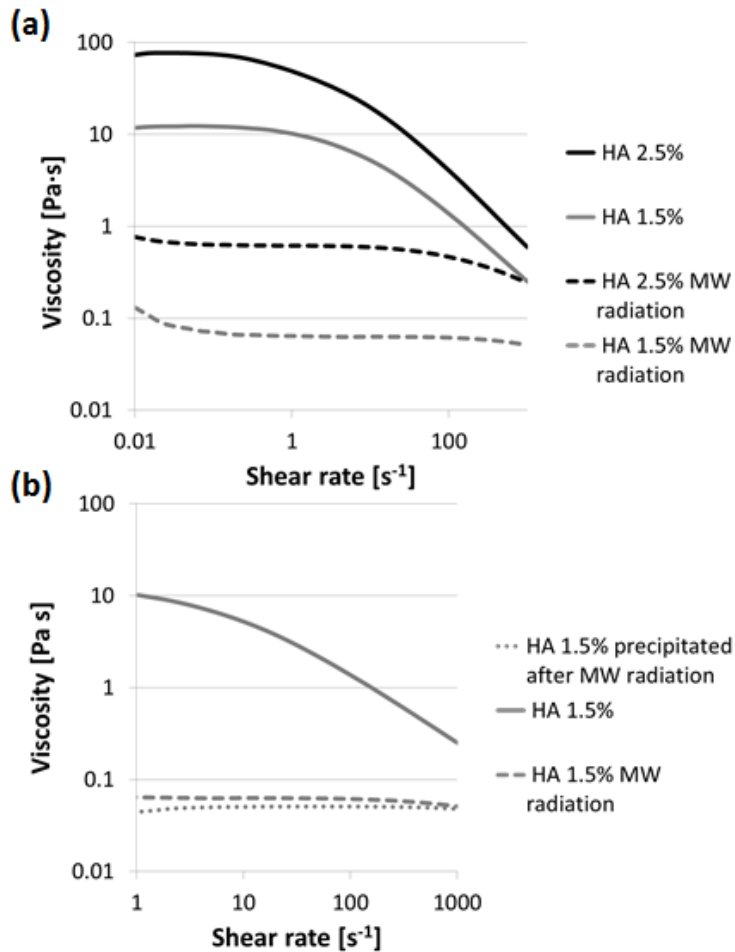


Fig. 4.37: Curves of viscosity as function of shear rate: (a) HA solutions in FA/DMF/H<sub>2</sub>O at two different concentrations, 1.5% and 2.5% w/v, before and after MW radiation; (b) 1.5% HA solutions before and after MW radiation, and after HA precipitation and re-dissolution by mechanical stirring in FA/DMF/H<sub>2</sub>O.

HA in solutions undergone MW radiations was precipitated by rapid addition of ethanol and the re-dissolved in FA/DMF/H<sub>2</sub>O by mechanical stirring ( $c = 1.5\%$  w/v). If MW process had caused chain degradation, the viscosity of the solution prepared with precipitated HA should have been lower than that prepared from “raw” HA. Unfortunately, rheological analysis confirmed this hypothesis: viscosity of 1.5% precipitated HA solution was significantly lower than that of the original 1.5% HA solution, and its rheological behavior was very close to that of 1.5% HA solution undergone MW radiation (Fig. 4.6b). Therefore,

it was possible to conclude that MW process caused disruption of HA molecular chains to a great extent, thus resulting in extensive biopolymer degradation.

Lower values of power and of the energy given during MW radiation were not sufficient to obtain a decrease in solution viscosity, thus suggesting that MW treatment, which is potentially useful to lower solution viscosity, was not suitable in this case.

Another important parameter affecting the formation of core-shell fibers concerns the interactions between the solvents of the two phases. In fact, it is reported that bicomponent fiber structure is favored by the use of immiscible solvents or, in alternative, by means of solvents with low interfacial tension<sup>8</sup>. From the results of solubility tests conducted for Gel and HA (see Tables 2.6 and 2.8 of Chapter 2), it was evident that it was not possible to use immiscible solvents for the two polymers; however, a good solvent for both the polymer existed: formic acid. Moreover, ES process of Gel in pure FA proved to be stable and excellent fiber morphology could be obtained. Therefore, we considered pure FA as solvent also for HA shell solution, even if ES of HA in this solvent has never been reported in literature before. Solutions with two different HA concentration values were considered, i.e. 2% and 4% w/v; however, the latter appeared more like a gel than like a fluid, so it was not possible to use it for ES purposes. For 2% HA solution, the effect of stirring time as possible means to reduce solution viscosity was also evaluated. In fact, as for Gel solution, decrease of viscosity for increasing stirring time had already been reported in literature for HA in FA<sup>32</sup>.

Curves of viscosity as function of shear rate for 2% HA solutions stirred for different times are shown in Fig. 4.7: it was evident that viscosity values greatly decreased for increasing stirring time. Initially, solutions had a high viscosity: in fact, HA is a high molecular weight polymer, whose long chains increase the amount of chain entanglements; moreover, it presents an acidic group and a glucosamine segment along its structure, that in the presence of weak acid makes HA a polyelectrolyte, favoring intermolecular associations<sup>27</sup>. These two characteristics resulted in solutions with unusually high viscosity. Furthermore, for solutions up to 5 days of stirring, pseudoplastic behavior was evident (as already reported for HA solutions in FA/DMF/H<sub>2</sub>O) and shear thinning occurred. In fact, at low shear

rate, HA molecules had an irregular internal order and greater resistance to flow, causing the viscosity value to be high. For increasing shear rate, equilibrium interaction of macromolecules was disrupted as molecules aligned with the flow, slipping over one another more easily, leading to lower viscosity values. Pseudoplastic behavior became less evident for increasing stirring time, and finally HA solutions stirred for 28 and 38 days had a Newtonian behavior, with constant viscosity in the whole range of shear rate tested. Therefore, increasing the stirring time had two main effects: the decrease of solution viscosity and the change of solution rheological behavior from pseudoplastic to Newtonian fluid. A possible explanation for both these effects is that FA causes the break of polymer chains by cleavage of glycosidic bonds along HA molecule <sup>32</sup>. The rupture of molecular chains results in a decrease of viscosity and, for longer times, it becomes so extensive that connectivity of the polymeric network is lost, resulting in a Newtonian behavior of the solution. If, from one side, this effect could be useful as the high viscosity of HA solutions was a problem for their processability by ES, on the other side extensive chain degradation was not suitable for the final application; therefore, the adequate stirring time had to be carefully considered.

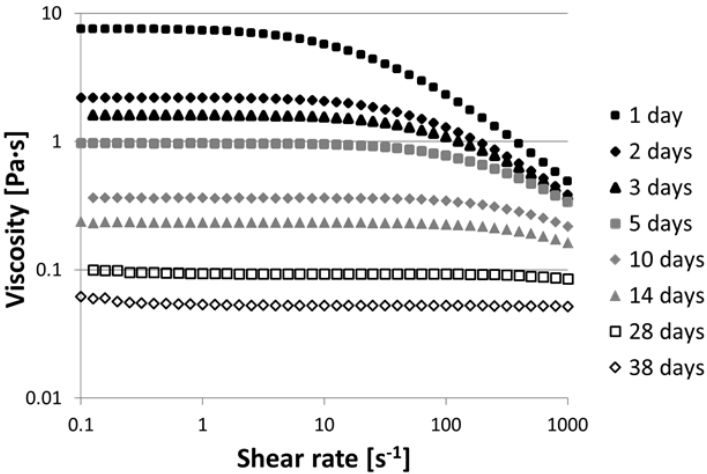


Fig. 4.38: Curves of viscosity as function of shear rate for 2% w/v HA solution in FA at different stirring time, from 1 to 38 days.

In order to evaluate how the stirring time, and therefore the viscosity, affected electrospinnability of the solution, ES of 2% HA solutions considered for rheological analyses was carried out. Even if ES parameters were varied in a wide range, it was not possible to obtain adequate fiber morphology. In particular, for solutions stirred up to 3 days, a drop of viscous fluid was formed at the tip of the spinneret and even for high values of voltage it was not possible to have any jet formation or deposition on the collector (Fig. 4.8a): solution viscosity was too high. For longer stirring times, i.e. 5 to 11 days, jet formation occurred and a whitish small deposition on the collector was visible; however, SEM analysis revealed that the process was more similar to electro spraying than to ES, as only small fragments of fibers and a lot of beads were obtained (Fig. 4.8b, c). Evidently, solution concentration was too low to have adequate fiber formation; optimization of solution concentration while maintaining adequate solution viscosity is a common problem for ES of HA. Finally, for stirring times longer than 14 days, less deposition on the collector occurred (Fig. 4.8d): probably the chain degradation was too extensive and intermolecular entanglements, which favored fiber formation, were no longer present.

Even if it was not possible to obtain good fiber morphology from 2% HA in FA, it could be interesting to employ this solution in co-axial ES in combination with Gel solution in FA, in order to evaluate if the use of the same solvent for the two phases effectively promote the formation of bicomponent fibers. In particular, HA solution stirred for 5 days was used for co-axial ES; in fact, this solution did not have too high viscosity which could prevent ES process, its rheological behavior was still pseudoplastic, and some initial fragments of fiber were formed by ES, meaning that no great chain degradation had occurred.

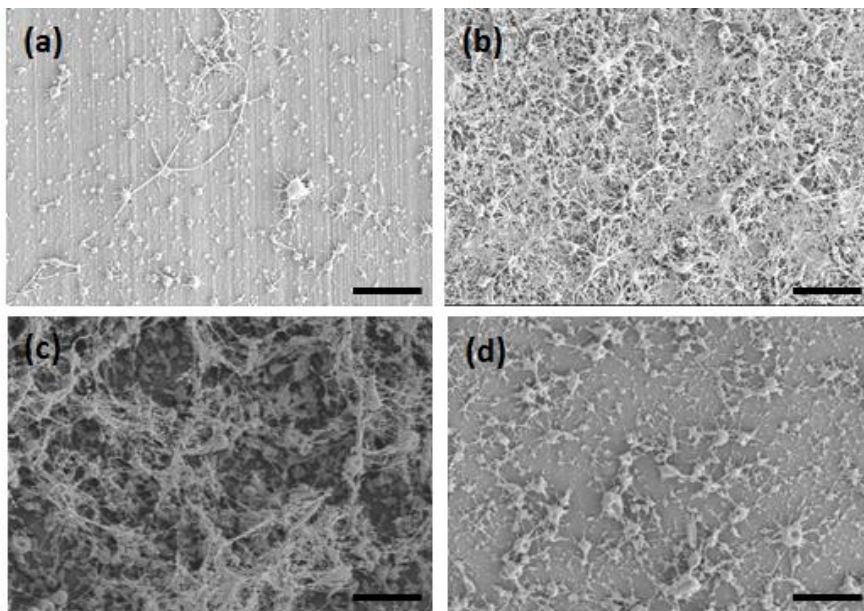


Fig. 4.39: SEM images of 2% w/v HA in FA electrospun at different solution stirring time: (a) 3 days; (b) 5 days; (c) 11 days, (d) 14 days. Scale bar: 5  $\mu$ m.

#### Core-shell electrospinning

The optimized parameters used for co-axial ES are reported in Table 4.6. The process proved to be stable only when 1.5% HA solution in FA/DMF/H<sub>2</sub>O or 2% HA in FA were employed as shell; for 2.5% HA in FA/DMF/H<sub>2</sub>O, ES became non-continuous and a drop of solution at the tip of the spinneret was periodically formed. Also co-axial ES process of 1.5% HA in NH<sub>4</sub>OH/DMF as shell and 3% Gel in HFIP/H<sub>2</sub>O as core was not stable for more than few minutes, because when the two solutions mixed at the end of the spinneret gelification occurred and the process was completely blocked. Therefore, these two shell solutions were not further considered for co-axial ES.

Fig. 4.9 shows the SEM images of samples obtained using 1.5% HA solution in FA/DMF/H<sub>2</sub>O as shell, and three Gel solutions in different solvents as core (only one concentration value of Gel per solvent system is reported to avoid useless repetition): for each solution combination, electrospun morphology was good with homogeneous fibers and no defects. As expected, fiber dimensions decreased for decreasing Gel concentrations of the core solution. Moreover, while fiber morphology was not affected by changes of spinneret-to-

collector distance and voltage applied, flow rate was a critical parameter to be optimized for all the Gel solutions used: in fact, when the two feed rates used for core and shell were very different (e.g. 0.1 vs 0.5 mL/h), fibers with several beads were obtained. The best morphology was achieved using the same flow rate or slightly greater for Gel solution.

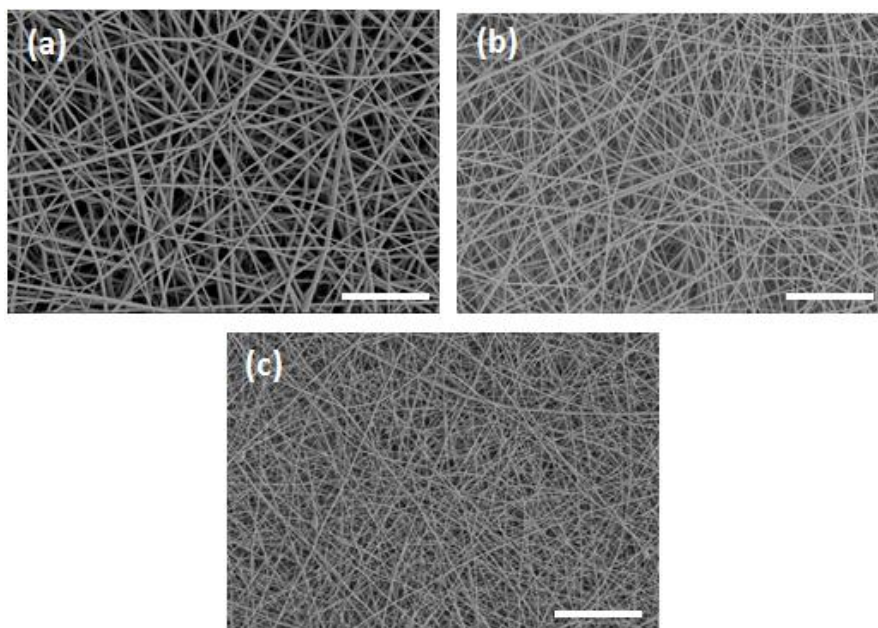


Fig. 4.40: SEM images of fibers electrospun with co-axial needle, using 1.5% w/v HA in FA/DMF/H<sub>2</sub>O as shell solution and different core solutions: (a) 15% w/v Gel in FA; (b) 7% w/v Gel in AA/H<sub>2</sub>O; (c) 3% Gel in HFIP/H<sub>2</sub>O (T = 40 °C). Scale bar: 5  $\mu$ m.

Even if 2.5% HA in FA/DMF/H<sub>2</sub>O and 1.5% HA in NH<sub>4</sub>OH/DMF as shell solutions did not allow stable ES process, fiber obtained from co-axial process still showed excellent morphology with none or very few beads present (Fig. 4.10, 4.11); probably, Gel core solution was still properly electrospun and produced adequate fibers, while the shell solution was too viscous to be elongated and form a jet, even for increasing values of voltage applied. This hypothesis would suggest that no shell formation was taking place using these HA solutions, even if specific analyses were necessary to confirm it.



Table 4.21: Optimized solutions and parameters for co-axial ES.

Solution	Flow rate [q, mL/h]	Voltage [ΔV, kV]	Distance [d, cm]	Temperature [°C]	Relative humidity [%]
Core: Gel in FA, c = 10–15% w/v	0.1	+12/-5	14	20 – 22	20 – 40
Shell: HA in FA/DMF/H <sub>2</sub> O, c = 1.5–2.5% w/v	0.05 – 0.1				
Core: Gel in AA/H <sub>2</sub> O, c = 10% w/v	0.6	+12/-5	14	20 – 22	20 – 40
Shell: HA in FA/DMF/H <sub>2</sub> O, c = 1.5–2.5% w/v	0.5 – 0.6				
Core: Gel in AA/H <sub>2</sub> O, c = 7% w/v	0.2	+12/-5	14	20 – 22	20 – 40
Shell: HA in FA/DMF/H <sub>2</sub> O, c = 1.5–2.5% w/v	0.2				
Core: Gel in HFIP/H <sub>2</sub> O, c = 3–5% w/v	0.3	+10/-4	14	40	20 – 40
Shell: HA in FA/DMF/H <sub>2</sub> O, c = 1.5% w/v	0.3				
Core: Gel in HFIP/H <sub>2</sub> O, c = 3–5% w/v	0.1	+10/-4	14	40	20 – 35
Shell: HA in FA/DMF/H <sub>2</sub> O, c = 2.5% w/v	0.1				
Core: Gel in HFIP/H <sub>2</sub> O, c = 3–5% w/v	0.1	+12/-5	12	40	20 – 35
Shell: HA in NH <sub>4</sub> OH/DMF, c = 1.5% w/v	0.1				
Core: Gel in FA, c = 10% w/v	0.2	+12/-5	12	20	25
Shell: HA in FA, c = 2% w/v	0.2				

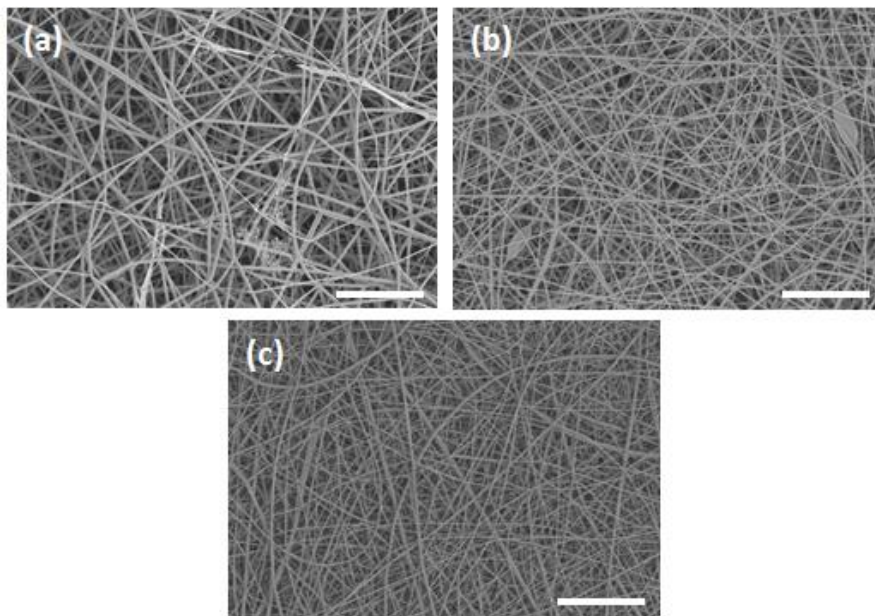


Fig. 4.41: SEM images of fibers electrospun with co-axial needle, using 2.5% w/v HA in FA/DMF/H<sub>2</sub>O as shell solution and different core solutions: (a) 15% w/v Gel in FA; (b) 7% w/v Gel in AA/H<sub>2</sub>O; (c) 3% Gel in HFIP/H<sub>2</sub>O (T = 40 °C). Scale bar: 5 μm.

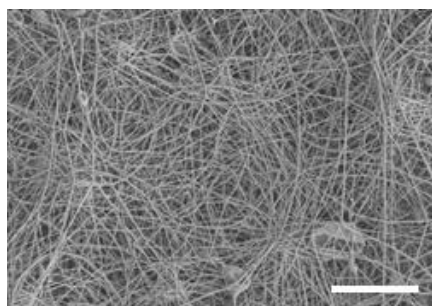


Fig. 4.42: SEM images of fibers electrospun with co-axial needle, using 1.5% w/v HA in NH<sub>4</sub>OH/DMF as shell solution and 3% Gel in HFIP/H<sub>2</sub>O (T = 40 °C) as core solution. Scale bar: 5 μm.

Finally, 10% Gel and 2% HA in FA as core and shell solutions respectively were co-axially electrospun. The process was stable and continuous, and no solution gelification nor drop formation occurred, thus indicating that also HA solution was entirely electrospun. This was possible because of the Gel core solution that guided nanofiber formation process, but also by means of the same solvent used, FA, which reduced interfacial tension between the two

fluids. Fig. 4.12 shows the morphology of the fibers obtained: they were homogeneous and thin ( $\varnothing = 112 \pm 32$  nm). Small fiber dimensions derived from the relatively low solution concentrations and the high conductivity values, which were 0.306 mS/cm and 0.275 mS/cm for Gel and HA solutions respectively. Fiber diameters of bicomponent fibers were not statistically different from 10% Gel fibers ( $\varnothing = 109 \pm 19$  nm,  $p > 0.05$ ), thus suggesting that, if present, the shell should have been much thinner than the core.

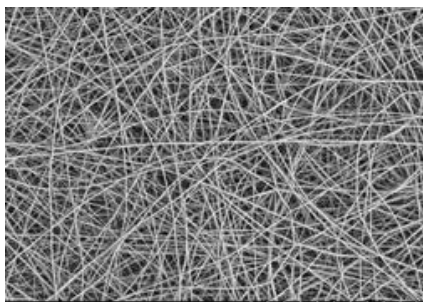


Fig. 4.43: SEM image of fibers electrospun with co-axial needle, using 10% w/v Gel in FA as core solution and 2% w/v HA in FA as shell. Scale bar: 5  $\mu$ m.

In order to investigate the formation of core-shell structure, different characterization techniques were employed. Initially, XPS analyses were carried out to evaluate surface chemical composition of co-axial electrospun membranes. Table 4.7 reports the results of XPS analyses on Gel and HA raw materials, used for comparison, and on representative bicomponent electrospun samples; in particular, only one Gel concentration value per solvent system is reported, as the results obtained for different concentrations of the same core solution were similar. Elemental composition of the co-axial electrospun Gel/HA matrices was almost identical to that of pure Gel; only few traces of Na were present in some samples, but this was not a prove of the presence of HA on the surface, as the biopolymer is sold as sodium salt and probably Na dissociation in solution occurred. These findings were not promising; nevertheless, the results could be affected by the intrinsic roughness of the electrospun samples, which did not allow the analysis of a perfectly flat surface, i.e. the “real” outer surface of the fibers, thus causing errors due to spatial resolution (in the order of tenths of  $\mu$ m). Moreover, the XPS instrument used had an information depth of about 10 nm, and, considering the small diameter of the fibers

(generally about 100 nm), it was possible that the dimensions of the shell thickness were similar or even smaller than the information depth of XPS, and therefore the instrument was not able to correctly measure it.

Therefore, other techniques for investigation of fiber structure were employed: in particular, SEM images of fiber cross-sections, TEM and CLSM analyses were used. As the results were analogous for all the samples analyzed, only the most representative images are reported.

Table 4.22: Elemental surface composition by XPS analyses of fibers electrospun with co-axial needle, and of raw Gel and HA for comparison.

Sample	C [%]	N [%]	O [%]	Na [%]
Gel powder	61.9	18.2	19.8	–
HA powder	55.0	3.7	36.6	4.7
Co-axial ES fibers - Core: 15% Gel in FA Shell: 1.5% HA in FA/DMF/H <sub>2</sub> O	62.2	16.9	20.5	0.3
Co-axial ES fibers - Core: 7% Gel in AA/H <sub>2</sub> O Shell: 1.5% HA in FA/DMF/H <sub>2</sub> O	62.0	17.0	20.1	0.6
Co-axial ES fibers - Core: 3% Gel in HFIP/H <sub>2</sub> O Shell: 1.5% HA in FA/DMF/H <sub>2</sub> O	62.5	16.6	19.7	1.1
Co-axial ES fibers – Core: 10% Gel in FA Shell: 2% HA in FA	61.1	17.4	21.4	–

Fig. 4.13 shows the SEM image of the cross-section after freeze-fracture (Fig. 4.13a) and TEM image (Fig. 4.13b) of fibers electrospun using 15% Gel in FA as core and 1.5% w/v HA in FA/DMF/H<sub>2</sub>O as shell. Unluckily, the similar chemical composition of the two biopolymers (that are both mainly composed of carbon, hydrogen and nitrogen) did not help in recognizing the eventual presence of the two phases. The same problem was obviously present also in TEM images of fibers electrospun from 3% Gel in HFIP/H<sub>2</sub>O as core and 1.5% w/v HA in FA/DMF/H<sub>2</sub>O as shell, where no core-shell structure was visible (Fig. 4.14a).

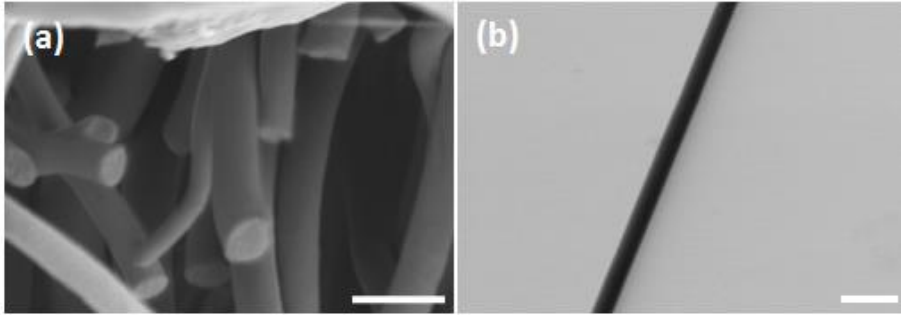


Fig. 4.44: (a) SEM image of cross-section and (b) STEM image at 30 kV accelerating voltage of fibers electrospun with co-axial needle, using 1.5% w/v HA in FA/DMF/H<sub>2</sub>O as shell solution and 15% w/v Gel in FA as core solution. Scale bar: 500 nm.

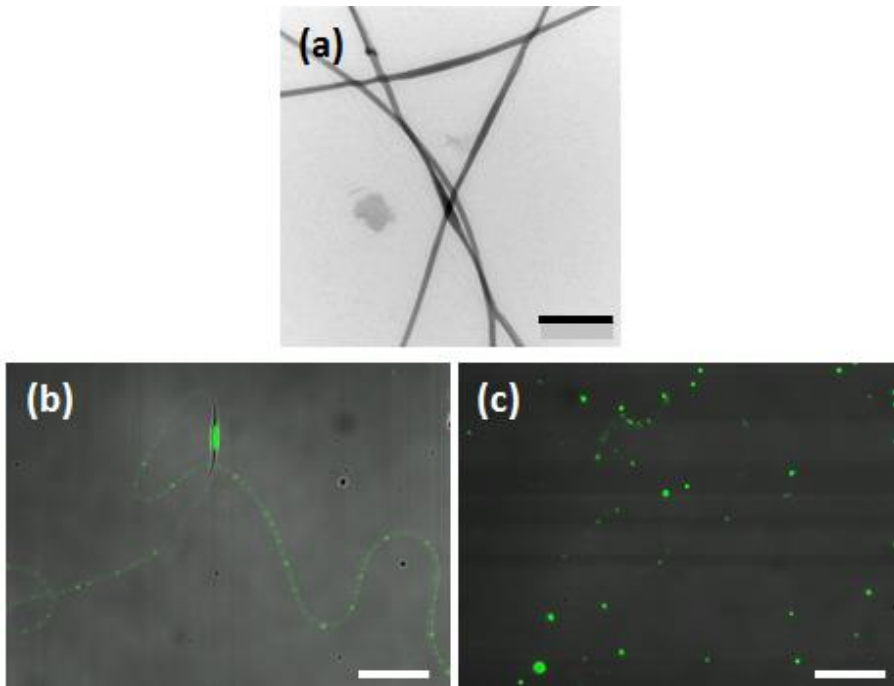


Fig. 4.45: (a) STEM image of fibers electrospun with co-axial needle using HA 1.5% w/v in FA/DMF/H<sub>2</sub>O as shell solution and Gel 3% w/v in HFIP/H<sub>2</sub>O (T = 40°C) as core solution. Scale bar: 500 nm. (b, c) CLSM images of fibers electrospun with co-axial needle using FITC-HA 1.5% w/v in FA/DMF/H<sub>2</sub>O as shell solution and Gel 3% w/v in HFIP/H<sub>2</sub>O. Scale bar: 20  $\mu$ m.

In order to better evaluate the distribution of HA within the fibers, before ES process HA was covalently bonded to FITC, a fluorophore that emits in the green region, and then fluorescence images of the fibers were taken by CLSM. Results are shown in Fig. 4.14: HA

did not form a continuous fiber, but it was present as dots along the fibers (Fig. 4.14b). Moreover, undesired spraying of HA over the sample occurred (Fig. 4.14c). These images proved that HA solutions used as shell was not spinnable even if combined with core Gel solutions with excellent processability by ES, and as a consequence formation of a continuous shell was not possible.

Finally, fibers co-axially electrospun using 10% Gel in FA as core and 2% HA in FA as shell were analyzed. Here again, SEM images of the cross-section after freeze-fracture did not allow to distinguish between two eventual phases within the section of the fibers, because of the poor contrast (Fig. 4.15). In order to evaluate the distribution of the two polymers within the fibers, not only HA was labeled to FITC (emission in the green region) as previously reported, but also Gel was covalently attached to RITC (emission in the red region). Then, RITC-Gel and FITC-HA solutions were co-axially electrospun. The fibers obtained were examined by CLSM and the results are reported in Fig. 4.16: these images confirmed that HA, which had proved not to be spinnable alone in FA, was here present forming fibers (and not dots as previously showed in Fig. 4.14). From Fig. 4.16c it was possible to observe that even if the distribution of the two polymers was not perfectly homogeneous, both Gel (red) and HA (green) were present in the vast majority of the fibers.

Core-shell structure of the fibers was finally demonstrated by TEM images when bromophenol blue was added at different concentrations to Gel and HA solutions before ES in order to enhance the contrast for the analysis<sup>34</sup>. Fig. 4.17 shows TEM images of fibers: the shell layer was present and homogeneous around a continuous core. The shell was very thin (about 10 nm) with respect to the core (about 70-80 nm), and this was in agreement with our hypothesis, as HA concentration in solution was much lower than Gel one.

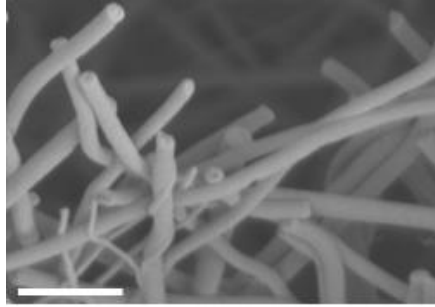


Fig. 4.46: SEM image of cross-section of fibers electrospun with co-axial needle, using 10% w/v Gel in FA as core solution and 2% w/v HA in FA as shell. Scale bar: 500 nm.

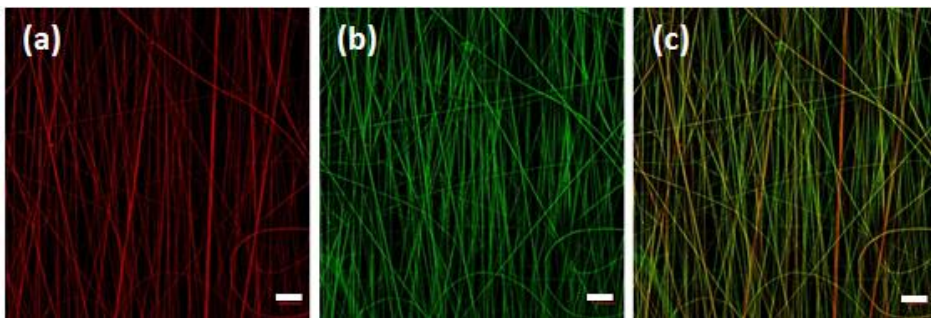


Fig. 4.47: CLSM images of fibers electrospun with co-axial needle, using 10% w/v RITC-Gel in FA as core solution and 2% w/v FITC-HA as shell solution; (a) RITC-Gel (red); (b) FITC-HA (green); (c) RITC-Gel and FITC-HA superimposed. Scale bar: 10  $\mu\text{m}$ .

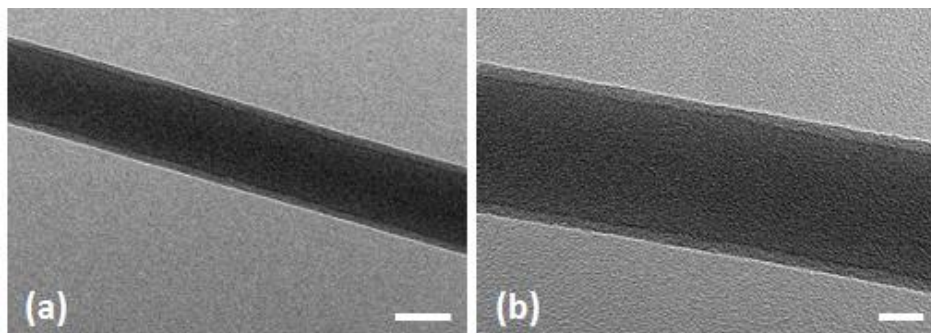


Fig. 4.48: TEM images of core-shell fibers obtained by co-axial ES of Gel 10% w/v in FA as core solution and HA 2% w/v in FA as shell solution. Scale bar: (a) 50 nm; (b) 20 nm.

### 3.2 Characterization of the crosslinking process

Before further characterization of core-shell fibrous matrices, electrospun membranes underwent crosslinking treatment. In fact, both Gel and HA are rapidly soluble in aqueous media, and therefore it was necessary to increase membrane stability for their application as wound dressing. Crosslinking methods for electrospun matrices that are intended to be used in biomedical field should not only preserve fiber structure and increase membrane stability at human body temperature, but also avoid any possible cytotoxic effects due to the crosslinking agent. In particular, for the application intended in this work, i.e. drug-loaded wound dressing, a crosslinking procedure that did not imply immersion of the membrane in solution was required, as this would have caused the untimely release of the drug incorporated within the fibers. The most studied crosslinking method for Gel is GA vapor; it was also particularly useful in this study as it does not consider a crosslinking solution, but it is a “dry” process. Optimization of GA\_CL process had been performed in Chapter 2, so the same parameters were used in this work, where they proved once again not to affect fiber morphology, as it is evident in Fig. 4.18. However, analysis of fiber diameters highlighted that there was a statistical increase in average fiber dimension after GA\_CL 2h: from  $109 \pm 19$  nm to  $119 \pm 27$  nm after crosslinking ( $p < 0.05$ ). This difference was very small and it was not particularly meaningful for the application intended. Regarding the morphology, another important characteristic of the membranes that could be affected by crosslinking process was the porosity, and, in particular, pore dimensions. Results by porometer analysis showed that before crosslinking the average pore size of Gel samples was  $325 \pm 3$  nm, with pore dimensions in the range of 304 – 593 nm. After GA\_CL 2h, the average pore size was  $355 \pm 26$  nm, and pore dimensions varied from 312 to 690 nm. These results indicated that the crosslinking treatment chosen did not reduce membrane porosity, which is usually a critical point for crosslinking procedures; on the contrary, pore dimensions increased after GA\_CL 2h. In fact, as the electrospun membranes would have shrunk because of the crosslinking process, they were fixed to a Petri dish in order to maintain their shape during the procedure; this resulted in an increase of pore size within the membranes after the process.



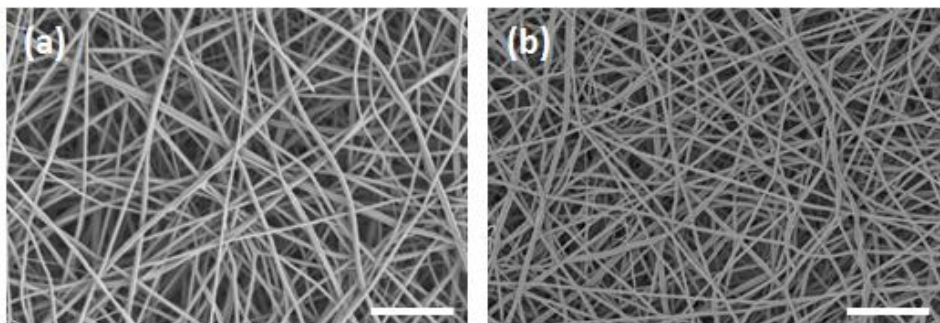


Fig. 4.49: SEM images of electrospun Gel (a) before and (b) after GA\_CL 2h. Scale bar: 2  $\mu$ m.

In order to demonstrate that crosslinking reaction between GA and Gel had occurred, we further examined GA\_CL samples by XPS and FTIR analyses. For this purpose, we considered Gel electrospun samples crosslinked for different times, from 2 to 6 hours, to better compare the effect of different process durations. In particular, XPS was initially used to examine the elemental composition of GA\_CL Gel samples: results showed that carbon amount slightly increased for increasing crosslinking time, and consequently nitrogen and oxygen contents decreased (Table 4.8).

Table 4.23: Elemental surface composition by XPS analyses of electrospun Gel fibers before and after GA\_CL for different times (2 to 6 hours).

Sample	C [%]	N [%]	O [%]
E-spun Gel fibers	61.5	16.8	21.6
E-spun Gel fibers GA_CL 2h	62.0	17.3	20.6
E-spun Gel fibers GA_CL 3h	61.5	17.3	21.1
E-spun Gel fibers GA_CL 4h	64.5	15.7	19.7
E-spun Gel fibers GA_CL 6h	66.2	14.6	19.1

This could be explained by the presence on the membrane surface of GA molecules, which are mainly formed by carbon atoms; evidently, the longer the GA\_CL process, the more GA molecules had time to interact with or deposited on Gel membranes. However, these data alone were not sufficient to prove that the crosslinking reaction had occurred, because GA

molecules present could be both reacted and non-reacted with Gel. Therefore, it was necessary to analyze elemental chemical state. GA molecule reacted with amino group ( $\text{NH}_2$ ) of lysine residues of Gel, forming imino group ( $\text{N}=\text{H}$ ). Amino and imino groups have different binding energy values in XPS spectrum: 399 and 398 eV, respectively. Fitting of nitrogen peak was carried out to evaluate the contribution and therefore the relative amount of amino and imino groups, for different GA\_CL times. Fig. 4.19a reports the survey scans spectra of nitrogen peak for Gel sample before crosslinking, and after GA\_CL 2h and 6h: by comparing the spectra it was possible to see that for the sample GA\_CL 6h there was an evident shift towards lower values of binding energy, which corresponds to nitrogen present as imino groups. To better quantify this phenomenon, fitting of the peak was performed and the results, in terms of percentage of amino and imino groups, were plotted as function of GA\_CL time (Fig. 4.19b). The curves show that for increasing crosslinking durations, the  $\text{NH}_2$  component of nitrogen peak decreased, while the percentage of imino bonds increased. In particular, there was not an important difference of nitrogen chemical state for GA\_CL times of 2 and 3 hours, while the content of imino group further increased for 4 and 6 hours of crosslinking. These results confirmed that GA present on sample surface has reacted with Gel molecules thus crosslinking them.

To evaluate if Gel molecular structure was extensively affected by the crosslinking process, FTIR analyses were conducted. Fig. 4.20 reports Gel IR spectrum, which shows the typical peaks of protein spectra, corresponding to the vibrations of amide groups: amide I ( $\text{C}=\text{O}$  stretching, 1656-44), amide II ( $\text{C}-\text{H}$  stretching and  $\text{N}-\text{H}$  bending, 1560-1335), and amide III ( $\text{C}-\text{N}$  stretching and  $\text{N}-\text{H}$  bending, 1240-670)<sup>41</sup>. Comparing the spectrum of electrospun Gel with those of Gel GA\_CL 2 and 6 hours (Fig. 4.20) it was evident that the crosslinking reaction did not cause any substantial variations in the IR spectra of Gel. Imino groups, which are formed during the crosslinking reaction, were not detectable in IR spectra as the band corresponding to their vibration, which is in the range 1615-1700  $\text{cm}^{-1}$ , overlaps the band of  $\text{C}=\text{O}$  vibrations, in the range 1630-1700  $\text{cm}^{-1}$ , that are groups naturally present in non-crosslinked Gel. The only difference in the spectra was that, for increasing GA\_CL durations, all the peaks were slightly shifted towards lower wave numbers: this effect could

be ascribed to the presence of longer polymeric chains consequently to crosslinking reaction.

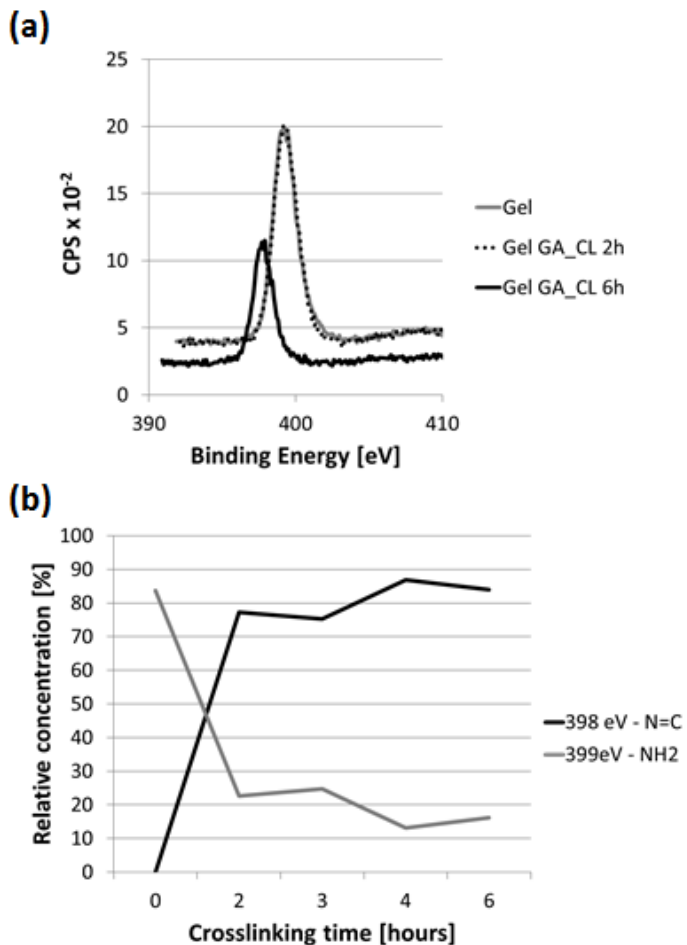


Fig. 4.50: Analysis of the shift of gelatin nitrogen peak after GA\_CL: (a) XPS survey scans spectra for nitrogen of e-spun Gel before and after glutaraldehyde crosslinking treatment for 2 and 6 hours; (b) plot of the percentage of two different nitrogen chemical states, i.e. N=C (formed by crosslinking reaction between Gel and GA) and NH<sub>2</sub> (related to lysine residues in non-crosslinked Gel), as function of crosslinking time of e-spun Gel membranes.

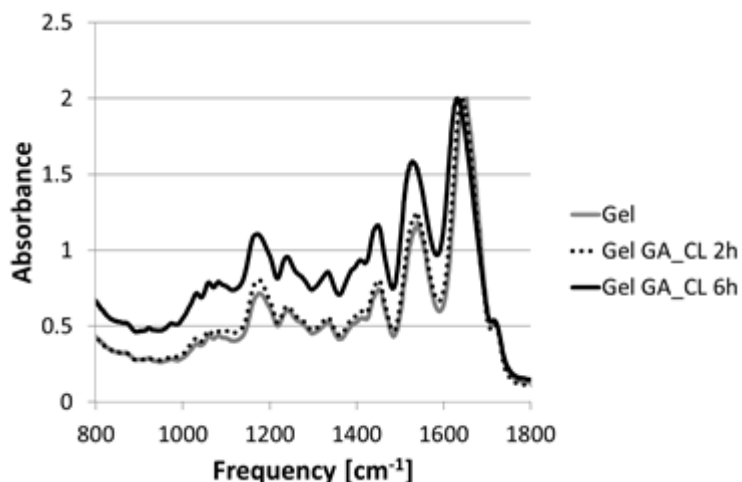


Fig. 4.51: FTIR spectra of e-spun Gel before and after GA\_CL for 2 and 6 hours.

Finally, for the application intended it was important that the membranes were fast-degrading, i.e. they completely dissolved in 5-10 days. Qualitative results of the degradation test in PBS at 37 °C revealed that the samples were degraded after 4-7 days. Unluckily, degradation kinetics was not homogeneous for all the samples, even if crosslinking conditions were carefully controlled and reproduced for all the matrices. However, the time of degradation was always in the desired range, so we concluded that the crosslinking procedure employed was extremely useful for our application. Fig. 4.21 shows the morphology of crosslinked fibers after 24-hour immersion in PBS at 37°C: the electrospun structure is still visible, but as Gel is a hydrophilic polymer, the fibers have swollen in the aqueous medium up to diameter of about 210 nm, and, as a consequence, the porosity has decreased.

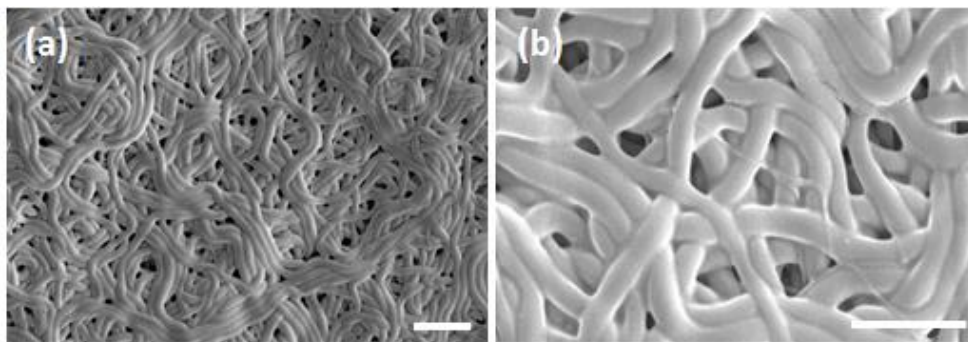


Fig. 4.52: SEM images of e-spun Gel fibers GA\_CL 2h after 24 hours in PBS at 37°C.  
Scale bar: (a) 1 μm; (b) 2 μm.

### 3.3 Evaluation of CCG-203971 cytotoxicity and efficacy

The drug employed in this work, namely CCG-203971, is a novel drug, studied for the suppression of several pathological processes, including cancer cell migration and tissue fibrosis. In particular, few studies present in literature have investigated its ability to reduce expression of genes associated with fibrosis and to inhibit TGF- $\beta$  induced myofibroblast transition of normal fibroblasts<sup>21-22</sup>. In fact, myofibroblast differentiation plays an important role during the fibrotic response to tissue injury and is thought to be a key pathologic step in the origin of wound healing disorders such as fibrosis<sup>17</sup>.

Previous works in literature reported that concentrations of 17.5 and 25  $\mu$ M inhibit TGF- $\beta$  induced  $\alpha$ SMA protein expression ( $\alpha$ SMA is a well-recognized protein marker for myofibroblasts)<sup>23</sup>. Another study found that, after 72 hours, 10  $\mu$ M concentration of the drug completely blocks TGF- $\beta$  stimulated myofibroblast transition of fibroblasts<sup>22</sup>. No cytotoxic effect for the concentrations tested have been reported. Therefore, this molecule appeared promising for applications in wound healing; in particular, sustained release of CCG-203971 from a wound dressing can be beneficial in reducing myofibroblast differentiation, thus preventing excessive collagen deposition and extensive scar formation in the wound area. Before adding the drug in the solution for ES, it was necessary to investigate the cytotoxic effect of different concentrations and their efficacy in the differentiation model used. In order to evaluate drug cytotoxicity, HDFs were cultured in standard DMEM with different drug concentrations or DMSO as control, and cell viability

was assessed by MTS assay. Considering 70% of control viability as threshold for defining a substance as toxic, results showed that up to about 10-15  $\mu\text{M}$  concentration CCG-203971 proved not to have cytotoxic effect, while for greater concentrations, i.e. 20 and 30  $\mu\text{M}$ , cell viability was about the half of the control, thus indicating that these values significantly affected cell normal proliferation and metabolic activity (Fig. 4.22).

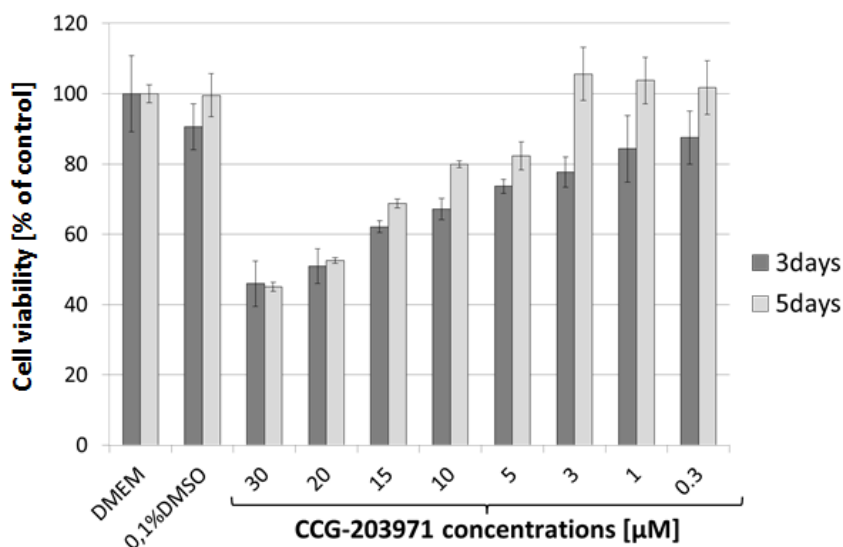


Fig. 4.53: Results of MTS assay on HDFs cultured for 3 or 5 days with different CCG-203971 concentrations.

The same drug concentrations were considered to evaluate the efficacy of CCG-203971 in preventing myofibroblast differentiation. For this test, HDFs were cultured in RPMI medium with 1% of horse serum and TGF- $\beta$  to induce myofibroblast differentiation; different drug concentrations were added and cell morphology was evaluated after 3 days by selective staining of  $\alpha\text{SMA}$  filaments (and nuclei by DAPI). Fig. 4.23 shows the images at CLSM with for different drug concentrations and for the controls (positive, i.e. cells without drug, and negative, i.e. cells without TGF- $\beta$  and drug): starting from the highest concentrations, with 30  $\mu\text{M}$  few cells were present, as apparently this value was too high to allow adequate cell viability. 20, 15, and 10  $\mu\text{M}$  concentrations partially block  $\alpha\text{SMA}$  expression and therefore myofibroblast differentiation, in a dose-dependent manner. Furthermore, from CLSM images it was possible to qualitatively confirm the results from cytotoxic test, as for 15 and

20  $\mu\text{M}$  concentrations less cells were present on the well. Below 10  $\mu\text{M}$  concentration, i.e. for 5, 3, 1 and 0.3  $\mu\text{M}$ , inhibition of  $\alpha\text{SMA}$  expression was no longer observable, and the image reported for 1  $\mu\text{M}$  concentration is representative for all.

To better quantify the inhibitory effect on myofibroblast differentiation of different drug concentrations, FACS tests were carried out, using 20, 15, 10, and 1  $\mu\text{M}$  as concentrations to be tested and compared to positive and negative controls. Cells were cultured for 3 days in the same conditions described before, and again  $\alpha\text{SMA}$  filaments and nuclei were stained with proper fluorophores. Results, in term of differentiation inhibition, are summarized in Table 4.9: as observed with CLSM images, for 10 to 20  $\mu\text{M}$  there was an inhibitory effect, which was proportional to the concentration, while concentration of 1  $\mu\text{M}$  was too low and the drug was not effective.

Taking into consideration the results on drug concentration cytotoxicity and efficacy, we decided to fabricate core-shell fibers for CCG-203971 release with two different drug amounts: 0.1% and 0.2% w/w with respect to Gel amount in the solution. In fact, even if these quantities appear extremely small, they correspond to 15 and 30  $\mu\text{M}$  concentrations in subsequently drug release and cell tests, according to electrospun sample dimensions (and therefore weight) chosen, to the medium volume necessary for the release or the cell test, and to the hypotheses that CCG-203971 was homogeneously distributed in the solution used for ES and that all the drug present in the sample would have been released. Concentration value of 15  $\mu\text{M}$  was selected as it did not cause important cytotoxic effect, and in the same time it was adequate to partially inhibit myofibroblast differentiation. To investigate possible different effects both on release kinetics and cell tests due to different drug amount loaded into the membranes, a second concentration value, which is quiet far from the first one, was chosen, i.e. 30  $\mu\text{M}$ . In fact, even if this concentration value proved to be too high for cell survival, at this point we did not know if the drug incorporated in the electrospun membranes would have been completely released, or if it would have retained its entire efficacy even after the ES process; therefore, we preferred to use high concentration value as “safe coefficient”.

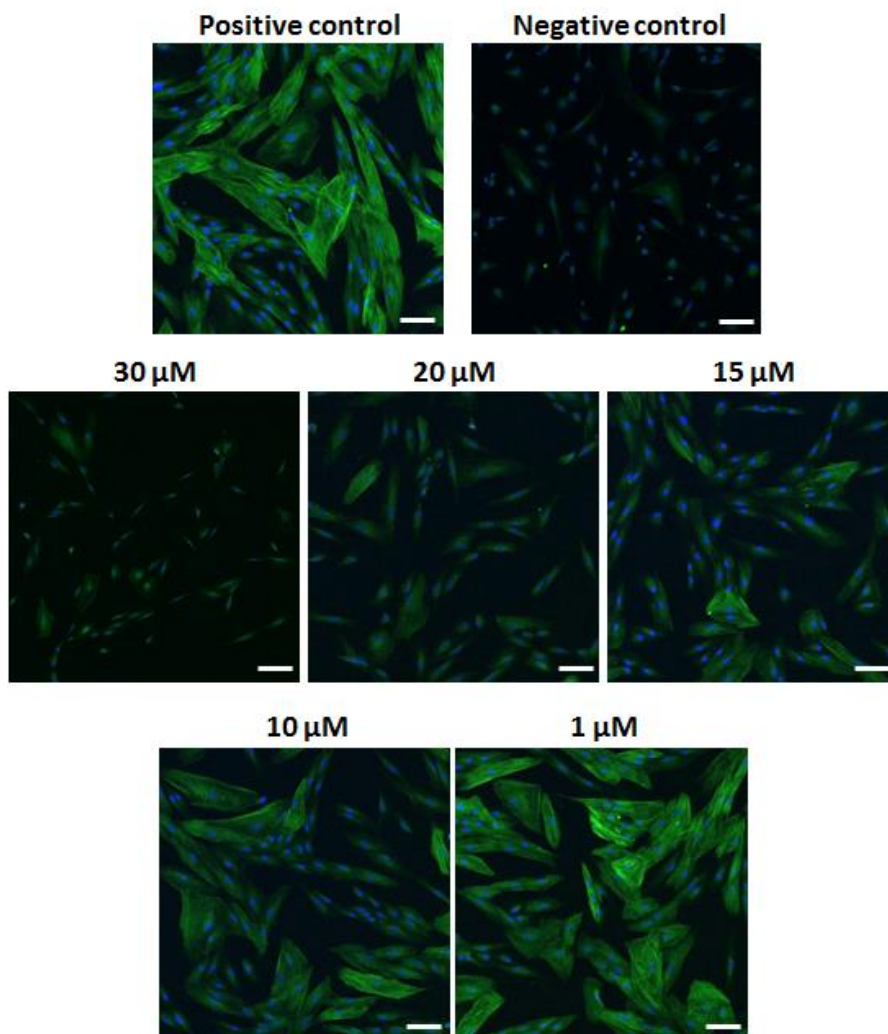


Fig. 4.54: CLSM images of HDFs after 3 days of differentiation test, with different CCG-203971 concentrations; nuclei are stained by DAPI, and  $\alpha$ SMA filaments by FITC-conjugated antibody. Scale bar: 100  $\mu$ m.

Table 4.24: FACS test results – percentage of differentiation inhibition for different drug concentrations.

<b>CCG-203971 concentration</b>	<b>20 <math>\mu</math>M</b>	<b>15 <math>\mu</math>M</b>	<b>10 <math>\mu</math>M</b>	<b>1 <math>\mu</math>M</b>
Differentiation inhibition [%]	62 $\pm$ 3	35.5 $\pm$ 10	15.5 $\pm$ 0.5	2 $\pm$ 1



### 3.4 Core-shell electrospinning of drug loaded fibers: release kinetics and cell tests

Fig. 4.24 shows the SEM images of Gel and Gel/HA fibers loaded with the two different amounts of CCG-203971 selected, namely 0.1% and 0.2%. The drug was dissolved in ethanol and a small amount of this solution was added in the core solution immediately before starting the ES. The addition of a small amount of ethanol did not affect the stability of the process nor the fiber morphology. In particular Gel 15  $\mu\text{M}$  and Gel 30  $\mu\text{M}$  fiber diameters were  $106 \pm 25$  nm and  $111 \pm 23$  nm respectively, which were not statistically different from Gel fibers. Also for Gel/HA samples there was no significantly variation in fiber diameter due to drug loading: fiber diameter was  $108 \pm 21$  nm for Gel/HA 15  $\mu\text{M}$  and  $105 \pm 22$  nm for Gel/HA 30  $\mu\text{M}$ .

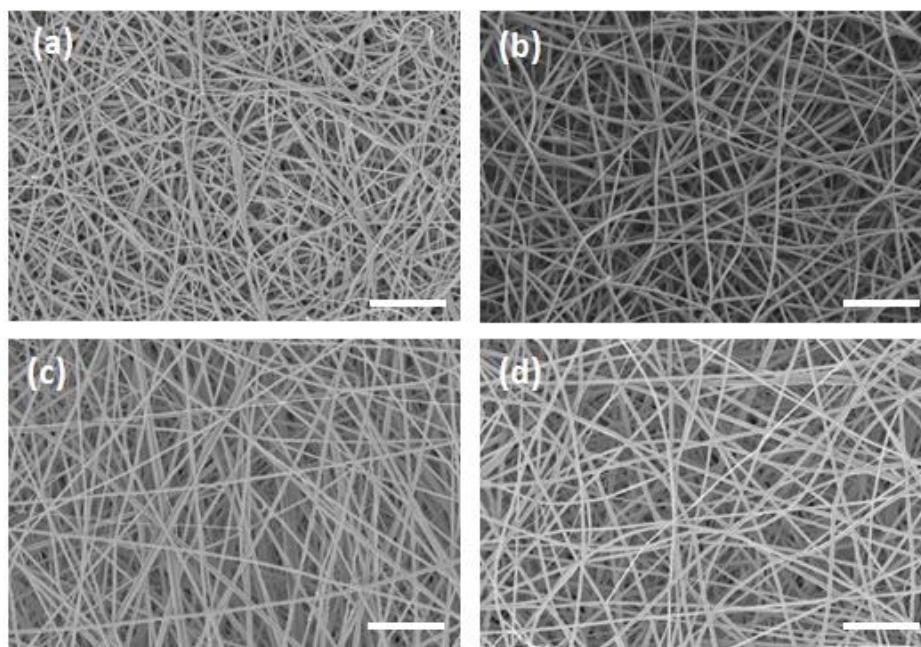


Fig. 4.55: SEM images of electrospun Gel and Gel/HA membranes loaded with CCG-203971: (a) Gel 15  $\mu\text{M}$  (0.1% w/w); (b) Gel/HA 15  $\mu\text{M}$  (0.1% w/w); (c) Gel 30  $\mu\text{M}$  (0.2% w/w); (d) Gel-HA 30  $\mu\text{M}$  (0.2% w/w). Scale bar: 2  $\mu\text{m}$ .

#### Drug release test

Core-shell nanofiber structure is particularly useful in drug release applications where a sustained release is desired, as it offers the possibility to prevent burst release<sup>1,3</sup>.

Accordingly, this was one of the main reason for the fabrication of drug-loaded core-shell fibers in the present Chapter. However, results from drug release tests could not prove any difference in drug release kinetics between Gel and Gel/HA samples. In fact, the results obtained were not meaningful, as there was a huge variability between different samples of the same type of membrane. For example, considering the release at the first time point, i.e. 1 hour, in PBS from the four samples used for Gel 15  $\mu\text{M}$  (0.1% w/w), we obtained the following values: 15%, 49%, 80%, 95% (% of drug released on the total drug loaded in the sample). The same trend was observable for Gel/HA matrices; for example, the release of the four Gel/HA 30  $\mu\text{M}$  samples in RPMI after 1 hour was: 13%, 40%, 58%, 97%. Even if the test was repeated two times, we were not able to obtain more reproducible results. The variability among different specimens of the same type was probably due to the different degradation kinetics of each sample, which greatly affected the release. In fact, even if the GA\_CL procedure was carried out in a very precise and reproducible way, with careful control over the crosslinking parameters and the environmental conditions, the membranes did not degrade all contemporary, and even a slight difference in degradation kinetics could greatly affect the release.

### **Cell tests**

Cell viability on the electrospun membranes was evaluated by Live/Dead assay after 3 days from seeding. As previously described, the amount of drug loaded within the fibers was derived from precise calculations, taking into consideration the size of the sample (and therefore its weight) and the volume of medium necessary during the test, which in this case was 500  $\mu\text{L}$ . However, after the seeding of the cells on the membrane it was clear that the glass ring, used to maintain the samples on the bottom of the well, caused the meniscus to assume a non-flat surface, because of the interfacial tension. As a consequence, a very thin layer of medium was present on the central region of the sample, thus not allowing optimal conditions for cell growth during the following three days of the test. Therefore, 200  $\mu\text{L}$  of DMEM were added after 12 hours from the seeding; the concentration values tested during this test, therefore, were of 21  $\mu\text{M}$  (instead of 30) and 10.5  $\mu\text{M}$  (instead of 15). Even if experimental conditions were responsible for a change of the selected

concentration values, the results obtained were satisfactory: as shown in Fig. 4.25, almost all the cells seeded on the membranes were alive (green), and their morphology proved that fibroblasts were well adhered on the samples. As cytotoxicity of the drug had already been evaluated, the main scope of this test was to investigate cytocompatibility of the electrospun membranes, and the precise amount of drug loaded within them was not a fundamental parameter according to this aim. Images of cells on Gel/HA samples loaded with drug are missing because of some technical problems. However, from the excellent viability of cells on Gel/HA specimen it was possible to infer that also on the two missing samples cell viability would have been good.

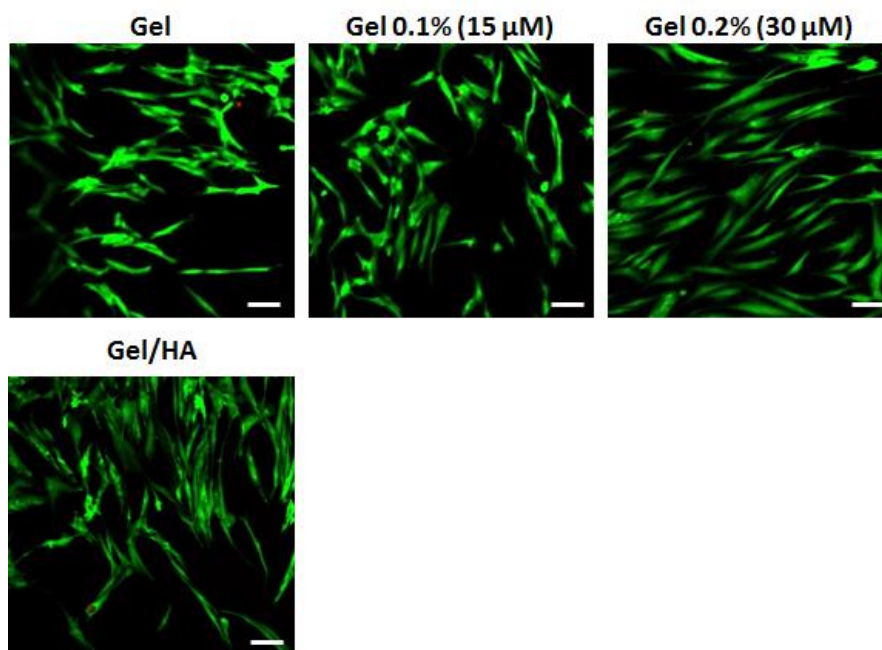


Fig. 4.56: CLSM images showing HDFs growing on e-spun membranes 3 days after seeding and stained with Live (green)/Dead (red) viability assay. Scale bar: 100 μm.

Furthermore, the results from MTS assay confirmed the good cytocompatibility of the electrospun samples (Fig. 4.26): viability of cells seeded on Gel and Gel/HA without drug was 93% and 77% of the control, while for samples loaded with drug these values decreased, but viability was always above or around 70% of the control. The decrease in cell viability with increase amount of drug was an expected result and confirmed what

already observed during the drug cytotoxicity test. Both the Live/Dead and the MTS assays confirmed that the cytocompatibility of the electrospun membranes was very good, and in particular cells on Gel samples had better viability than Gel/HA. This can be explained by the well-known excellent cytocompatibility properties of Gel, while HA has sometimes been reported to inhibit cell attachment<sup>42-44</sup>. However, cell viability on Gel/HA samples was still very good, and the beneficial effects that HA can have during the wound healing process lie above a slight decrease in cell viability at 3 days. In fact, HA inhibits scar formation during wound healing when topically applied. This effect may be related to its ability to stimulate fibroblast migration, inhibit fibroblast-induced collagen matrix contraction, and modulation of collagen synthesis.

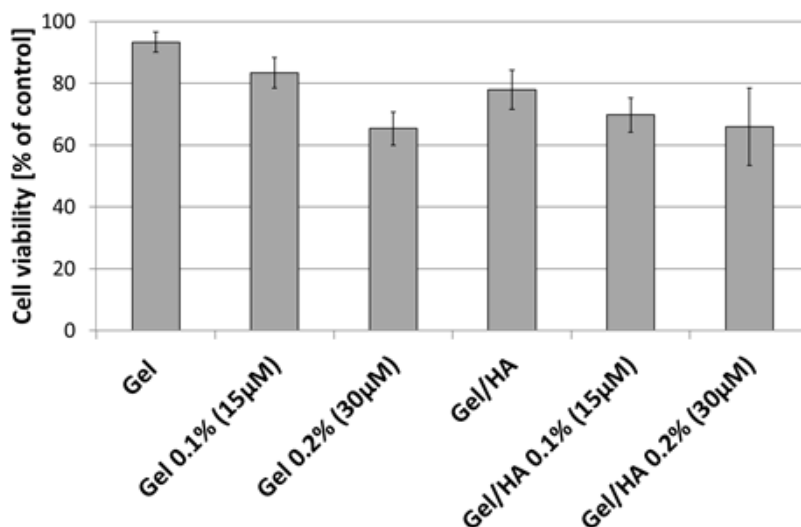


Fig. 4.57: Results of MTS assay on HDFs 3 days after seeding on Gel and Gel/HA electrospun membranes loaded with different drug amounts.

Another key point in this study was the evaluation of CCG-203971 activity after ES process; in fact, the acidic solvent used for Gel ES and the presence of high electric field could potentially affect molecule integrity and efficacy. Stability of the drug released from electrospun membranes was investigated by assessing its inhibitory effect on myofibroblast differentiation through an indirect cell test. Therefore, 24-hour eluates for all the samples considered (i.e. Gel and Gel/HA without drug or with 15 and 30 µM drug

concentrations) were prepared. CLSM images of cells exposed to eluates for 3 days are shown in Fig. 4.27: these results revealed that HDFs in contact with drug-loaded sample eluates expressed lower level of  $\alpha$ SMA, thus indicating that CCG-203971 released from electrospun specimen retained its activity and was able to inhibit cell differentiation. The effect was still dependent on the concentration: in fact, Gel and Gel/HA loaded with 15  $\mu$ M slightly decreased HDF differentiation, while for sample loaded with 30  $\mu$ M differentiation inhibition was more evident. Moreover, the images show that there was no significant difference in the number of viable cells present on the well among all the samples. Therefore, we speculated that not all the drug loaded within the samples was released in the 24 hours for eluates preparation, so that the real drug concentration of the eluates was lower than 15 and 30  $\mu$ M respectively, thus leading to lower extent of differentiation inhibition and lower cytotoxicity.

After being proved that CCG-203971 retained its activity during ES process, it would have been necessary to evaluate the morphology (in particular the differentiation) of HDFs seeded on electrospun membranes and cultured according to the differentiation protocol. In this case, it was difficult to acquire good CLSM images, as the fluorophores used for cell staining, in particular DAPI and FITC, were also absorbed by the samples, which subsequently gave a huge fluorescence signal during CLSM analysis. Another fluorescent probes, namely Alexa Fluor 546 phalloidin, was used for actin staining, in order to evaluate if a fluorophore emitting in the orange-red region could be a solution to the problem of membrane fluorescence signal. Incubation of the samples with Black Sudan solution partially helped in eliminating membrane fluorescence, but could not completely resolve the problem, as reported in Fig. 4.28: CLSM images showed that the phalloidin-actin staining of the cells was clearly visible, but also a strong fluorescence signal in the green region from the membrane was present. A possible solution could be the use of a different primary antibody for  $\alpha$ SMA labeling, in combination with a secondary antibody emitting in orange-red region, in order to avoid green fluorescence of the sample.

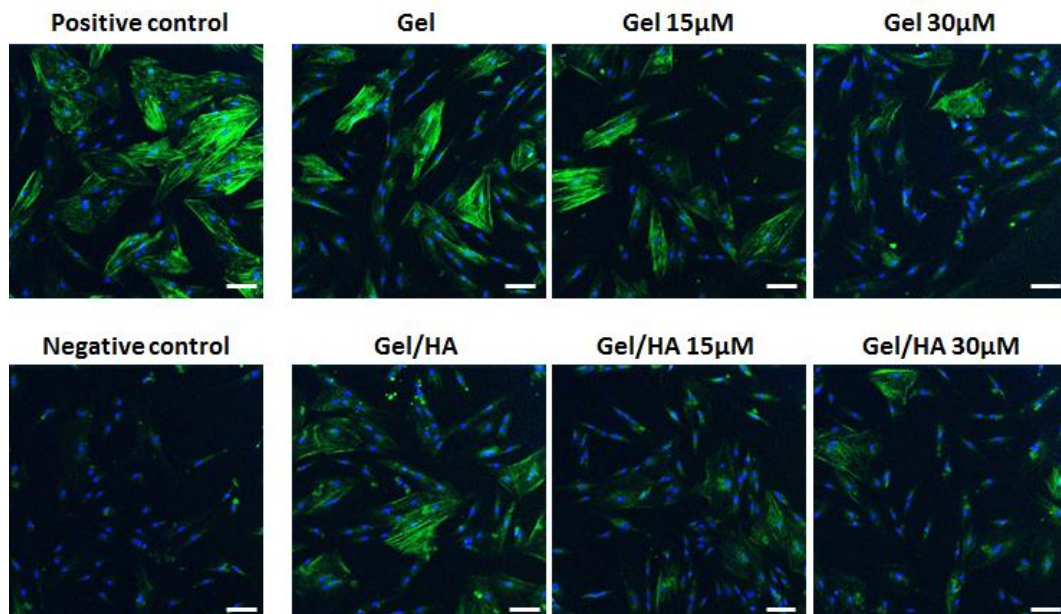


Fig. 4.58: CLSM images showing differentiation of HDFs in contact with 24-hour eluates of e-spun membranes 3 days after seeding; nuclei are stained by DAPI, and  $\alpha$ SMA filaments by FITC-conjugated antibody. Scale bar: 100  $\mu$ m.

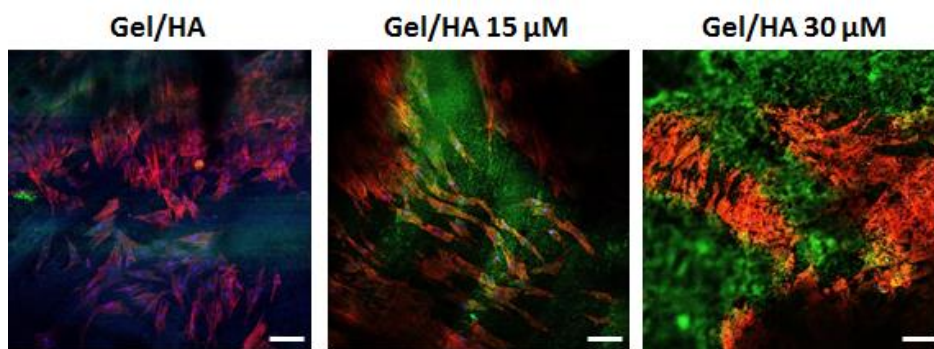


Fig. 4.59: CLSM images showing differentiation of HDFs on e-spun membranes 3 days after seeding; nuclei are stained by DAPI,  $\alpha$ SMA filaments by FITC-conjugated antibody, and actin by phalloidin. Scale bar: 100  $\mu$ m.

## 4. Conclusions

In order to obtain core-shell electrospun fibers, different solution combinations were tested, and in particular the effect of concentration ratio, viscosity, and surface tension at the interface were considered. Solution concentration and viscosity parameters need

careful optimization for ES of HA, as the biopolymer has very high molecular weight and charge nature, and therefore even low concentrated solutions present an extremely high viscosity value. 1.5 and 2.5% solution concentration of HA in FA/DMF/H<sub>2</sub>O were employed for co-axial ES: the process was stable when 1.5% solution was used, while for 2.5% HA a drop of solution was periodically formed at the tip of the spinneret, because the viscosity was too high to have electrified jet formation.

Two different strategies were investigated with the aim to reduce HA solution viscosity: MW radiation and HA stirring time in FA solution. Even if MW radiation were effective in decreasing solution viscosity, further analysis revealed that this treatment caused extensive and unwanted chain degradation of the biopolymer. Also by increasing the stirring time of HA solution in FA, a decrease of solution viscosity was observable, due to the cleavage of glycosidic bonds in HA molecular chains. In this case, degradation of HA chains was dependent on the stirring time.

Different characterization techniques were used for investigation of core-shell formation: SEM of fiber cross-section, TEM, CLSM of fluorophore-bonded biopolymers, and XPS. However, these techniques proved not to be adequate for the determination of fiber structure electrospun in this work, because of intrinsic resolution limit of the instruments and/or similar chemical composition of the two biopolymers, which did not allow to see any contrast between the two phases. Only by the addition of different concentrations of Bromophenol Blue to the Gel and HA solutions, the contrast was enhanced and finally by TEM analyses it was possible to see core-shell morphology in the majority of the fibers. In this regard, the use of the same solvent for the two phases, namely FA, was fundamental for core-shell fiber formation, as already stated in some works in literature<sup>8</sup>. To the best of author's knowledge, there are no works in literature describing co-axial fibers where both the inner and the outer phases are composed of natural polymers.

The crosslinking procedure used, i.e. glutaraldehyde vapor, proved to be adequate with respect to the application intended, as it did not affect membrane electrospun morphology nor pore dimensions. In particular, pores within the matrix have very small size, related to thin fiber diameter, thus possibly hindering cell migration. However, because of membrane

fast degradation kinetics (i.e. 4-7 days), it is probable that as the fibers degrade, the pore dimensions increase, thus favoring eventual cell migration.

The addition of CCG-203971 drug in the core solution did not affect electrospun fiber morphology. Unluckily, it was not possible to correctly evaluate the kinetics of drug release from the electrospun samples because of the huge influence of sample degradation on the measurements. However, cell tests proved that CCG-203971 loaded within the electrospun fibers retained its efficacy after the ES process. Moreover, HDFs seeded on the membranes well adhered and proliferated, thus demonstrating the good cytocompatibility of the materials.

In conclusion, core-shell membranes electrospun in this work are promising for wound healing applications, as their surface is made of hyaluronic acid, which favors healing process, and the core material is gelatin, a natural and fast-degradable biopolymer which ensures biocompatibility of the membrane; moreover, for future applications in clinic HA and gelatin degradability will avoid the need of repeated changing of the dressing. The presence of CCG-203971 in the fibers is particularly important for preventing excessive scar formation and tissue fibrosis, which is a key factor during wound healing.

In future it will be necessary to further improve some features of the electrospun membranes. For example, an unresolved issue is the reproducibility of GA\_CL membrane degradation rate, which however is a key factor for future application of the dressing. As crosslinking with GA vapor proved to be a difficult process to control and reproduce, a possible alternative is represented by chemically modified gelatin that can be photo-crosslinked: this method should avoid eventual cytotoxic effect of chemical crosslinking agents and improve outcome reproducibility. A more homogeneous membrane degradation rate will allow to more precisely measure drug release kinetics, which is another important key parameter for the application intended. Furthermore, a more complete *in vitro* characterization is necessary; in particular, it would be interesting to evaluate the degree of differentiation inhibition of myofibroblasts seeded directly on the membranes, by means of staining and CLSM analysis. Finally, the application of the matrices in an *in vitro* skin model of wound would allow to preliminary assess their efficacy.



## References

1. Yarin, A., Coaxial electrospinning and emulsion electrospinning of core–shell fibers. *Polym Advan Technol* **2011**, *22* (3), 310-317.
2. Khajavi, R.; Abbasipour, M., Electrospinning as a versatile method for fabricating coreshell, hollow and porous nanofibers. *Scientia Iranica* **2012**, *19* (6), 2029-2034.
3. Elahi, M. F.; Lu, W.; Guoping, G.; Khan, F., Core-shell fibers for biomedical applications-a review. *Journal of Bioengineering & Biomedical Science* **2013**, *2013*.
4. Reznik, S.; Yarin, A.; Zussman, E.; Bercovici, L., Evolution of a compound droplet attached to a core-shell nozzle under the action of a strong electric field. *Physics of Fluids (1994-present)* **2006**, *18* (6), 062101.
5. Wang, C.; Yan, K.-W.; Lin, Y.-D.; Hsieh, P. C., Biodegradable core/shell fibers by coaxial electrospinning: processing, fiber characterization, and its application in sustained drug release. *Macromolecules* **2010**, *43* (15), 6389-6397.
6. Zhang, H.; Zhao, C.; Zhao, Y.; Tang, G.; Yuan, X., Electrospinning of ultrafine core/shell fibers for biomedical applications. *Science China Chemistry* **2010**, *53* (6), 1246-1254.
7. Kurban, Z.; Lovell, A.; Bennington, S. M.; Jenkins, D. W.; Ryan, K. R.; Jones, M. O.; Skipper, N. T.; David, W. I., A solution selection model for coaxial electrospinning and its application to nanostructured hydrogen storage materials. *The Journal of Physical Chemistry C* **2010**, *114* (49), 21201-21213.
8. Nguyen, T. T. T.; Ghosh, C.; Hwang, S.-G.; Chanunpanich, N.; Park, J. S., Porous core/sheath composite nanofibers fabricated by coaxial electrospinning as a potential mat for drug release system. *Int J Pharm* **2012**, *439* (1), 296-306.
9. Zussman, E.; Yarin, A. L.; Bazilevsky, A. V.; Avrahami, R.; Feldman, M., Electrospun Polyaniline/Poly (methyl methacrylate)-Derived Turbostratic Carbon Micro-/Nanotubes. *Adv Mater* **2006**, *18* (3), 348-353.
10. Saraf, A.; Lozier, G.; Haesslein, A.; Kasper, F. K.; Raphael, R. M.; Baggett, L. S.; Mikos, A. G., Fabrication of nonwoven coaxial fiber meshes by electrospinning. *Tissue Engineering Part C: Methods* **2009**, *15* (3), 333-344.
11. Zhang, Y. Z.; Kouguchi, T.; Shimizu, K.; Sato, M.; Takahata, Y.; Mormatsu, F., Chicken Collagen Hydrolysate Reduces Proinflammatory Cytokine Production in C57BL/6.KOR-ApoE(shl) Mice. *J Nutr Sci Vitaminol* **2010**, *56* (3), 208-210.
12. Zhang, Y.; Wang, X.; Feng, Y.; Li, J.; Lim, C.; Ramakrishna, S., Coaxial electrospinning of (fluorescein isothiocyanate-conjugated bovine serum albumin)-encapsulated poly ( $\epsilon$ -caprolactone) nanofibers for sustained release. *Biomacromolecules* **2006**, *7* (4), 1049-1057.
13. Jiang, H.; Hu, Y.; Li, Y.; Zhao, P.; Zhu, K.; Chen, W., A facile technique to prepare biodegradable coaxial electrospun nanofibers for controlled release of bioactive agents. *J Control Release* **2005**, *108* (2), 237-243.
14. Bazilevsky, A. V.; Yarin, A. L.; Megaridis, C. M., Co-electrospinning of core-shell fibers using a single-nozzle technique. *Langmuir* **2007**, *23* (5), 2311-2314.

15. Angeles, M.; Cheng, H. L.; Velankar, S. S., Emulsion electrospinning: composite fibers from drop breakup during electrospinning. *Polym Advan Technol* **2008**, *19* (7), 728-733.
16. Bereznicki, L., Factors affecting wound healing. *Australian Pharmacist* **2012**, *31* (6), 484.
17. Tsou, P.-S.; Haak, A. J.; Khanna, D.; Neubig, R. R., Cellular mechanisms of tissue fibrosis. 8. Current and future drug targets in fibrosis: focus on Rho GTPase-regulated gene transcription. *Am J Physiol-Cell Ph* **2014**, *307* (1), C2-C13.
18. Boateng, J. S.; Matthews, K. H.; Stevens, H. N.; Eccleston, G. M., Wound healing dressings and drug delivery systems: a review. *J Pharm Sci-US* **2008**, *97* (8), 2892-2923.
19. Mogoşanu, G. D.; Grumezescu, A. M., Natural and synthetic polymers for wounds and burns dressing. *Int J Pharm* **2014**, *463* (2), 127-136.
20. Zahedi, P.; Rezaeian, I.; Ranaei-Siadat, S. O.; Jafari, S. H.; Supaphol, P., A review on wound dressings with an emphasis on electrospun nanofibrous polymeric bandages. *Polym Advan Technol* **2010**, *21* (2), 77-95.
21. Bell, J. L.; Haak, A. J.; Wade, S. M.; Kirchhoff, P. D.; Neubig, R. R.; Larsen, S. D., Optimization of novel nipecotin bis (amide) inhibitors of the Rho/MKL1/SRF transcriptional pathway as potential anti-metastasis agents. *Bioorg Med Chem Lett* **2013**, *23* (13), 3826-3832.
22. Haak, A. J.; Tsou, P.-S.; Amin, M. A.; Ruth, J. H.; Campbell, P.; Fox, D. A.; Khanna, D.; Larsen, S. D.; Neubig, R. R., Targeting the Myofibroblast Genetic Switch: Inhibitors of Myocardin-Related Transcription Factor/Serum Response Factor–Regulated Gene Transcription Prevent Fibrosis in a Murine Model of Skin Injury. *Journal of Pharmacology and Experimental Therapeutics* **2014**, *349* (3), 480-486.
23. Johnson, L. A.; Rodansky, E. S.; Haak, A. J.; Larsen, S. D.; Neubig, R. R.; Higgins, P. D., Novel Rho/MRTE/SRF Inhibitors Block Matrix-stiffness and TGF- $\beta$ –Induced Fibrogenesis in Human Colonic Myofibroblasts. *Inflammatory bowel diseases* **2014**, *20* (1), 154.
24. Uppal, R.; Ramaswamy, G. N.; Arnold, C.; Goodband, R.; Wang, Y., Hyaluronic acid nanofiber wound dressing—production, characterization, and in vivo behavior. *Journal of Biomedical Materials Research Part B: Applied Biomaterials* **2011**, *97* (1), 20-29.
25. Kogan, G.; Šoltés, L.; Stern, R.; Gemeiner, P., Hyaluronic acid: a natural biopolymer with a broad range of biomedical and industrial applications. *Biotechnology letters* **2007**, *29* (1), 17-25.
26. Ellis, I. R.; Schor, S. L., Differential effects of TGF- $\beta$ 1 on hyaluronan synthesis by fetal and adult skin fibroblasts: implications for cell migration and wound healing. *Exp Cell Res* **1996**, *228* (2), 326-333.
27. Um, I. C.; Fang, D.; Hsiao, B. S.; Okamoto, A.; Chu, B., Electro-spinning and electro-blowing of hyaluronic acid. *Biomacromolecules* **2004**, *5* (4), 1428-1436.
28. Thakur, R.; Florek, C.; Kohn, J.; Michniak, B., Electrospun nanofibrous polymeric scaffold with targeted drug release profiles for potential application as wound dressing. *Int J Pharm* **2008**, *364* (1), 87-93.
29. Ki, C. S.; Baek, D. H.; Gang, K. D.; Lee, K. H.; Um, I. C.; Park, Y. H., Characterization of gelatin nanofiber prepared from gelatin–formic acid solution. *Polymer* **2005**, *46* (14), 5094-5102.

30. Song, J.-H.; Kim, H.-E.; Kim, H.-W., Production of electrospun gelatin nanofiber by water-based co-solvent approach. *Journal of Materials Science: Materials in Medicine* **2008**, *19* (1), 95-102.
31. Heydarkhan-Hagvall, S.; Schenke-Layland, K.; Dhanasopon, A. P.; Rofail, F.; Smith, H.; Wu, B. M.; Shemin, R.; Beygui, R. E.; MacLellan, W. R., Three-dimensional electrospun ECM-based hybrid scaffolds for cardiovascular tissue engineering. *Biomaterials* **2008**, *29* (19), 2907-2914.
32. Liu, Y.; Ma, G.; Fang, D.; Xu, J.; Zhang, H.; Nie, J., Effects of solution properties and electric field on the electrospinning of hyaluronic acid. *Carbohydrate Polymers* **2011**, *83* (2), 1011-1015.
33. Brenner, E. K.; Schiffman, J. D.; Thompson, E. A.; Toth, L. J.; Schauer, C. L., Electrospinning of hyaluronic acid nanofibers from aqueous ammonium solutions. *Carbohydrate Polymers* **2012**, *87* (1), 926-929.
34. Sun, Z.; Zussman, E.; Yarin, A. L.; Wendorff, J. H.; Greiner, A., Compound core-shell polymer nanofibers by co-electrospinning. *Adv Mater* **2003**, *15* (22), 1929-1932.
35. Hsu, F.-Y.; Hung, Y.-S.; Liou, H.-M.; Shen, C.-H., Electrospun hyaluronate-collagen nanofibrous matrix and the effects of varying the concentration of hyaluronate on the characteristics of foreskin fibroblast cells. *Acta Biomater* **2010**, *6* (6), 2140-2147.
36. Chang, C. F.; Lee, M. W.; Kuo, P. Y.; Wang, Y. J.; Tu, Y. H.; Hung, S. C., Three-dimensional collagen fiber remodeling by mesenchymal stem cells requires the integrin-matrix interaction. *J Biomed Mater Res A* **2007**, *80* (2), 466-474.
37. Fuentes, S.; Retuert, J.; González, G., Preparation and properties of chitosan hybrid films from microwave irradiated solutions. *Journal of the Chilean Chemical Society* **2008**, *53* (2), 1511-1514.
38. Zhang, Y.; Venugopal, J.; Huang, Z.-M.; Lim, C.; Ramakrishna, S., Crosslinking of the electrospun gelatin nanofibers. *Polymer* **2006**, *47* (8), 2911-2917.
39. Jaafar, I. H.; LeBlon, C. E.; Wei, M.-T.; Ou-Yang, D.; Coulter, J. P.; Jedlicka, S. S., Improving fluorescence imaging of biological cells on biomedical polymers. *Acta Biomater* **2011**, *7* (4), 1588-1598.
40. Yao, S.; Wang, X.; Liu, X.; Wang, R.; Deng, C.; Cui, F., Effects of ambient relative humidity and solvent properties on the electrospinning of pure hyaluronic acid nanofibers. *J Nanosci Nanotechnol* **2013**, *13* (7), 4752-4758.
41. Hashim, D.; Man, Y. C.; Norakasha, R.; Shuhaimi, M.; Salmah, Y.; Syahariza, Z., Potential use of Fourier transform infrared spectroscopy for differentiation of bovine and porcine gelatins. *Food Chemistry* **2010**, *118* (3), 856-860.
42. Shu, X. Z.; Liu, Y.; Palumbo, F.; Prestwich, G. D., Disulfide-crosslinked hyaluronan-gelatin hydrogel films: a covalent mimic of the extracellular matrix for in vitro cell growth. *Biomaterials* **2003**, *24* (21), 3825-3834.
43. Yoldemir, T.; Sagol, S.; Adakan, S.; Oztekin, K.; Ozsener, S.; Karadadas, N., Comparison of the reduction of postoperative adhesions by two barriers, one solution, and two pharmacologic agents in the rat uterine model. *Fertil Steril* **2002**, *78* (2), 335-339.
44. Sawada, T.; Hasegawa, K.; Tsukada, K.; Kawakami, S., Adhesion preventive effect of hyaluronic acid after intraperitoneal surgery in mice. *Human Reproduction* **1999**, *14* (6), 1470-1472.

## Chapter 5 - Final remarks

---

Electrospinning (ES) of natural polymers, and in particular of biopolymers, is an extremely fascinating and challenging field, as it offers unique possibility to produce matrices whose morphology and chemical composition closely resemble those of physiological extra-cellular matrix (ECM). Therefore, these matrices have promising applications as scaffold for tissue engineering and wound healing.

ES is a simple and versatile technique that allows the production of micro- and nano-fibers from a wide range of polymers. In particular, ES of natural polymers has been extensively studied in literature, but it still presents some limitations. In fact, biopolymers are generally difficult to dissolve; moreover, the solvent system used should have adequate properties (e.g. vapor pressure, surface tension) to allow successful ES outcome, and at the same time it should not compromise biopolymer structure. Some natural polymers (e.g. hyaluronic acid, chitosan) have very high molecular weight or charged nature, that further complicate their processability by ES. Moreover, natural polymer composition is not always controlled and tends to vary by batch, thus limiting ES process reproducibility. Last but not least, rigidity of natural polymers due to their stable three-dimensional structure prevents process continuity, as the solution lacks the viscoelastic properties essential for stable jet formation.

One biopolymer that presents good processability by ES is gelatin, which derives from collagen denaturation, and has lost the intra-molecular forces responsible for the stability of protein structure. Gelatin has been successfully electrospun in many works in literature, from different solvents. For other biomolecules, e.g. collagen, fibrinogen, elastin (in its precursor form, tropoelastin), the most used solvent for ES is hexafluoro-isopropanol (HFIP); however, HFIP is toxic and expensive. In addition, for collagen ES, it was demonstrated that HFIP induced extensive protein denaturation.

A strategy often used in literature to improve natural polymer ES processability consists in blend them with synthetic polymers (e.g. PEO, PVA, PLA, PCL), that are usually easier to spin. However, in this case the biological compatibility and functionality of the scaffold is partially lost, and degradation kinetics is greatly affected. Therefore, in this thesis no

synthetic polymers were used, and alternative strategies to solve biopolymer ES problems were found.

The present work investigates the possibility to fabricate electrospun membranes made of biopolymers with different properties and for different applications in tissue engineering field, with special attention to process stability, reproducibility, and ability to be scaled up to industrial level in the future.

ES of collagen was investigated and, in particular, influence of collagen batch variability on ES outcome was demonstrated. Gelatin, instead, proved to be stable during ES from different solvent systems, thus confirming its good processability. Therefore, gelatin was chosen as main component in the preparation of natural polymer blends for ES: in particular, gelatin/elastin blends and gelatin/elastin/hyaluronic acid blends were used. Elastin and hyaluronic acid are two of the main ECM components of connective tissues, and previous works in literature have demonstrated their beneficial properties for tissue engineering applications.

Combination of different biopolymers within the same electrospun matrix is advantageous as it offers the possibility to better mimic the complex chemical structure of ECM in different tissues and to have different chemico-physical properties according to the tunable composition. Moreover, the present work focused on the choice of alternative solvents for ES, less toxic and expensive than those currently used in literature for collagen-elastin blends.

As one drawback of natural polymers is their degradability, crosslinking of the electrospun membranes was necessary to improve their stability. The most used crosslinking methods in literature, i.e. UV-radiation, dehydrothermal treatment (DHT), glutaraldehyde vapor (GA), genipin (GP) and dimethylaminopropyl ethyl carbodiimide (EDC) crosslinking, were compared. Results showed that only DHT and GA were able to improve sample stability without affecting electrospun morphology; in fact, samples after UV-radiation immediately dissolved in aqueous environment, while GP and EDC solutions used for crosslinking cause complete loss of fiber structure.

Apart from ECM macromolecule components, also fibrinogen, that constitutes the physiological provisional scaffold during tissue repair, appears interesting for tissue engineering application. In literature, fibrinogen was electrospun only from HFIP or trifluoro ethanol (TFE) solutions. We tested a less expensive and less toxic solvent system composed by formic and acetic acids: even if the morphology of the fibers obtained was excellent, solution gelification occurred thus preventing process stability. Detailed investigation on this phenomenon revealed that gelification process was favored by solvent evaporation rate and increasing fibrinogen concentration, and it depended on the rearrangement of fibrinogen molecules, whose secondary and tertiary structure was greatly affected by the solvent. As it was not possible to change the solvent without greatly affect ES outcome, an alternative strategy was investigated; in particular, fibrinogen was blended with gelatin in formic acid solution in order to decrease its relative concentration. ES process of fibrinogen/gelatin blend was continuous and no gelification occurred. Moreover, the electrospun matrices proved to be stable in aqueous environment up to 7-10 days, thanks to fibrinogen good stability.

The versatility of ES process was employed also to fabricate non-standard fibers, in particular core-shell nanofibers for wound healing application. Here, gelatin was used as core material for its excellent cytocompatibility and good ES processability, whereas hyaluronic acid (HA) was chosen as shell material because of its well-established relevance in wound healing. Co-axial ES was carried out in order to favor HA spinnability by means of inner gelatin solution. Moreover, CCG-203971, a drug that is able to prevent myofibroblast differentiation and excessive scar formation during wound healing process, was loaded within the core solution to obtain a sustained release.

Fundamental parameters that affected core-shell fiber structure formation were the viscosity of the two solutions, their concentration and the solvents employed. In particular, the use of the same solvent (i.e. formic acid) was fundamental in order to obtain adequate fiber structuration. The characterization of core-shell structure was particularly complicated, as the two biopolymers have similar chemical compositions and therefore no contrast between the two phases was observable by SEM images of the cross-section nor

by TEM analysis. Moreover, investigation of the surface chemical composition by XPS analysis proved not to be useful in this case, as the shell thickness dimension was in the range of the instrument information depth (about 10 nm). Only when bromophenol blue was added to ES solutions for contrast enhancement, it was finally possible to observe the core-shell structure of the fibers by TEM.

Electrospun membranes demonstrated good cytocompatibility properties; in addition, the drug loaded within the fibers retained its efficacy after the ES process, and was effective in preventing myofibroblast differentiation. Therefore, the matrices appear extremely interesting for wound healing applications.

In conclusion ES technique has been successfully applied on different natural biopolymers allowing to obtain nanofibers with different features mimicking the main architecture of natural ECM but also core-shell fibers functionalized with a new drug.



## Figure Index

Fig. 1.1: Cellular microenvironment showing the main components of ECM <sup>3</sup> . .....	9
Fig. 1.2: Electrospinning setup scheme with indication of possible variables as example. 15	
Fig. 1.3: Four regions of ES process: (I) Taylor cone, (II) jet, (III) whipping jet, and (IV) collection of the fibers.....	17
Fig. 2.1: SDS-PAGE analysis of collagen and fibrinogen used as control: fibrinogen (lanes 1-2), batch #1 collagen after solubilisation in formic acid (lanes 4-5), batch #2 collagen after solubilisation in formic acid (Lanes 7-8), “raw” batch #1 collagen (lanes 8-9). Lanes 3 and 10 contain molecular weight standards. Lanes 1, 4, 6, 8 were loaded with 10 µg of fibrinogen; Lanes 2, 5, 7, 9 with 5µg. ....	62
Fig. 2.2: SEM image of electrospun gelatin in acetic acid/water (9/1). Scale bar: 5 µm....	64
Fig. 2.3: SEM image of electrospun gelatin in water/ethanol/formic acid (3/1/1). Scale bar: 5 µm.....	64
Fig. 2.4: SEM image of electrospun gelatin in formic acid at different concentrations: .....	65
Fig. 2.5: SEM images of electrospun gelatin/elastin blend, c = 8% w/v, at different ratios: .....	68
Fig. 2.6: SEM images of electrospun gelatin/elastin blend, c = 10% w/v, at different ratios: .....	69
Fig. 2.7: Images of the Taylor cone during ES process of gelatin (a) and 5/5 gelatin/elastin blend (b); in both cases, total concentration was 10% w/v. ....	69
Fig. 2.8: SEM images of electrospun gelatin/elastin blend, c = 15% w/v, at different ratios: (a) 9/1; (b) 7/3. Scale bar: 20 µm. ....	70
Fig. 2.9: SEM images of electrospun gelatin/elastin blend, c = 20% w/v, at different ratios: (a) 9/1; (b) 7/3. Scale bar: 20µm. ....	71
Fig. 2.10: SEM image of electrospun 9/1 gelatin/elastin blend, c = 20% w/v. ....	71
Fig. 2.11: SEM images of electrospun gelatin/elastin/HA blend, c = 10% w/v, with different HA amount: (a) c <sub>HA</sub> = 5% w/w; (b) c <sub>HA</sub> = 8% w/w. Scale bar: 5 µm. ....	74
Fig. 2.12: SEM image of electrospun gelatin/elastin/HA blend, c = 13% w/v, c <sub>HA</sub> = 5% w/w. Scale bar: 5 µm. ....	75
Fig. 2.13: Electrospun gelatin fibers after DHT treatment. Scale bar: 5 µm. ....	77
Fig. 2.14: SEM images of electrospun gelatin samples after GA crosslinking (c <sub>GA</sub> = 50%, V = 5 ml) for different times: (a) 2 hours; (b) 3 hours; (c) 4 hours; (d) 6 hours. Scale bar: 10 µm. ....	79
Fig. 2.15: SEM images of electrospun gelatin samples after immersion in 2.5% w/v GP crosslinking solution after different time: (a) 1 day; (b) 2 days; (c) 3 days. Scale bar = 20 µm. ....	80

Fig. 2.16: SEM images of electrospun gelatin samples after 2 days of immersion in EDC crosslinking solution at different concentrations: (a) 0.5% w/v; (b) 1% w/v; (c) 2% w/v; (d) 2.5% w/v; (e) 5% w/v. Scale bar = 20 $\mu\text{m}$ . .....	<b>Errore. Il segnalibro non è definito.</b>
Fig. 3.1: Crystal structure of a) human fibrinogen and b) fibrinogen monomer considered for the MD simulations in this Chapter, with indication of head and tail regions. ....	98
Fig. 3.2: Representative CD spectra in far-UV region for different types of secondary structure. ....	99
Fig. 3.3: SEM image of electrospun fibrinogen from acidic solvent system. Scale bar: 5 $\mu\text{m}$ . ....	105
Fig. 3.4: SEM image of electrospun fibrinogen from 100 mg/mL solution concentration. ....	106
Fig. 3.5: SEM images of electrospun fibrinogen for high flow rate values. In particular, (a) shows the presence of drops of solution on the electrospun sample. Scale bar: (a) 1 mm, (b) 5 $\mu\text{m}$ . ....	107
Fig. 3.6: SDS-PAGE analysis of fibrinogen after treatment with different solvents: formic acid (pH = 1, Lanes 1,3), HFIP (Lanes 4-5), formic acid aqueous solution pH = 4 (Lanes 7-8), PBS (pH = 7, Lanes 9-10). Lanes 2 and 6 contain molecular weight standards. Lanes 1, 4, 7, 9 were loaded with 10 $\mu\text{g}$ of fibrinogen; Lanes 3, 5, 8, 10 with 15 $\mu\text{g}$ . ....	108
Fig. 3.7: RMSD plot of tail and head regions of fibrinogen at pH 1. ....	109
Fig. 3.8: Fibrinogen monomer conformation and secondary structure at different pH values: (a) pH = 7, and (b) pH = 1. Images were obtained using VMD software; in particular, $\alpha$ -helices are depicted in orange, $\beta$ -sheets in green, random coil and turn in blue.....	110
Fig. 3.9: CD spectra of fibrinogen in different solvents: PBS (pH 7), aqueous solutions of formic acid at pHs 4 and 1, pure formic acid, and HFIP. ....	112
Fig. 3.10: Results of rheological measurements of fibrinogen solution: (a) viscosity (green) and shear stress (blue) as a function of shear rate; (b) strain-dependence of elastic modulus ( $G'$ , blue), viscous modulus ( $G''$ , red), and $\tan\delta$ (grey).....	113
Fig. 3.11: Images of structures formed by fibrinogen in acidic solution at different conditions: (a-b) higher evaporation rate (glass coverslip); (c-d) lower evaporation rate (cuvette). (b-d) show light depolarization due to molecular organization at nanometric scale. Scale bar: 100 $\mu\text{m}$ . ....	115
Fig. 3.12: SEM image of fibrinogen/gelatin electrospun sample after immersion in PBS at 37°C for 24 hours. Scale bar: 5 $\mu\text{m}$ . ....	118
Fig. 4.1: Fibroblast to myofibroblast transition can be caused by microenvironment conditions such as growth factors, cytokines, and mechanical stress. $\alpha$ -SMA expressing myofibroblasts are responsible for the excess deposition of collagen observed in pathological fibrosis. ....	128

Fig. 4.2: SEM images of gelatin electrospun in FA at different solution concentrations: (a) c = 15% w/v; (b) c = 10% w/v; (c) c = 5% w/v. Scale bar: 5 $\mu$ m. ....	142
Fig. 4.3: SEM images of gelatin electrospun in AA/H <sub>2</sub> O at different solution concentrations: (a) c = 10% w/v; (b) c = 7% w/v; (c) c = 5% w/v. Scale bar: 5 $\mu$ m. ....	142
Fig. 4.4: SEM images of gelatin electrospun in HFIP/H <sub>2</sub> O at different solution concentrations and temperature: (a) c = 5% w/v, T = 20°C; (b) c = 3% w/v, T = 20°C; (c) c = 3% w/v, T = 40°C. Scale bar: 5 $\mu$ m. ....	144
Fig. 4.5: Curves of viscosity as function of shear rate for 10% w/v Gel solution in FA at different stirring time, from 1 to 12 days.....	145
Fig. 4.6: Curves of viscosity as function of shear rate: (a) HA solutions in FA/DMF/H <sub>2</sub> O at two different concentrations, 1.5% and 2.5% w/v, before and after MW radiation; (b) 1.5% HA solutions before and after MW radiation, and after HA precipitation and re-dissolution by mechanical stirring in FA/DMF/H <sub>2</sub> O. ....	147
Fig. 4.7: Curves of viscosity as function of shear rate for 2% w/v HA solution in FA at different stirring time, from 1 to 38 days.....	149
Fig. 4.8: SEM images of 2% w/v HA in FA electrospun at different solution stirring time: (a) 3 days; (b) 5 days; (c) 11 days, (d) 14 days. Scale bar: 5 $\mu$ m. ....	151
Fig. 4.9: SEM images of fibers electrospun with co-axial needle, using 1.5% w/v HA in FA/DMF/H <sub>2</sub> O as shell solution and different core solutions: (a) 15% w/v Gel in FA; (b) 7% w/v Gel in AA/H <sub>2</sub> O; (c) 3% Gel in HFIP/H <sub>2</sub> O (T = 40 °C). Scale bar: 5 $\mu$ m.....	152
Fig. 4.10: SEM images of fibers electrospun with co-axial needle, using 2.5% w/v HA in FA/DMF/H <sub>2</sub> O as shell solution and different core solutions: (a) 15% w/v Gel in FA; (b) 7% w/v Gel in AA/H <sub>2</sub> O; (c) 3% Gel in HFIP/H <sub>2</sub> O (T = 40 °C). Scale bar: 5 $\mu$ m.....	154
Fig. 4.11: SEM images of fibers electrospun with co-axial needle, using 1.5% w/v HA in NH <sub>4</sub> OH/DMF as shell solution and 3% Gel in HFIP/H <sub>2</sub> O (T = 40 °C) as core solution. Scale bar: 5 $\mu$ m.....	154
Fig. 4.12: SEM image of fibers electrospun with co-axial needle, using 10% w/v Gel in FA as core solution and 2% w/v HA in FA as shell. Scale bar: 5 $\mu$ m.....	155
Fig. 4.13: (a) SEM image of cross-section and (b) STEM image at 30 kV accelerating voltage of fibers electrospun with co-axial needle, using 1.5% w/v HA in FA/DMF/H <sub>2</sub> O as shell solution and 15% w/v Gel in FA as core solution. Scale bar: 500 nm.....	157
Fig. 4.14: (a) STEM image of fibers electrospun with co-axial needle using HA 1.5% w/v in FA/DMF/H <sub>2</sub> O as shell solution and Gel 3% w/v in HFIP/H <sub>2</sub> O (T = 40°C) as core solution. Scale bar: 500 nm. (b, c) CLSM images of fibers electrospun with co-axial needle using FITC-HA 1.5% w/v in FA/DMF/H <sub>2</sub> O as shell solution and Gel 3% w/v in HFIP/H <sub>2</sub> O. Scale bar: 20 $\mu$ m. ....	157
Fig. 4.15: SEM image of cross-section of fibers electrospun with co-axial needle, using 10% w/v Gel in FA as core solution and 2% w/v HA in FA as shell. Scale bar: 500 nm. ....	159

Fig. 4.16: CLSM images of fibers electrospun with co-axial needle, using 10% w/v RITC-Gel in FA as core solution and 2% w/v FITC-HA as shell solution; (a) RITC-Gel (red); (b) FITC-HA (green); (c) RITC-Gel and FITC-HA superimposed. Scale bar: 10 $\mu\text{m}$ .	159
Fig. 4.17: TEM images of core-shell fibers obtained by co-axial ES of Gel 10% w/v in FA as core solution and HA 2% w/v in FA as shell solution. Scale bar: (a) 50 nm; (b) 20 nm.	159
Fig. 4.18: SEM images of electrospun Gel (a) before and (b) after GA_CL 2h. Scale bar: 2 $\mu\text{m}$ .	161
Fig. 4.19: Analysis of the shift of gelatin nitrogen peak after GA_CL: (a) XPS survey scans spectra for nitrogen of e-spun Gel before and after glutaraldehyde crosslinking treatment for 2 and 6 hours; (b) plot of the percentage of two different nitrogen chemical states, i.e. N=C (formed by crosslinking reaction between Gel and GA) and $\text{NH}_2$ (related to lysine residues in non-crosslinked Gel), as function of crosslinking time of e-spun Gel membranes.	163
Fig. 4.20: FTIR spectra of e-spun Gel before and after GA_CL for 2 and 6 hours.	164
Fig. 4.21: SEM images of e-spun Gel fibers GA_CL 2h after 24 hours in PBS at 37°C. Scale bar: (a) 1 $\mu\text{m}$ ; (b) 2 $\mu\text{m}$ .	165
Fig. 4.22: Results of MTS assay on HDFs cultured for 3 or 5 days with different CCG-203971 concentrations.	166
Fig. 4.23: CLSM images of HDFs after 3 days of differentiation test, with different CCG-203971 concentrations; nuclei are stained by DAPI, and $\alpha\text{SMA}$ filaments by FITC-conjugated antibody. Scale bar: 100 $\mu\text{m}$ .	168
Fig. 4.24: SEM images of electrospun Gel and Gel/HA membranes loaded with CCG-203971: (a) Gel 15 $\mu\text{M}$ (0.1% w/w); (b) Gel/HA 15 $\mu\text{M}$ (0.1% w/w); (c) Gel 30 $\mu\text{M}$ (0.2% w/w); (d) Gel-HA 30 $\mu\text{M}$ (0.2% w/w). Scale bar: 2 $\mu\text{m}$ .	169
Fig. 4.25: CLSM images showing HDFs growing on e-spun membranes 3 days after seeding and stained with Live (green)/Dead (red) viability assay. Scale bar: 100 $\mu\text{m}$ .	171
Fig. 4.26: Results of MTS assay on HDFs 3 days after seeding on Gel and Gel/HA e-spun membranes loaded with different drug amounts.	172
Fig. 4.27: CLSM images showing differentiation of HDFs in contact with 24-hour eluates of e-spun membranes 3 days after seeding; nuclei are stained by DAPI, and $\alpha\text{SMA}$ filaments by FITC-conjugated antibody. Scale bar: 100 $\mu\text{m}$ .	174
Fig. 4.28: CLSM images showing differentiation of HDFs on e-spun membranes 3 days after seeding; nuclei are stained by DAPI, $\alpha\text{SMA}$ filaments by FITC-conjugated antibody, and actin by phalloidin. Scale bar: 100 $\mu\text{m}$ .	174

## Table Index

Table 1.1: Major component of native ECM, their locations, and functions in the body <sup>4</sup> ..	10
Table 2.1: Molecular weight of the biopolymers used.....	48
Table 2.2: Values of vapor pressure and surface tension of the solvents considered for ES- .....	48
Table 2.3: Polymeric solutions and range of parameters tested for ES. ....	51
Table 2.4: Results of collagen solubility tests.....	57
Table 2.5: SEM images of electrospun collagen solutions for both the batches used and for different concentrations. Scale bar: 5 $\mu\text{m}$ .....	59
Table 2.6: Results of gelatin solubility tests. ....	63
Table 2.7: Results of elastin solubility tests.....	66
Table 2.8: Results of HA solubility tests.....	73
Table 2.9: composition of gelatin/elastin and gelatin/elastin/HA solutions optimized for ES process.....	82
Table 3.1: Product information of fibrinogen and gelatin used with indication of their molecular weight.....	90
Table 3.2: Solution, process and ambient parameters used for electrospinning .....	92
Table 3.3: Results of fibrinogen solubility tests.....	105
Table 3.4: SASA value, number of H-bonds, and percentage of $\alpha$ -helix and random coil in fibrinogen secondary structure for the different pH values tested. ....	110
Table 3.5: SEM images and indication of gelification rate during ES for different fibrinogen/gelatin blend compositions. Scale bar: 5 $\mu\text{m}$ . ....	117
Table 4.1: Solvent systems and concentration values of Gel investigated as possible core solutions. ....	130
Table 4.2: Solvent systems and concentration values of HA investigated as possible shell solutions. ....	131
Table 4.3: Solutions and parameter tested for traditional ES. ....	133
Table 4.4: Combinations of core and shell solutions used for co-axial ES and optimized parameters. ....	133
Table 4.5: Optimized solutions and parameters for traditional ES. ....	143
Table 4.6: Optimized solutions and parameters for co-axial ES.....	153
Table 4.7: Elemental surface composition by XPS analyses of fibers electrospun with co- axial needle, and of raw Gel and HA for comparison.....	156
Table 4.8: Elemental surface composition by XPS analyses of electrospun Gel fibers before and after GA_CL for different times (2 to 6 hours). ....	161
Table 4.9: FACS test results – percentage of differentiation inhibition for different drug concentrations.....	168

## Acknowledgements

This work has been performed in the Biomaterial group of the Department of Chemistry, Materials and Chemical Engineering of Politecnico di Milano. I would like to thank my advisor, Lorenza Draghi, and all the other colleagues of the group. In particular, I thank Professor Candiani for his kind suggestions and support, Monica Moscatelli for all the SEM images, Andrea Serafini for the TEM analyses, Elena Tallarita and Paolo Tarsini for helping me with SDS-PAGE.

Thanks also to Dott. Elena Rosini for the CD analysis and the discussion about it, and to Dott. Stefano Buzzaccaro for the part of my study regarding the Photon correlation imaging.

A special thank goes to the Biomechanics group of the Politecnico di Milano, and in particular to Federica Rigoldi and Professor Simone Vesentini, who gave me the access to the computational biomechanics lab where I performed all my MD simulations under their supervision.

Last but not least, I thank Dott. Giuseppino Fortunato and Dott. Markus Rottmar, who were my supervisors for my period abroad at Empa in St. Gallen. Thank you again for your experience, your open-minded attitude, your kindness, and your neverending support. In this group I met a number of researchers that gave me the possibility to develop my skills and my attitude toward research. In particular, I would like to thank Yvonne Elbs-Glatz for her neverending patience and contagious passion for her job.

